THE CRUSTAL STRUCTURE OF THE CENTRAL ANATOLIA USING RECEIVER FUNCTION ANALYSIS

by

Seda YELKENCİ

B. Sc in Department of Geophysics, Istanbul University, 2002

Submitted to the Kandilli Observatory and Earthquake Research Institute
In partial fulfillment of the requirements for the degree of
Master of Science
in
Geophysics

Boğaziçi University

June 2006

TABLE OF CONTENTS

ACKNOWLEDGEMENTS

First of all, I would like to thank to my advisor Prof. Dr. Cemil GÜRBÜZ for his guidance, constructive support and suggestions during this work. I am also thankful to him for providing me opportunity to work with my thesis in Massachusetts Institute of Technology, U.S.A.

I would like to thank Prof. Dr. Nafi TOKSÖZ who provided me an office and access to their laboratory and computing facilities and all members in Earth Resources Laboratory (ERL) for their assistance and helps whenever I needed throughout my study there. Especially, this thesis could not have been completed without postdoctoral fellow Margaret BENOIT and Dr. H. Sadi KULELİ who gave me great deal of guidance, as well as providing me computer programs to advance my study during the analysis stages. I am also appreciated Esen ARPAT who shared his experiences for me in interpreting stage.

I would like to special thanks to Dr. H. Sadi KULELİ for his motivations and invaluable advices about life as well as my study and his family for their hospitalities and friendships that could help to reduce my homesick situation during my staying in U.S.A. Special thanks also go to Gülten POLAT, Tuğce AFACAN and Doğan AKSARI for their support. Especially, I am grateful to my officemate, Gülten POLAT who was very helpful for office work during my thesis and, encouraged and make me smiled whenever I was in trouble.

On the personal side, I would like to acknowledge the infinite moral support of my family who encouraged me throughout all my life.

ÖZET

Orta Anadolu, çevresindeki plakaların hareketlerine bağlı olarak termal ve jeo-dinamik gelişmelerin etkisinde kalmış karmaşık bir bölge özelliği taşımaktadır. Orta Anadolu bölgesinin kabuk yapısı ile ilgili yapılan bilimsel araştırmalara, 2002 yılında başlayan ve Massachusetts Institute of Technology (MIT), Lawrance Livermore National Laboratory (LLNL) ve Boğaziçi Üniversitesi tarafından desteklenen Kalibrasyon Projesi kapsamındaki calışmalar büyük ölçüde katkıda bulunmuştur. Bu çalışmalara destek olmak adına, alıcı fonksiyonlarının analizi ile bölgenin kabuk yapısı ortaya koyulmaya çalışıldı. Çalışmada, Kalibrasyon projesi kapsamında kurulan geçici sismik istasyonlarda kaydedilmiş ve daha önceki çalışmalarda kullanılmamış veriler analiz edildi. Ayrıca, 2002 yılının Ekim ve Kasım ayları boyunca yaklasık bir buçuk aylık bir süre boyunca çalışan bu geçici istasyonlara ek olarak, ISP, ANTO ve MALT kalıcı istasyonlarına ait veriler de analizde kullanıldı. Alıcı fonksiyonu bir istasyon altında, yerin sismik cevabı olarak tanımlanmakla birlikte, tektonik ve jeodinamik gelişmelerin daha iyi araştırılmasına yardımcı olabilen bir yöntemdir. Bu çalışmada, elde edilen alıcı fonksiyonlarına, Moho derinliği ve Vp/ Vs oranlarını bir sonuç olarak verebilen H-κ yığma algoritması uygulandı. Analizde geniş bir episantr aralığına (30°-103°) sahip veriler seçilerek, herbir üç bileşen telesismik kayıt için bir alıcı fonksiyonu oluşturuldu ve orta Anadolu altındaki Moho derinliği araştırıldı. Sonuçta, bölgenin kabuk yapısı belirlendi ve daha önceki çalışmalarla karşılaştırıldı. Yapılan alıcı fonksiyonu analizi sonucunda, orta Anadolu'nun doğu kesimlerinde yaklaşık 43 km'ye varan kabuk kalınlıklarından, batı kesimlere doğru 35 km'ye ulaşan bir azalma gözlendi. Fakat, Orta Anadolu metamorfik masifi, Tuz Gölü baseni ve Isparta çevresinde bu azalmanın uyumlu bir şekilde gerçekleşmesini engelleyen ani derinlik değişimleri gözlendi. Ayrıca bölgenin termal yapısına işaret edebilecek, genellikle yüksek Vp/Vs oranları bulundu. Alıcı fonksiyonlarının analizine ek olarak, geçici sismik istasyonlarda aynı süre içinde kaydedilmiş olan yerel depremlerden yararlanarak, bu depremlerin tekrar lokasyonu yapıldı. Sonuçlar alıcı fonksiyonları ile elde edilen sonuçlar ile karşılaştırıldı. Bu çalışmanın devamında dalgacık modelleme tekniği ile Orta Anadolu'nun kabuk yapısının daha ayrıntılı araştırılması amaçlanmaktadır.

ABSTRACT

Central Anatolia has complicated crustal and upper mantle structure that is influenced by the thermal and geodynamic process related to motions of surrounding plates. Few studies of the crustal structure of Central Anatolia have been done. Basically, studies of the nature of the crust have been performed for central Anatolia under the Calibration project started in 2002. To further investigate the crustal structure in the region, we present results from receiver function analysis using new data from temporary network which was installed under the same project. These temporary stations operated for period of one and half months between October and November, 2002. In addition, permanent stations ANTO, ISP and MALT were alsò used to compute receiver functions. Receiver function that is the seismic response of the Earth beneath the seismic station leads to investigation of tectonic and geodynamic processes. In this study, H-κ stacking algorithm which gives crustal thicknesses and Vp/Vs ratios as outputs of method has been used for receiver function analysis. Three component teleseismic data with epicentral distances between 30 and 103 degrees has been preferred to obtain single-event RFs and to investigate Moho depth under the Central Anatolia. Consequently, the structure of the region has been reasonably defined and compared with other geophysical studies. As a result of the RF analysis, although it has found that Moho depth decreases from about 43 km eastern part of central Anatolia to about 35 km western part, we observed sharp changes for some regions in which Tuz Gölü basin, central Anatolia core complex and Isparta that may prevent smooth changes in crustal thickness. Furthermore, we found almost high Vp/Vs ratios that can indicate thermal structure in the study area. Additionally, we acquired information concerning the thickness of central Anatolia from relocating local earthquakes, which were recorded by the temporary stations during recording periods. Then obtained outcomes were discussed with results of RF analysis. In the light of this study, new treaties based on waveform modeling technique in the future can allow us getting detailed investigation concerning crustal structure of the Central Anatolia.

LIST OF FIGURES

LIST OF TABLES

CHAPTER.I. INTRODUCTION

From the seismologic point of view, much of the information about the earth's interior has been derived from a knowledge of the variation of seismic velocities with depth. The efforts to determine crustal thickness dates back to 1910, when Mohorovicic first identified an increase of velocity beneath the shallow rocks in Europe. The compositional boundary between crustal rocks and mantle rocks is called as the Moho discontinuity. The depth of Moho is a crucial parameter to characterize overall structure of a crust and can be related to geology and tectonic evolution of the region. Therefore, its physical properties strongly encourage researchers to investigate it.

For the purpose of finding out Moho depth, crustal and lithospheric structures; teleseismic body waves have been used extensively for a long time under the name of crustal transfer function method ever since the early studies of Phinney (1964). The method has been subsequently improved by several researchers (Burdick and Langston, 1977; Vinnik and Kosarev, 1981). Owens et al. (1984) further improved the method for the application to newly available broadband data using linearized time-domain inversion. It is now commonly referred to the Receiver Function analysis, one of the most favored and effective technique to analyse the structure of the crust and uppermost mantle. Receiver function analysis has proven to be useful tool which provides a good measurement of crustal thickness under a seismic station. The depth estimation is less affected by lateral velocity variation due to the fact that P to S conversion point is so close to the station. As a result, this advantage makes receiver function a preferable technique for estimating crustal thickness.

As taking into account the usefulness of the method, we applied receiver function analysis method for the central Anatolia to determine the depth of the Mohorovicic discontinuity and Vp/Vs ratio. In the study area, stations operated for period of one and half months between the October and November, 2002 and yielded high quality data which is suitable for the receiver function analysis. Stations used in this study consist of 7 portable broadband three-component STS-2 and 13 portable short period three-component S-13 sensors across the central Anatolia (Figure 1.1). Additionally, permanent IRIS stations MALT, ISP, and ANTO were also used to complete the data set.

In the case of data analysis; after some usual processes such as rotating three component teleseismic records to obtain radial and transverse components and filtering to improve signal to noise ratio, we applied frequency domain deconvolution procedure in order to produce receiver functions. Deconvolving the vertical component of teleseismic P-wave records from the radial components removes source and instrument response from waveforms (Langston, 1979). The P to S converted phase and reverberated phases, PpPs and PpSs+PsPs, are generally apparent in the receiver function waveforms. After obtaining receiver function, we applied H-κ stacking analysis method which is consists of a transformation from a time domain representation of the receiver function into a new domain that is H (depth) and the Vp / Vs ratio.

H-κ stack method has been used by several scientists (eg. Zhu and Kanamori, 2000; Julia et al., 2005; Julia and Mejia, 2004) recently. This method takes advantage of the relative moveout of the secondary arrivals generated at a seismic discontinuity beneath the station to infer the depth and Vp/Vs ratio above the discontinuity. By stacking receiver functions from different distances and directions, effects of lateral structural variations were suppressed and an average crustal model was obtained. Finally, we map out the lateral variations of Moho depth under the central Anatolia. We will discuss the methodology of obtaining teleseismic receiver functions, H-κ stack analysis and associated uncertainties in Chapter II. In addition to the receiver function analysis, to recognize signature of laterally varying media and have information about changes of crustal thickness in Central Anatolia we attempted a relocation procedure which was discussed in Chapter IV. A number of regional and local events that have been recorded by broadband and short period stations in the region have been considered by using HYPO71PC program. Comparing the results of relocation with H-κ stack analysis's results gives us implicitly determination of the Moho depth.

1.1. Previous studies

Various seismological treaties have been done in the region due to the fact that Central Anatolia lies in a transitional region between the extentional tectonics of western Anatolia and the complex transpressional tectonics of Eastern Anatolia, and has complicated thermal structural history. The crustal structure and seismic velocities of the Anatolian plateau have been studied by several researchers.

Canıtez and Toksöz (1980) used travel-time residuals of teleseismically recorded P wave velocities, concluded that P wave velocities in the uppermost mantle are 7.9 km/s in central and the Eastern Turkey. Gürbüz and Evans (1991) determined basement depths as between 6 and 10 km with a velocity of 6.15 km/s in the Salt Lake (Tuz Gölü) basin using time-term analysis and ray tracing method. Hearn and Ni (1994) used a tomographic technique to obtain Pn velocities for Anatolia and surrounding regions. They used data from the International Seismological Centre (ISC) catalog and found that Pn velocity is approximately 7.8 km/s in central Anatolia.

Sandvol et al. (1998) applied a grid-search approach to receiver function waveform modeling to determine site-specific crustal velocity and thickness models and they estimated crustal thickness of 37.0 and average crustal shear velocity of 3.6 km/s under the ANTO station. Mindevalli and Mitchell (1989) measured fundamental mode Rayleigh and Love wave group velocities in the 8- to 50-s period range for the ANTO seismic station. They realized that the shear wave (Sn) velocity is 4.2 km/s and an approximate crustal thickness is 40 km. Gürbüz *et al.* (2003) used seismic refraction method for the purpose of determining velocity structure and propagation characteristics of seismic waves in the central Anatolia. They found that Pn velocity is 7.8 km/sec. and the crust is 36 km thick under Keskin area. Crustal velocities and Moho depth were estimated to be 3.6km/s and 36 km thick, respectively beneath the Belbaşı array (BRAR) by Kuleli et al. (2001) using receiver function modeling technique. These studies will be compared with our result of receiver function analysis in Chapter V.

1.2. Tectonic and Geological Settings

Turkey is a tectonically very active and surrounded by major plates, Eurasian, African and Arabian Plates (Figure.1.2). The first studies on the tectonic evolution of Turkey with regarding to tectonic elements were initiated by McKenzie (1972) as a systematic approach. Ketin (1973) also initiated the study with his finding on the right lateral movement of the North Anatolian Fault following the Erzincan earthquake in 1939. His studies were later followed and expanded by several earth scientists (Barka and Kadisky-Cade, 1988; Şengör and Yılmaz, 1983; Aydan, 1997). Tectonic evolution of Turkey was associated with the closing of the Tethys ocean between Eurasian and African plates as a result of the northward motion of the African plate and Arabian plate (McKenzie 1972; Barka and Reilinger, 1997; Aydan, 1997).

Tectonic framework of the eastern Turkey is dominated by the continent-continent collision where the Arabian plate is colliding with Eurasian plate along the Zagros and Bitlis suture zones (McKenzie, 1970; Jackson and McKenzie, 1988; Al-Lazki, 2004) and subduction beneath the Agean and Anatolian (Şengör and Yılmaz, 1981). According to the plate tectonic models, the Arabian plate is moving in a north-northwest direction relative to Eurasian. This was resulted high topography and earthquake activity in the Eastern Turkey, and African plate is being subducted along the Hellenic arc that creates extention in the Agean region. According to Şengör et al. (1985) and Barka (1996), the movement of Arabian plate has taken place since the late Miocene. In the Early Pliocene, continued convergence of the Eurasian and Arabian plates (Figure1.2) causes development of the North Anatolian fault (NAF) and East Anatolian fault (EAF) zones (Sengor & Yılmaz 1981; Sengor et al. 1985). These fault systems can be thought as boundaries that separate the eastern compression from westward moving of Anatolian block.

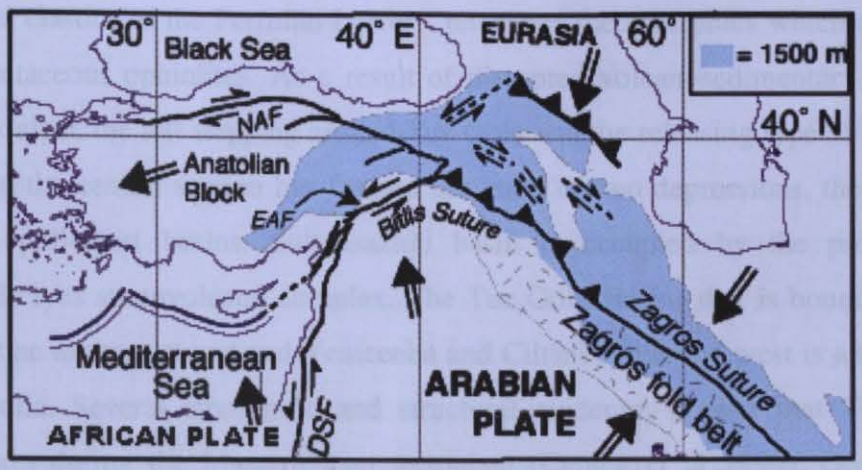

Figure 1.2 Map showing major tectonic structures of Turkey and adjacent areas. (modified after Şeber et al., 1997)

The Central Anatolia has complex Neotectonic deformation with Alpine-Himalayan collision and subduction of Neotethyan seaways prior to collision since Late Miocene-Pliocene times. It includes metamorphic rocks and associated structures like many faults and basins that formed during this collision period. More recent geological studies carried out by many scientist show that there is a long and broad belt that is called Ecemiş fault zone between Düzyayla Town (Sivas) in the northeast and Anamur County in the southwest. This sinistral, approximately NE-trending, intracontinental structure has been described and renamed by Koçyiğit and Beyhan (1997) as Central Anatolian fault zone (CAFZ). It is thought that it have originated from the north-northeastward propagation of a paleotectonic structure during the neotectonic period (Plio-Quaternary times). Another well-known great structure in central Anatolia is the Lake Salt fault zone. The Lake Salt (Tuz Gölü) is active, dextral strike-slip fault interacts with the WSW-ENE-trending Kayseri-Karaman volcanic lineament, leading to the continuous rise of magmas from the Late Miocene to Recent (Innocenti et al., 1975; Görür et al., 1984).

In central Anatolia there are several important basins such as the Haymana, Tuzgölü, Ulukışla, Kızılırmak, Çankırı-Çorum and Sivas. They developed mainly after closure of the Neotethys (Dirik et al., 1999). Sivas basin is one of the largest basins of Anatolia inherited from the closure of the Inner Tauride ocean (Şengör and Yılmaz, 1981). The Sivas Basin is located in the eastern part of central Anatolia between the Central Anatolian Crystalline Complex (CACC) in the north and Taurides in the south (Figure.1.3). According to the Dirik

et al. (1999), the basement to the southeastern part of the basin consists of recrystallized limestone and clastics of the Permian-Lower Cretaceous metamorphics which are overlain by an Upper Cretaceous ophiolites. As a result of disrupted volcanosedimentary infill by Mio-Pliocene tectonism, the left stepping around Tuz Gölü and the releasing type of bending on the CAFZ around the central section has formed initiation of two depressions, the Tuz Gölü and Sultansazlığı pull-apart basins. Sultansazlığı basin is occupied by the product of Plio-Quaternary Erciyes stratovolcano complex. The Tuz Gölü Basin that is bounded by the Tuz Gölü Fault zone to the east and and Yeniceoba and Cihanbeyli to the west is a typical basin in central Anatolia. Several stratigrafic and structural evidence suggest that Tuz Gölü basin started to form during the Maastrichtian tectonism (Çemen et al.,1999). Göncüoglu et al., (1991) proposed that underlying metamorphic rocks in the area were subjected to medium- to high grade metamorphism with high temperature reaching partial melting conditions.

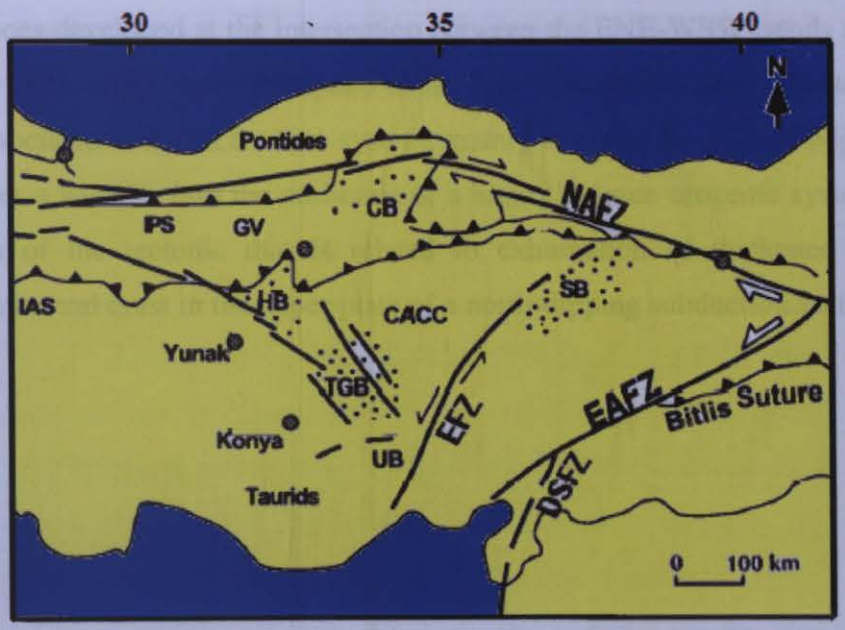

Figure 1.3 Map showing major basins and tectonic elements of Central Anatolia. *CACC*= Anatolian Crystalline Complex, fault Central *CB*= Çankiri basin, *EAFZ* = East Anatolian fault zone *EFZ*= Ecemis fault zone, *IAS* = İzmir-Ankara suture zone, *DSFZ* = Dead Sea fault zone *GV*= Galatian Volcanics, *HB*= Haymana Basin, IAS= İzmir-Ankara suture zone, *TGB* = Tuz Gölü basin, *IPS* = Intrapontide suture zone *UB* = Ulukisla basin, *SB* = Sivas basin. (Çemen et al., 1999).

The Central Anatolian Volcanism has developed since the Late Miocene over an Oligocene foredeep basin located between the central Taurus Range and the Kirsehir crystalline massif (Innocenti et al., 1982; Pasquare et al., 1988) . However, the origin of the magmatism of this province dominated by calc-alkaline products is not clearly understood (Temel, 1992).

The Neogene and Quaternarry volcanism of Central Anatolia represent the central part of the Anatolian Volcanic Arc, related to continental collision between the African, Arabian and Eurasian plates (İlkışık et al., 1997). İlkışık (1997) suggested that the volcanism is described as three main periods of activity for central Anatolia. The first one is represented by mostly andesitic activity. The second period is characterized by the emplacement of a thick ignimbritic sequence like the Cappadocian ignimbritic units. Cappadocia is located in the central part of Central Anatolian Volcanic Province and is characterized by Miocene ignimbritic sequence. Since the Pleistocene, volcanic activity has been essentially represented by two stratovolcanoes, Hasan Dağ and Erciyes Dağ in the region. The third period of volcanism for Central Anatolia is represented by great andesitic- basaltic stratovolcanos. Most of the great central volcanoes developed at the intersection between the ENE-WSW trends and the Ecemiş and Tuz Gölü transcurrent faults (Pasquare et al., 1988). Moreover, many Quatemary volcanic centers are associated with this fracture system, mainly between Acıgöl and Niğde. The Niğde massif provides a window into the mid-crust of a highly oblique orogenic system and permits reconstruction of the tectonic that is related to exhumation of thickened and thermally weakened continental crust in the upper plate of a north-dipping subduction zone (Whitney and Dilek, 1997).

CHAPTER.II. Receiver Function Method

2.1 Introduction

Determination of the detailed structure of the crust and the upper mantle is a continuous goal of geophysical studies. In the light of this aim, the receiver function method has been used as a relatively powerful and alternative technique in obtaining information about Moho depth, discontinuities in the crust and the upper mantle beneath three component seismic stations. Receiver functions define a time series corresponding to the relative response of Earth structure under the station. In Receiver function technique, the teleseismic body waveforms which produce a series of reflections, refractions, and conversions are used to image the crustal structures. These waveforms contain information related to the source time function, propagation effect through the mantle and local structures beneath the recording site.

The basic aspect of this method is that part of the incoming P wave energy from distant events was converted into SV wave at Moho discontinuity by owing to the large velocity contrast across the discontinuity. This wave arrives at the station within the P wave coda directly after the direct P wave. Commonly observed propagation modes in receiver functions include a pulse associated with the incoming P wave field, P to S (Ps) converted modes generated by the upcoming wave field at each discontinuity and reverberated modes which are generated by the upcoming wave field being reflected downward off the earth's free surface as P or S and finally reflecting upward as S at each discontinuity (Figure 2.1.a). As a result, receiver function trace includes the direct, Ps converted and PpPs phases which have a positive polarity, PpSs+PsPs reverberated phases which has a negative polarity (Figure 2.1.b). The polarity implies whether the impedance contrast is negative or positive.

The arrival times of the converted phases and multiples which have much stronger amplitude on the horizontal component, depend on the depth of the velocity contrast, the P and S velocity between the contrast and the surface, and the P-wave incidence angle, or ray parameter.

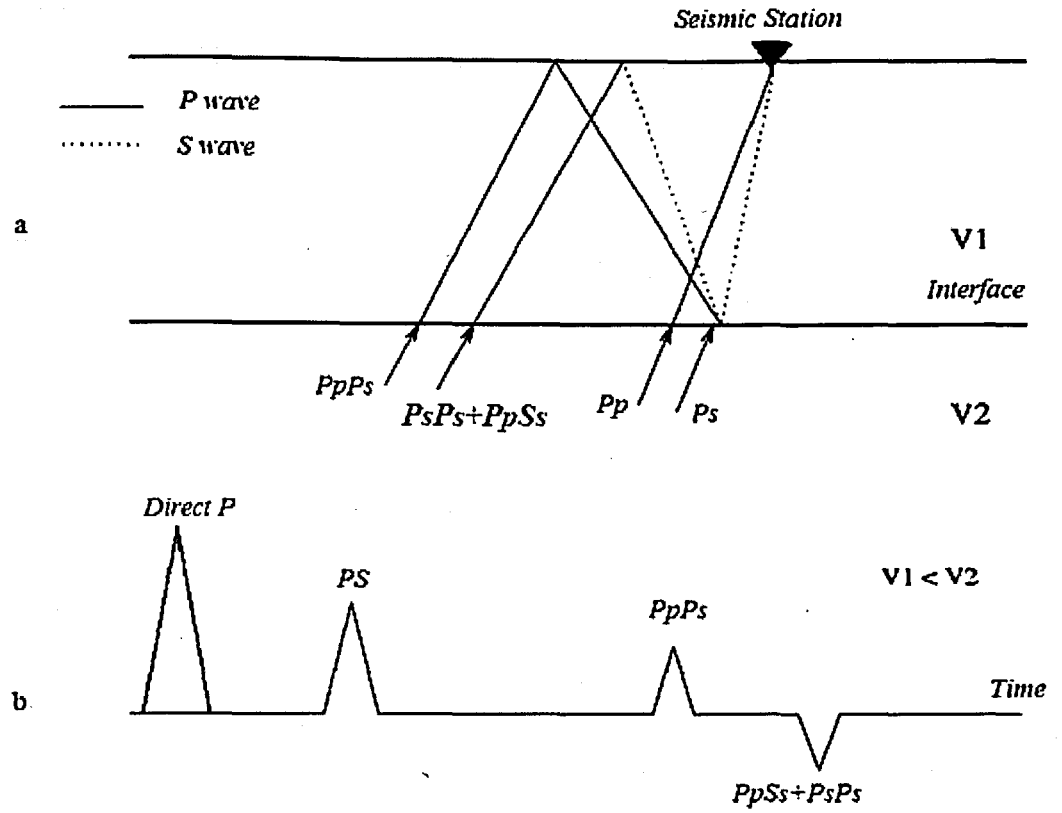

Figure 2.1.a. The major Ps converted phases for a layer over a half space model.
b. Receiver function that show the direct P and the Ps conversions from the Moho and its multiples corresponding to the model above.

Both radial and transverse component receiver functions obtained from cluster of backazimuths can be computed to study about anisotropy and dipping receiver structures. (McNamara and Owens 1993; Zhang and Langston 1995; Peng and Humphreys 1997; Levin and Park 1997). While radial RF is defined as spectral division of the radial and vertical seismograms, transverse RF is defined as the spectral division of tangential and vertical seismograms in the frequency domain.

2.2. Receiver Function Analysis

For the teleseismic earthquakes which is more than 30° distant, P waves are steeply incident and dominate vertical component of ground motion, P to S converted phases dominate horizontal component of ground motion. Therefore, frequency responses of the three component seismometers are useful for receiver function analysis. Broadband seismometers

are generally used because of having better seismic energy coverage, short period seismograms are also useful to analyze RFs. Since P to S conversions on horizontal component can be studied directly, deep events are preferable for RFs. According to observation from teleseismic deep events, vertical component of ground motion has minor structural response.

Filtering, windowing and rotating the waveform are very crucial steps to obtain high quality waveforms to analyze the data. Filtering of waveforms can eliminate their high frequency component that are effected by small-scale heterogenities. For receiver function studies, useful teleseismic waves have frequencies in the range of 0.1 Hz to 1 Hz. Windowing waveform is also prominent because of choosing large window length makes reverberated phases more obvious. For the teleseismic distances (30° to 95°), 60 seconds of pre-signal and 60 seconds after the P wave are used. Generally, the first 20 s of the P wave coda can be considered to represent features of the crust and uppermost mantle. However, variations can be compared by various lengths of signal during the source equalization procedure.

Another procedure that receiver function analysis requires the rotation of original Z, NS and EW components into the L, Q and T coordinate system (Figure 3.3) for the purpose of isolating the converted S phases from the direct P wave. The L-component points in the direction of the direct P wave and the Q-component is perpendicular to L-component. The T component is perpendicular to both L and Q components. The L, Q and T components contain mainly P-energy, SV-energy and SH-energy, respectively. The rotation can be performed using the theoretical back-azimuth and incidence angle of an incoming P wave. The back-azimuth and incidence angle can be determined by knowing the coordinates of earthquake hypocenter and the recording station for a global velocity model. The alternate way to determine the angles of incidence and back-azimuth is by calculating the eigenvalues of the covariance matrix over a time window spanning the first few seconds following the P-arrival.

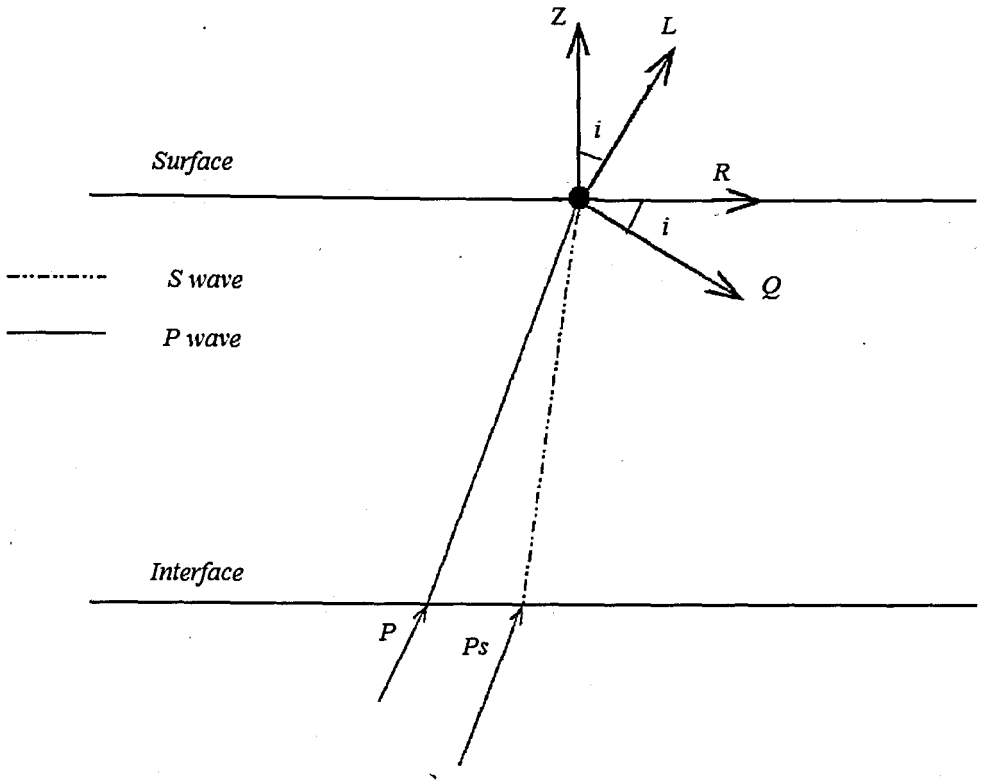

Figure 2.2 Showing the earth-oriented coordinate system Z and R. Labels L and Q represent the axes of the ray coordinate system, L component is in the direction of the incident P wave, Q component is perpendicular to L and points away from the source. T component is perpendicular to both L and Q components.

In case of the medium is isotropic and the layers are horizontal, the L component contains mainly the P-energy, Q component contains mainly the SV-energy, and no energy should be seen on the T component. However, anisotropic media and lateral inhomogeneities under the seismic station may produce energy on the T component. The reason of obtaining radial and transverse component is that P to SV mode conversions are radially polarized on the radial component while the P to SH mode conversions are transversally polarized on the tangential component. The advantage of using the Q-component instead of the radial component, is the disappearance of projected P-energy at the P arrival time. Because of this characteristic of Q component, receiver functions are identified on the Q-component seismogram.

2.2.1. Deconvolution Procedure

In receiver function studies, the response of the structure must be isolated from the factors such as source structure and propagation path effects which are the composition of each seismogram. The source equalization procedure can be computed both in time and frequency domain for receiver structure studies. Phinney (1964) developed a deconvolution process in the frequency domain and Langston (1979) extended this technique by using a water-level stabilization method and a low-pass Gaussian filter as an addition to inverse transformation back into the time domain.

The theoretical displacement response, *D(t),* of three component stations is explained by the convolution of instrumental response, source-time function and structural response in time domain. This convolution process for teleseismic P wave under a horizontal or dipping layers is given by;

$$\begin{aligned} D_V(t) &= I(t) * S(t) * E_V(t) \\ D_R(t) &= I(t) * S(t) * E_R(t) \\ D_T(t) &= I(t) * S(t) * E_T(t) \end{aligned} \tag{2.1}$$

where $E_V(t)$, $E_R(t)$ and $E_T(t)$ represent vertical, radial and tangential component of Earth's impulse response, respectively. $I(t)$ is impulse response of recording instrument and $S(t)$ is seismic source-time function. The Earth's impulse response is also given by,

$$E(t) = \sum_{i=1}^{n} \left\{ \alpha_i \delta\,(t-\tau_i) + \beta_i H[\delta(t-\tau_i)] \right\} \tag{2.2}$$

where α_i and β_i are constant reflection transmission coefficients, δ (t) is Dirac delta function, τ_i is travel time of the ray and $H[\delta(t-\tau_i)]$ represents Hilbert transformation operator.

Horizontal component of ground motion is different from the vertical component due to the fact that structure under a station produce conversion of P to S type modes. Vertical component which includes unwanted source and path effects for P wave consists of large direct arrivals followed by small arrivals from crustal reverberations. As a result, it gives vertical displacement response and behaves like Dirac delta function.

Therefore, assuming $E_V\ (t) \sim \delta(t)$ at teleseismic distances, vertical component displacement deviation can be represented by,

$$D_V(t) \sim I(t) * S(t) \tag{2.3}$$

After this assumption, radial component earth response that is called receiver function $E_R\ (t)$ can be found by deconvolving vertical component with radial component $D_R\ (t)$. This process can be also produced for $E_T(t)$. Radial and transverse receiver functions in frequency domain are expressed by,

$$\begin{aligned} E_R(\omega) &= \frac{D_R(\omega)}{I(\omega)S(\omega)} \sim \frac{D_R(\omega)}{D_V(\omega)} \\ E_T(\omega) &= \frac{D_T(\omega)}{I(\omega)S(\omega)} \sim \frac{D_T(\omega)}{D_V(\omega)} \end{aligned} \tag{2.4}$$

$E_R(\omega)$ and $E_T(\omega)$ are retransformed back into the time domain. For the purpose of making dominator real in equation 2.4, it is multiplied with complex conjugate $D_V^*\ (\omega)$ and radial receiver function is expressed by,

$$E_R(\omega) = \frac{D_R(\omega)\, D_V^*(\omega)}{D_V(\omega)\, D_V^*(\omega)} \tag{2.5}$$

This estimation is defined for the whole frequency band of the spectrum. In order to remove high-frequency noise in the receiver functions and smooth the results, low pass Gaussian filter G(ω) is taken into account.

$$E_R(\omega) = \frac{D_R(\omega)\, D_V^*(\omega)}{D_V(\omega)\, D_V^*(\omega)}\, G(\omega) \tag{2.6}$$

where,

$$G(\omega) = e^{-\omega^2/4\alpha^2}$$

α is Gaussian filter-width parameter controlling the frequency content (Table.2.1).

Table 2.1 Showing frequencies for chosen α values at which G(ω) value equals to 0.1.

α	**Frequency (Hz) at which G(ω)= 0.1**
10.0	4.8
5.0	2.4
2.5	1.2
1.25	0.6
0.625	0.3
0.5	0.24
0.4	0.2
0.2	0.1

The division of deconvolution in frequency domain causes some numerical problems in calculations in the case of small or zero values of $D_V(\omega)D_V^*(\omega)$. Therefore, receiver function which is defined in equation 2.5 can not be used to compute radial Earth's response. The simplest way is to use a water-level technique which is developed by Helmberger and Wiggins (1971) and Dey-Sarkar and Wiggins (1976) to avoid this problem.

In the case of this consideration, implementation of the receiver function in the frequency domain takes the form by replacing $D_V(\omega)D_V^*(\omega)$ in equation 2.5 with $\varphi(\omega)$:

$$E_R(\omega) = \frac{D_R(\omega)\, D_V^*(\omega)}{\varphi(\omega)}\, G(\omega) \tag{2.7}$$

$\varphi(\omega)$ that represents autocorrelation of $D_V(\omega)$ can be expressed by,

$$\varphi(\omega) = \max\{D_V(\omega)\, D_V^*(\omega),\ c \max[D_V(\omega)\, D_V^*(\omega)]\} \tag{2.8}$$

The water-level creates the stabilization of deconvolution by replacing small values with a fraction of the maximum value of the denominator. The fraction is called as the water level parameter, c. The consequence of replacing small values with larger ones in the denominator is an attenuation of frequencies for which the vertical component has a small amplitude (Ammon, 1991). Water level parameter is ranging from 0.001 to 0.1. It is chosen by examining the

results of several trial water-level fractions until reaching to an ideal result. Since the water-level filter can cause distortions of the receiver function, it can give better results by choosing smaller values.

The averaging function shows a good way to see the effects of the water-level and Gaussian filter on the waveform. The averaging function is calculated by deconvolving the vertical component of motion from itself by using the chosen water-level parameter (Ammon, 1991). Large water-level values produce a broadened and often distorted averaging function which can be guided for interpretation of receiver functions.

2.3. Receiver Function Estimation Methods

2.3.1. Inversion Technique

Since Phinney (1964), several researchers employed waveform modeling in various forms. Because frequency domain technique has some disadvantageous, Burdick and Langston (1977), they improved time domain modeling and Langston pointed out the sensitivity of the structure to shear waves. For the purpose of recovering detailed information from the P waveform, Owens et al., (1984) and Owens et al., (1987) developed this inversion technique and demonstrated that the shear-wave partial derivatives are much larger than the compressional wave partial derivatives, so the inversion is formulated to estimate the shear-velocity.

Nowadays, receiver function inversion has become a widely used technique which inverts RFs to an S wave velocity model to obtain shear wave velocity structure beneath stations. The inversion method is a non-linear inversion scheme, which requires an initial velocity model and then improves the model iteratively by a sequence of relatively thin layers with an increase or decrease of the velocity. For the initial model, information from reflection/refraction studies in the region can be used. The method investigates minimization of the differences between observed and synthetic receiver functions (equation 2.9, 2.10, 2.11), hence using a priori available information of the area under investigation will be helpful to have realistic solutions.

The general representation of the inversion form can be given below:

$$G\,dm = d \tag{2.9}$$

where m is the velocity model, dm is a velocity correction vector, d is the residual vector, and G is the matrix whose i' th column is the partial derivative of the receiver function with respect to the shear velocity in layer "i".

The initial model is m_o and the model is characterized by,

$$m = m_o + dm \tag{2.10}$$

By using this representation, a new inversion form (2.11) may be directly obtained and is given by,

$$Gm = d + Gm_o \tag{2.11}$$

Furthermore, many non-linear minimization procedures have recently been introduced such as Simulated Annealing (Velis, 2001) and Genetic Algorithm (Koper et al., 1999) in order to overcome the lack of stability of receiver function inversion. In addition, Cassidy (1995) and Baker et al. (1996) applied receiver function inversion to forward model waveforms for determining crustal structure. As another widely used technique, Grid Search Method (GSM) is based on searching each parameter in the predefined space (Walter, 1993; Sandvol et al., 1998) and minimize the misfit between the observed and predicted radial-horizantal seismograms. For this method, it is possible to reduce the number of model parameters in inverse problem under some assumptions based on Birch's law and Poissson's ratio. A Grid Search Method (GSM) can allow the estimation of average crustal thickness and shear wave velocity structure.

2.3.2. H-κ Stacking Technique

2.3.2.1. Introduction

Determination of accurate crustal thickness and average Vp/Vs ratios by using crustal multiples are important characteristics of receiver function analysis. The converted phase Ps and reverberated phases PpPs and PpPs+PsPs contain valuable information about the crustal properties. There are several developed techniques to estimate local depth and average Vp/Vs ratio between the surface and the discontinuity associated with each mode by measuring the

moveout of the direct converted and reverberated receiver function mode (e.g., Zandt and Ammon, 1995).

One of the useful techniqe is H-κ (depth-Vp/Vs ratio) stacking method proposed by Zhu and Kanamori (2000). The main assumptions in this method are that the incoming P wave is essentially a plane wave, the velocity structure consists of locally horizontal layers, and the crust is laterally uniform. This technique requires information about of average P velocity of the crust. In the light of these assumption, H-κ stacking technique makes a transformation from the time domain receiver functions directly into the H-Vp/Vs domain without a need to identify reverberated phases at Moho and to pick their arrival times, namely, the PpPs and PpPs+PsPs.

According to this stacking algorithm, estimation of the local thickness and average crustal Vp/Vs ratio underneath each station can be produced by stacking or summing the receiver amplitudes of receiver functions at the predicted arrival times of direct converted phase, Ps, and reverberated PpPs and PpSs+PsPs with assuming a starting average P wave velocity model. The stacked receiver function amplitudes will be maximized where the three phases add coherently. The best estimations of crustal thickness and Vp/Vs ratio are found and measurement variances and covariances can be calculated. An important consideration in accurately estimating the crustal velocity model is an accurate characterization of the thickness and velocity of near surface sediments. Seismic velocities, particularly for shear waves, can be much slower for sedimentary rocks than crystalline rocks. A high level of variability, along with lateral variability in crustal thickness estimates, may indicate strong lateral velocity heterogeneity or considerable Moho topography. .

2.3.2.2. H-κ Stack Analysis

Basic data preparation steps such as data selection, windowing, filtering and rotating are applied to three component data for preparation of H-κ stacking analysis. As a result of this, good quality waveforms are used to compute deconvolution to remove the effects of source and instrument response from waveforms that was expressed in the previous section in this chapter.

Deconvolution process creates receiver function including direct P, converted Ps and reverberated Moho multiples which have information concerning crustal structure, crust and upper mantle velocity discontinuity under the station. By using the time difference between the

phases in receiver function trace and given the average crustal velocities, receiver function amplitudes are stacked in H-K domain. After this straight forward stacking procedure Moho depth and Vp/Vs ratio can be identified under all available stations. This also provides an opportunity to map out lateral variation of Moho depth. Because of large velocity contrast at the crust–mantle boundary, the Moho P to S conversion is often the largest signal following the direct P. The time separation between Ps and P can be used to estimate crustal thickness.

Assuming that ray parameter is the same for the direct P and converted Ps, delay time of Ps converted wave is given by,

$$t_1 = t_{ps} - t_p = H(p_\alpha - p_\beta) \tag{2.12}$$

where α and β are velocities of P wave and S wave, respectively.

Since t_{ps} represents the differential travel time of S with respect to P wave in the crust, the dependence of H on Vp is not as strong as Vs. Most important problem of this method is that the crustal thickness calculated from delay times of Ps converted phase trades off with Vp/Vs ratio. The best way to reduce this incoherency situation is to take into account later multiple converted phase. Therefore, delay time of reverberated PpPs that has two P legs and one S leg can be calculated as a similar way to Ps and can be given by,

$$t_2 = t_{PpPs} - t_p = H(p_\alpha + p_\beta) \tag{2.13}$$

Other reverberated phase PpSs that has two P and S legs can also be expressed by,

$$t_3 = t_{PpSs} - t_p = 2Hp_\beta \tag{2.14}$$

In a similar definition, crustal thickness can be expressed in terms of delay times of direct converted and reverberated phases. These forms are given by,

$$H = \frac{t_{ps}}{\sqrt{1/V_s^2 - p^2} - \sqrt{1/V_p^2 - p^2}}$$

$$H = \frac{t_{PpPs}}{\sqrt{1/V_s^2 - p^2} + \sqrt{1/V_p^2 - p^2}} \qquad (2.15)$$

$$H = \frac{t_{PpSs+PsPs}}{2\sqrt{1/V_s^2 - p^2}}$$

where H is thickness and p is the ray parameter (slowness) of the incident wave.

In real situations observing the Moho Ps and the multiples and measuring their arrival times on a individual receiver function trace can be very difficult because of the background noise, scatterings from crustal heterogeneities, and P to S conversions from other velocity discontinuities. Therefore, stacking methodologies are commonly developed for receiver function in order to increase the signal to noise (S/N) ratio.

Generally, stacking procedure is performed in the time domain for a cluster of events (e.g., Owens *et al.*, 1984). However, a straightforward H-κ domain stacking is applied for the purpose of estimating crustal thickness in the content of the H-κ stacking technique and is described as,

$$s(H\text{-}\kappa) = \sum_i w_1 rf_i(t_1) + w_2 rf_i(t_2) - w_3 rf_i(t_3) \qquad (2.16)$$

where $rf_j(t)$ is the radial receiver function, t_1 ,t_2 and t_3 are the predicted Ps, PpPs and PsSs+ PsPs arrival times corresponding to crustal thickness (H) and Vp/Vs ratio (κ) The w_i's are weighting factors that are chosen to balance the contributions from three phases. The highest weighting factor is for direct conversion that has highest S/N ratio and because the later two converted phases have similar slopes (Figure 2.3), it can be set as w_1>w2+w3. As a result,

$$\sum w_i = 1.$$

In the stacking transformation, because of the depth velocity trade-off, the stacking analysis requires at least two phases to be identified in the waveform (Ammon et al.1990). The resulting

constraints are weak when the multiples are not clear. By stacking all three phases coherently with the correct H and κ, the s(H,κ) reaches a maximum. While inconsistent signals used to be eliminated in the case of the number of records is large enough, consistent phases are coherently stacked. In fact, seismic phases such as Ps, PpPs and PpSs + PsPs will add constructively only when the assumed depth of the reflector and the Vp/Vs ratio coincide with the actual values underneath the station (Julia, J. and J. Mejia, 2004). The location of the maximum in the stacking surface provides the estimates for H and Vp/Vs under the assumption, medium is laterally homogeneous and isotropic by assuming an acceptable value of the P wave velocity prior to stacking.

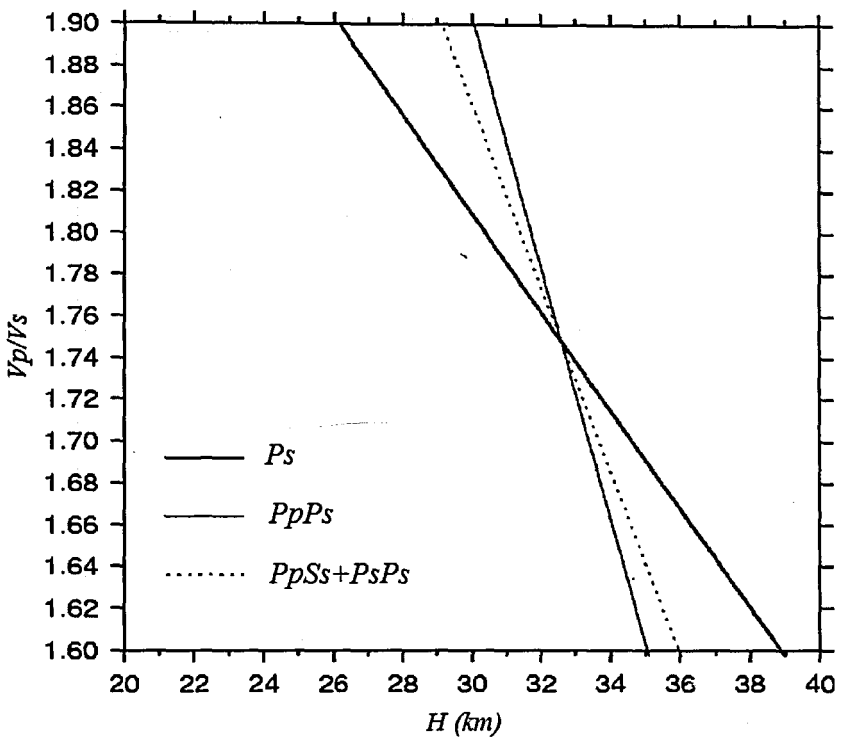

Figure 2.3 H-κ relations for Moho converted Ps and multiples PpPs, PpSs+PsPs.

2.3.2.3. Correlation and Uncertainties of H-κ Stacking Technique

H-κ stacking procedure requires confidence limits for obtained crustal thickness and Vp/Vs ratios by using stacking surface, s(H, κ). Using the Taylor expansion of s(H, κ) at the obtained maximum flatness and omitting the higher-order terms, the variances of H and κ can be expressed as,

$$\sigma^2 H = \frac{2\sigma_s}{\partial^2 s/\partial H^2}$$

$$\sigma^2 \kappa = \frac{2\sigma_s}{\partial^2 s/\partial \kappa^2} \tag{2.17}$$

where σ_s is the estimated variance of s(H, κ) from stacking (equation 2.16).

According to equations (2.17) there is no correlation between the crustal thickness and Vp/Vs ratio. However, a strong negative correlation should be expected because of the depth-velocity trade off. As explained in the previous section, Vp is defined before the stacking and kept constant during the analysis. Therefore, travel times can be preserved by increasing Vs and decreasing Vp/Vs ratio upon increasing H and vice versa. Taking into account a bivariate Gaussian distribution, the stacking surface that is explained in equation 2.16 can be better approximated. The variances σ^2_H and $\sigma^2\kappa$ and the covariance $\sigma_{H\kappa}$ can be defined as,

$$\sigma^2 H = \frac{2\sigma_s}{\partial^2 s/\partial \kappa^2} \Big/ \left[\frac{\partial^2 s}{\partial H^2}\frac{\partial^2 s}{\partial \kappa^2} - \frac{\partial^2 s}{\partial \kappa \partial H}\frac{\partial^2 s}{\partial \kappa \partial H}\right]$$

$$\sigma^2 \kappa = \frac{2\sigma_s}{\partial^2 s/\partial H^2} \Big/ \left[\frac{\partial^2 s}{\partial H^2}\frac{\partial^2 s}{\partial \kappa^2} - \frac{\partial^2 s}{\partial \kappa \partial H}\frac{\partial^2 s}{\partial \kappa \partial H}\right] \tag{2.18}$$

$$\sigma_{H\kappa} = \frac{2\sigma_s}{\partial^2 s/\partial H \partial \kappa} \Big/ \left[\frac{\partial^2 s}{\partial H^2}\frac{\partial^2 s}{\partial \kappa^2} - \frac{\partial^2 s}{\partial \kappa \partial H}\frac{\partial^2 s}{\partial \kappa \partial H}\right]$$

Even the more accurate expression (equation 2.18) implicitly assumes that the stacking surface (equation 2.16) is proportional to the true probability density for Vp/Vs and H (Julia, J. and J. Mejia, 2004). Since stacking surface is a weighted average for Vp/Vs and *H*, employing a bootstrap approach in order to estimate the uncertainities is more appropriate (e.g. Chevrot and Van der Hilst, 2000). Bootstrap approach was originally introduced by Efron and Tibshirani (1991) as an extending the root mean square error of the mean of a data set x =(x_1, x_2, x_3,….,x_n), and this expresssion is given by,

$$\sigma_x = \left[\sum_{i=1}^{n}(x_i - x)^2 / n(n-1)\right]^{1/2} \tag{2.19}$$

Bootstrap technique includes the creation of data sets of receiver functions at each station by randomly sampling with replacement from original sets. The sampled set has the same size as the original datasets. A stack is calculated from this new data sets and global maximum is noted. The resampling procedure is repeated for some number of tries. Therefore a set of thickness and Vp/Vs values on which a standard deviation can be calculated.

2.3.2.4. Advantage and Limitations of H-κ Stacking Technique

Processing a large number of teleseismic waveforms makes this technique advantageous. Since PS conversion point is very close to the station, estimation of crustal thickness or Vp/Vs ratio do not contain effect of lateral velocity variations. Moreover, there is no need to pick arrival times of the direct conversion from the Moho and its multiples; As a result, average crustal model is obtained and uncertainties can be estimated from the flatness of s(H,κ) at the maximum by stacking receiver functions from different distances and directions.

In addition to these advantages, the method has some limitations and tricky situations that result in different interpretations. The basic assumption for stacking procedure is that the Moho is a planar, horizontal interface. However, dipping Moho affects Vp/Vs ratio that indicates lateral heterogenities. Dipping of this interface will travel larger distances through the crust and will have longer relative travel times, with respect to those generated at a horizontal interface (Ligorria, 2000) whereas multiples travelling downdip will travel shorter distances. This effect might be significant in regions where the rapid crustal thickness variations.

The presence of a gradational crust-mantle transition instead of a well-defined Moho discontinuity is another situation which can cause failure of stacking process. A gradatinal crust-mantle boundary makes the energy from the boundary interaction phases spread in time, so that the corresponding pulses decrease in amplitude and increase in width (Cassidy, 1992; Ligorria, 2000). Another situation is that interfering Moho converted phase Ps and multiples from an intracrustal discontinuity. As common situation in sedimentary environments, multiples from sediment-bedrock interface overlap in time with the Ps converted phase at Moho (Cassidy, 1992; Zelt and Ellis, 1999). As a result of interference of phases, possible time shifting at the Ps converted phase may cause unrealistic results of Vp/Vs ratio.

CHAPTER.III. DATA ANALYSIS AND RESULTS

3.1. Seismic Stations

In the content of the Calibration project which purposes the calibration of seismic stations in Turkey and surrounding areas and determination of crustal structure by collaborating with Boğaziçi University, MIT (Massachusetts Institute of Technology) and LLNL (Lawrance Livermore National Laboratory), permanent short period and broadband KOERI stations, Ankara and Keskin array stations were used. Additionally, 13 portable short period and 10 broadband stations were installed across central Anatolia. Figure 3.1 shows stations used in the project.

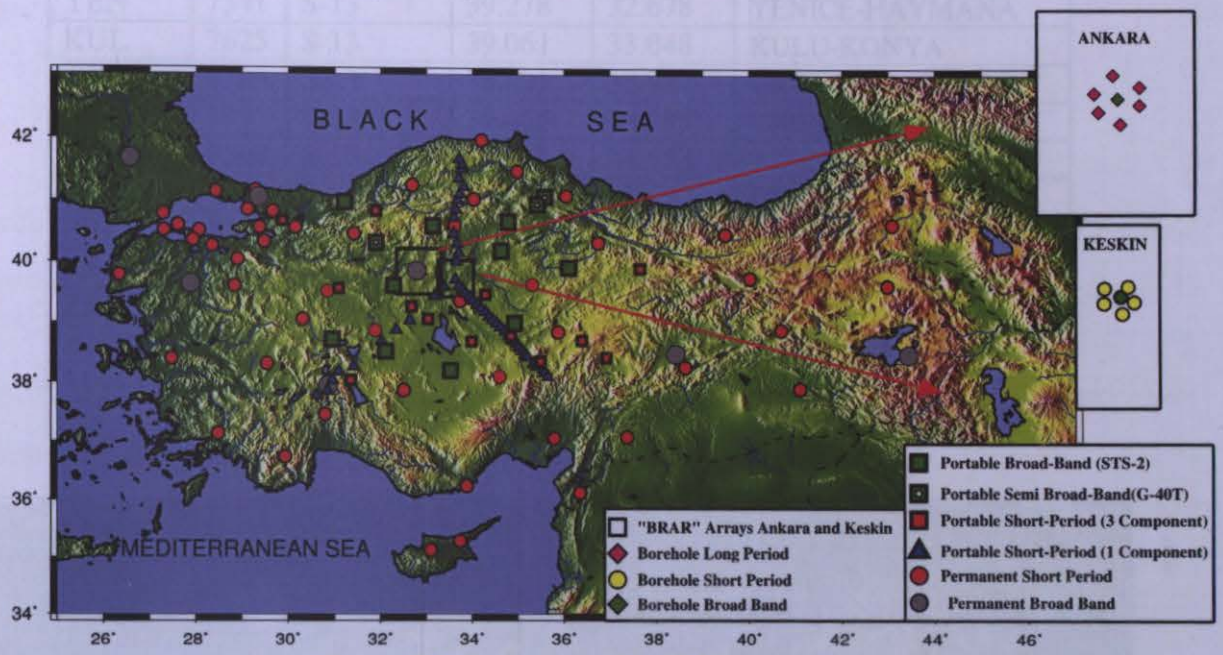

Figure 3.1 Stations used in Calibration Project

In this study, we processed data obtained from temporary seismic stations which have been operated between October, 22 and end of the November, 2002. The available seismic stations consist of 7 broadband three-component and 13 short period three-component equipments (Figure 3.2). Three of the broadband stations did not work during the recording period. Broadband and short period seismic stations were equipped with Streckeisen STS-2 covering a period from 20s to 0.01 Hz and S-13 covering a period 0.75s to 1.1 Hz, respectively. An example of STS-2 seismometer and its installation in the field is shown in Figure 3.3. In addition to these temporary seismic stations, ANTO, MALT and ISP permanent stations were also used to increase number of recording stations in study area. The characteristic properties of stations are shown in the Table 3.1.

Table 3.1 List of the stations used in the study

CODE	ID	SENSOR	LAT.	LON.	LOCATION
KAD	7435	STS-2	38.520	32.114	KADINHANI
POL	7428	STS-2	39.610	32.293	POLATLI
KAR	7300	STS-2	39.915	36.991	SIVAS
BOL	7286	STS-2	38.718	30.950	BOLVADIN
SUN	7350	STS-2	40.179	34.630	SUNGURLU-CORUM
AVO	7298	STS-2	38.995	34.931	NEVSEHIR
SUL	7447	STS-2	38.199	33.516	AKSARAY
GOL	7620	S-13	40.679	29.875	GOLCUK
MEN	7278	S-13	40.827	31.907	MENGEN-BOLU
BAL	7624	S-13	39.578	31.098	BALCIKHISAR
SAR	7326	S-13	38.046	31.354	ISPARTA
YEN	7341	S-13	39.278	32.678	YENICE-HAYMANA
KUL	7625	S-13	39.061	33.048	KULU-KONYA
AKS	7289	S-13	38.691	33.987	ORTAKOY-AKSARAY
KIR	7351	S-13	39.465	34.295	KIRSEHIR
NEV	7598	S-13	38.778	34.853	NEVSEHIR
DEV	7591	S-13	38.353	35.492	DEVELI
PIN	7288	S-13	38.719	36.399	PINARBASI
AFS	7342	S-13	38.419	36.923	AFSIN
ZAR	7456	S-13	39.902	37.650	SIVAS
ANTO	7435	STS-1	39.87	32.79	ANKARA
MALT	7428	STS-2	38.31	38.43	MALATYA
ISP	7300	STS-1	37.84	30.51	ISPARTA

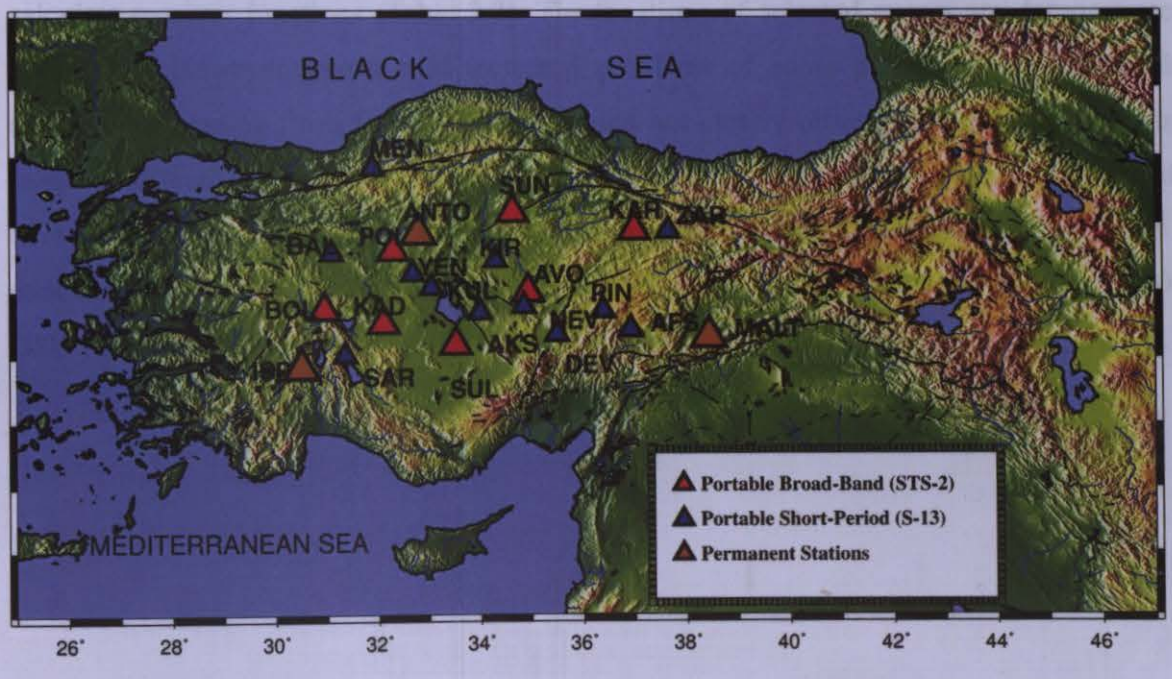

Figure 3.2 Stations used in this study

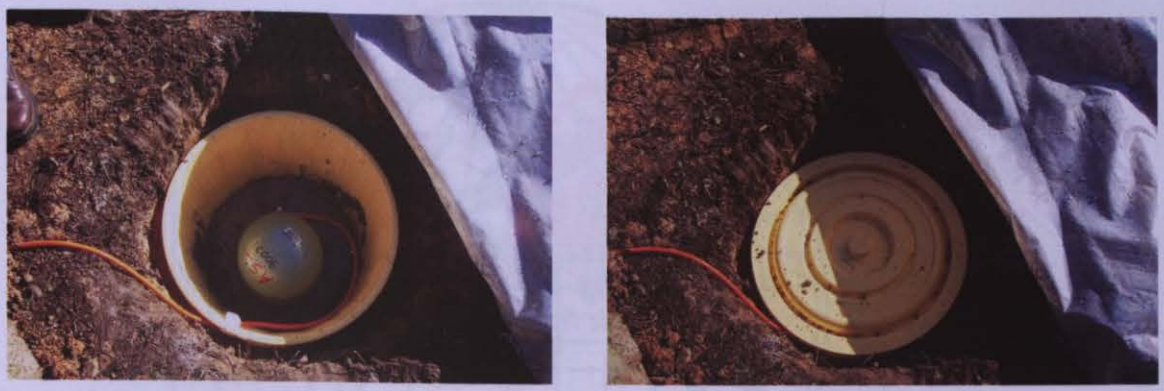

Figure 3.3 STS-2 seismometer is installed in a well and its upper part is covered by soil.

3.2. Data Selection

Approximately 160 teleseismic earthquakes worldwide with magnitudes greater than 5.0 and various focal depth range were occurred in the recording period. For a better receiver function analysis, earthquakes should be selected with epicentral distances ranging from 30 to 103 degrees, magnitudes greater than 5.0 and clear records with high signal to noise ratio. Earthquakes can be selected within shallow, intermediate or deep depth range for data analysis. Nearly 35 useful earthquakes were selected taking into account mentioned criteria above to calculate receiver functions (Table 3.2). The locations of selected events are demonstrated in Figure 3.4. However, because of technical problems of some portable seismic stations or earthquakes coming from far away distance and not clearly observed teleseismic records, all selected earthquakes couldn't be use to create receiver functions. Therefore, in the light of the criteria described above data recorded from the ANTO, MALT and ISP stations were also added to improve the dataset. Furthermore, teleseismic data were processed between 2000 and 2005 from these three component broadband stations.

Figure 3.4 Teleseismic earthquakes used in receiver function analysis

Table 3.2 Events which were used in receiver function analysis

Event Date yy:mm:dd	Origin Time (GMT)	Latitude	Longitude	Depth (km)	Magnitude
2002 10 24	033426.73	48.26	154.38	33	5.60
2002 10 24	215343.19	6.03	94.42	64	6.20
2002 10 25	024924.45	25.21	123.73	10	5.30
2002 10 28	023832.59	-33.90	-178.79	33	5.00
2002 10 30	144305.69	-17.61	-174.18	86	5.50
2002 10 31	103258.77	41.79	14.87	10	5.90
2002 11 01	150900.81	41.73	14.88	10	5.80
2002 11 01	220929.28	35.52	74.65	33	5.4
2002 11 02	012610.70	2.82	96.08	30	7.60
2002 11 02	094646.70	2.95	96.39	27	6.40
2002 11 00	033742.07	38.89	141.98	39	6.40
2002 11 03	221241.00	63.52	-147.44	4	8.50
2002 11 04	031918.38	-5.53	36.03	10	5.50
2002 11 04	043557.76	32.39	131.55	33	5.40
2002 11 05	084726.13	49.07	142.30	596	5.60
2002 11 07	151406.76	51.20	179.33	33	6.60
2002 11 09	052925.96	-2.62	68.00	10	5.70
2002 11 11	163902.32	-23.31	-179.90	539	5.70

2002 11 13	155309.14	3.01	96.09	39	5.60
2002 11 14	110520.54	-17.78	-178.78	553	5.60
2002 11 15	195831.78	-56.05	-36.40	10	6.60
2002 11 15	215604.62	-3.14	84.95	10	5.10
2002 11 16	120625.17	50.38	156.56	96	5.60
2002 11 16	204449.88	-26.40	178.20	633	5.50
2002 11 17	025837.47	-23.53	-175.61	10	5.50
2002 11 17	045348.46	47.95	146.42	470	5.80
2002 11 18	225156.49	-4.21	102.18	33	5.50
2002 11 20	213230.81	35.41	74.51	33	6.50
2002 11 21	165637.61	-9.54	117.28	59	5.10
2002 11 23	010500.63	-25.30	-177.30	99	5.2
2002 11 23	144841.66	-27.78	-177.09	33	5.10
2002 11 26	004815.04	51.47	-173.54	20	6.10
2002 11 26	152945.04	23.93	122.74	33	5.30
2002 11 26	224613.81	-21.09	-178.81	536	5.40
2002 11 27	013506.29	54.67	-160.74	33	5.60

3.3. Data Analysis

After selecting available data, basic preparation steps were applied to the data. These steps are shown in Figure 3.5 as a flow chart. Firstly, P arrival times of earthquakes were calculated according to IASPEI travel-time table and then all events were selected on each three component seismograms manually with a window approximately from 100 seconds before the P wave to 300 seconds after the P wave. If some waveforms contain gaps and they do not have all components, we rejected these types of records. Predicted P wave arrivals were marked using automatic picking program, Taup and data were cut with windowing from 20 seconds before P arrivals to 80 seconds after the predicted P arrival time. Large window length was selected to see late arrivals clearly. Then a taper and high pass filter of 0.02 was applied to data to enhance S/N ratio. To isolate the converted S phases from the P wave, each seismogram was rotated from the original N-S, E-W and Z component to longitudinal component L, SV component Q and SH component R by using backazimuth and incidence angle. After these preparation procedure, frequency domain deconvolution was applied the data to obtain receiver functions. Several possibilities are tried for water level and gauss filter width until reaching the best receiver function. As a result of testing water level from 0.1 to 0.5, we preferred water level value of 0.1 and gauss filter width of 2.0 which indicate a cutoff frequency of 0.9 Hz that gives us better deconvolution results. Because of the sensitivity of the first order features, we

consider the first 25 seconds in the receiver function waveforms. Some examples of original waveform data for broadband and short period seismic stations are shown in Figure 3.6 and 3.8, respectively. Rotated data and obtained receiver functions from these waveforms with selected available water level and gauss filter width are shown in Figure 3.7 and 3.9.

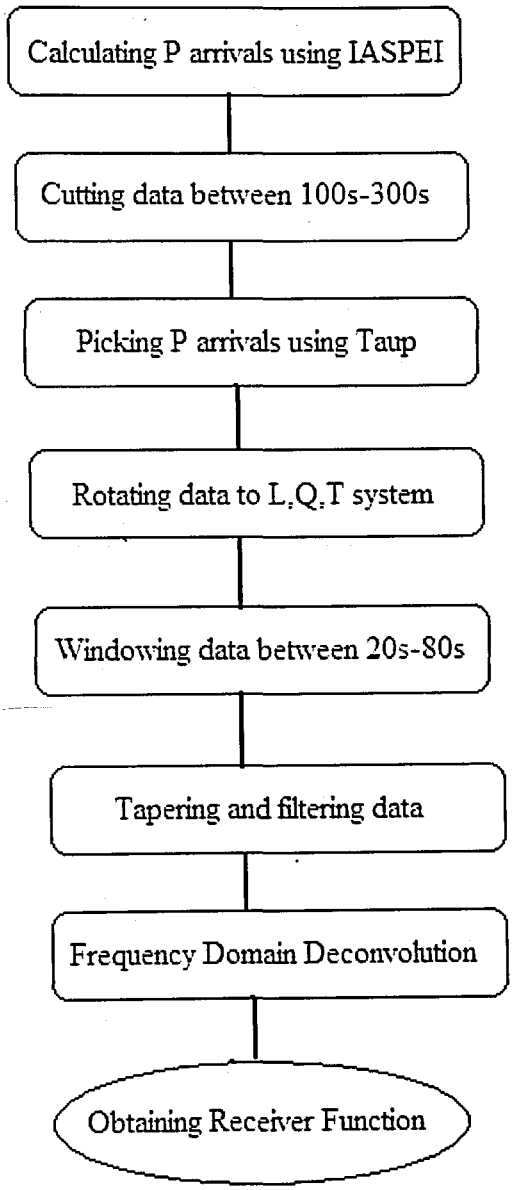

Figure.3.5 Basic steps in data analysis

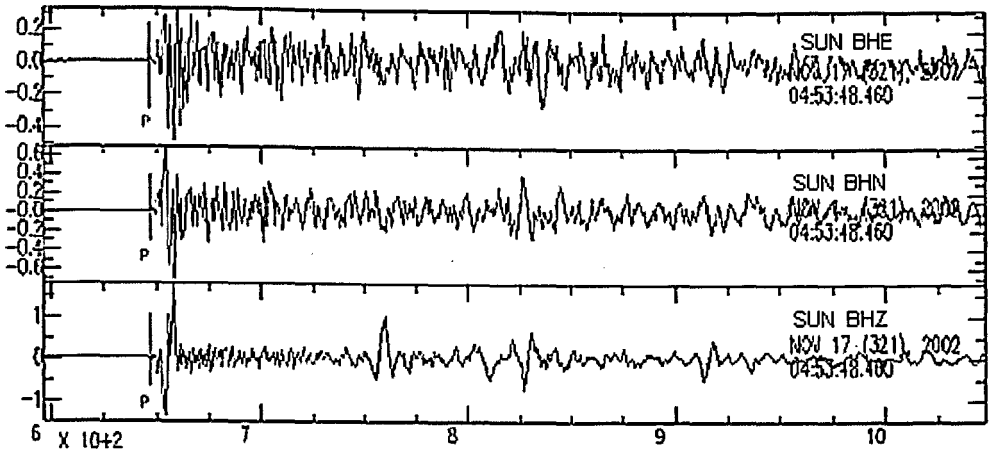

Figure 3.6 The original three component waveform recorded at SUN broadband seismic station.

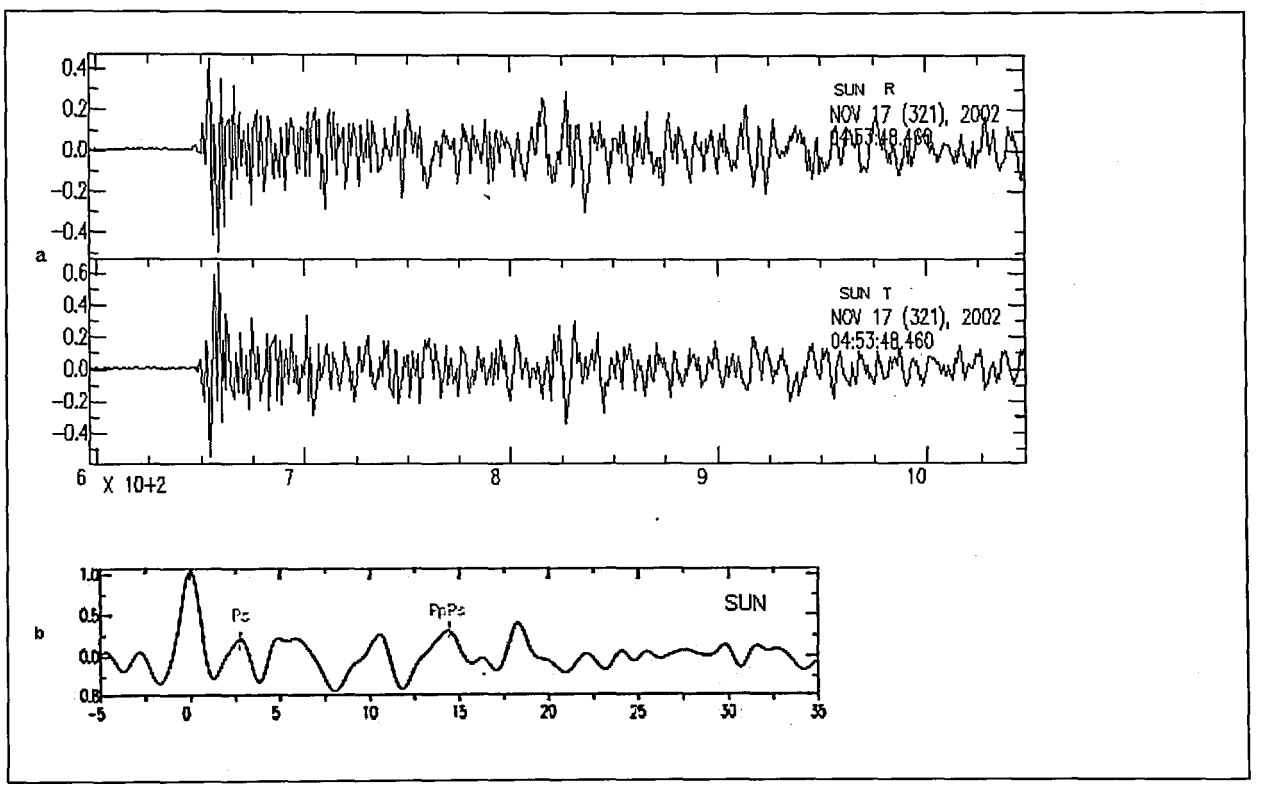

Figure 3.7.a The rotated (radial and transverse component) waveform recorded at SUN broadband station, **b.**Radial receiver function of the same event

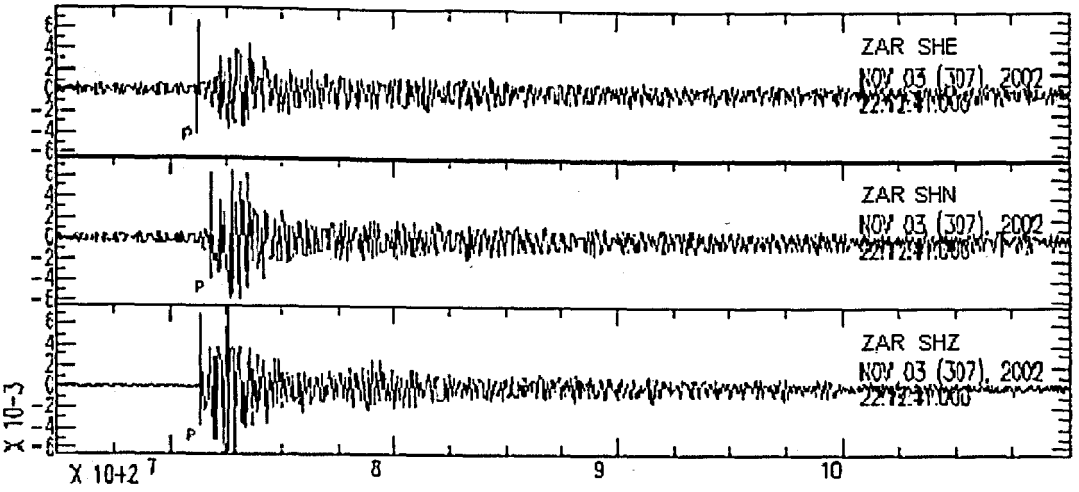

Figure 3.8 The original three component waveform recorded at ZAR short period seismic station.

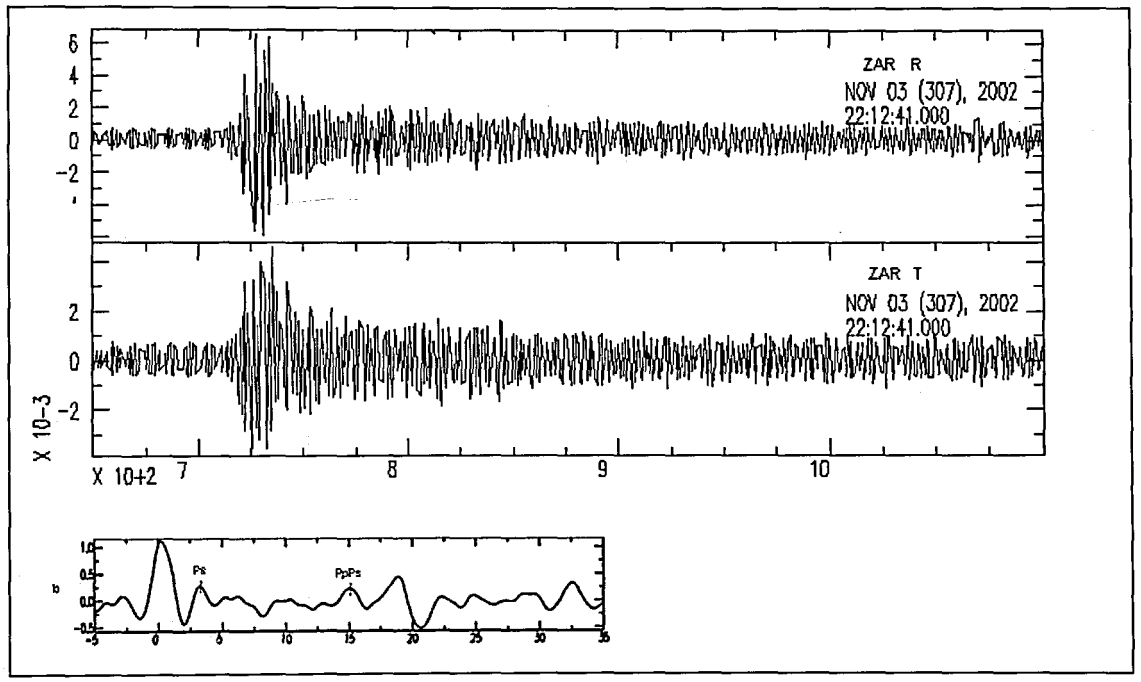

Figure 3.9.a The rotated (radial and transverse component) waveform recorded at ZAR short period station, **b.** Radial receiver function of the same event.

3.4. Results of H-κ stack Analysis

After the obtaining receiver function with deconvoution process, we eliminated some receiver functions which have not clearly observed Ps converted and multiple phases and selected RFs on low pre-signal noise and to perform receiver function analysis with more quality RFs. Events which are used to get receiver functions for each seismic stations and their radial receiver functions are plotted in Figure 3.10, 3.11 and 3.12 in a time window between -5 to 25 seconds which the Moho conversions and its multiples are clearly visible. Seismic stations in central Anatolia region have events that are coming from all directions with respect to back-azimuth. However, azimuthal coverage is dominantly between the backazimuth of 0 and 110 degree. When we consider the plotted receiver function traces for stations, we can identify easily several phases. The largest amplitude in the receiver function waveform infers the largest discontinuity under the station and the first phase after the direct P wave, is the conversion from the Moho. This first positive phase observed at all stations are between 4 and 5 seconds. The crustal multiples PpPs and PpSs which are generated between Moho and surface are clearly seen around 14-18 and 20-22 seconds, respectively. Sometimes we can see a phase that indicate sediments after the direct wave. In the case of the stations installed on crystalline basement, this phase can not be observed. In figures, although we can see Moho and multiples for some stations clearly, there are no coherent visible multiples in some stations. Additionally, another phase which is called lower crustal multiples (LCM) can be seen around 10 seconds in receiver function traces. This phase is observed between the Moho converted phase Ps and Moho multiples. Therefore, arrival of this phase is less than the arrival of Moho multiple and this phase must be generated in a discontinuity in the lower crust.

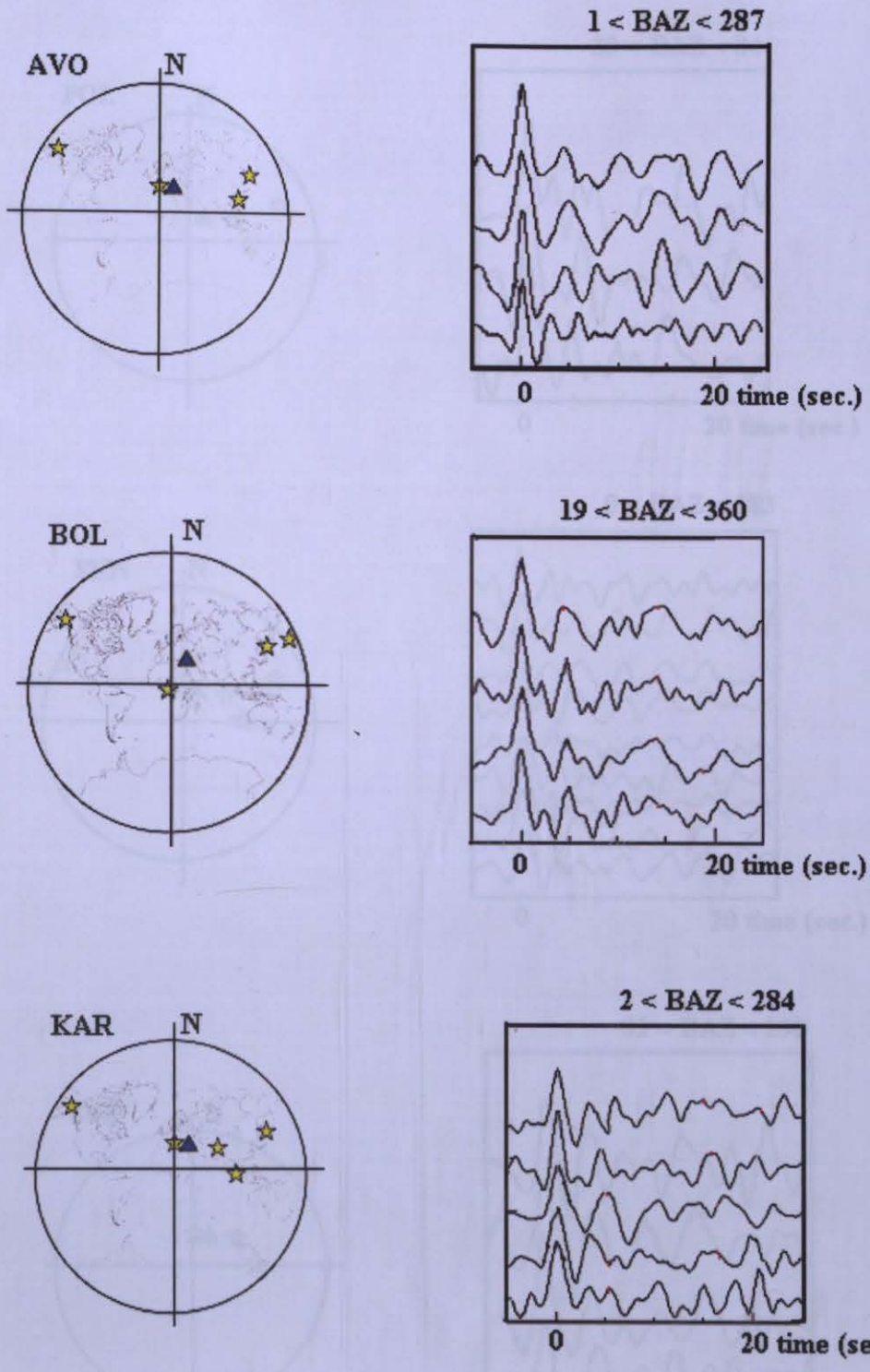

Figure 3.10 On the left column show the events which were used to get receiver function for statios. Radial receiver functions are shown on the right column for the AVO, BOL and KAR broad-band stations. Back-azimuth values (BAZ) are also shown on the graph. The horizontal axis in these figures represents the conversion time with respect to direct P arrival and it can be termed as delay time.

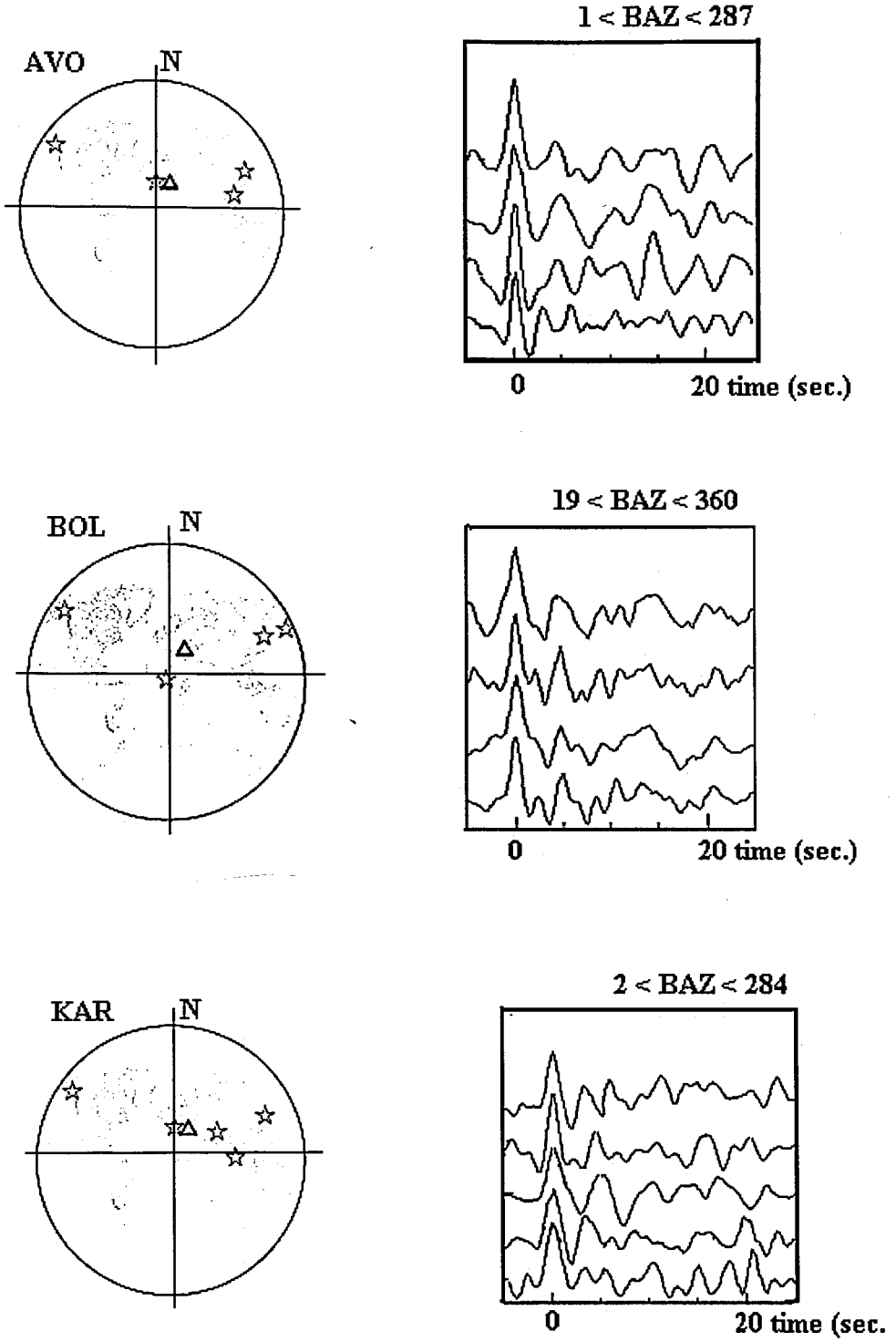

Figure 3.10 On the left column show the events which were used to get receiver function for statios. Radial receiver functions are shown on the right column for the AVO, BOL and KAR broad-band stations. Back-azimuth values (BAZ) are also shown on the graph. The horizontal axis in these figures represents the conversion time with respect to direct P arrival and it can be termed as delay time.

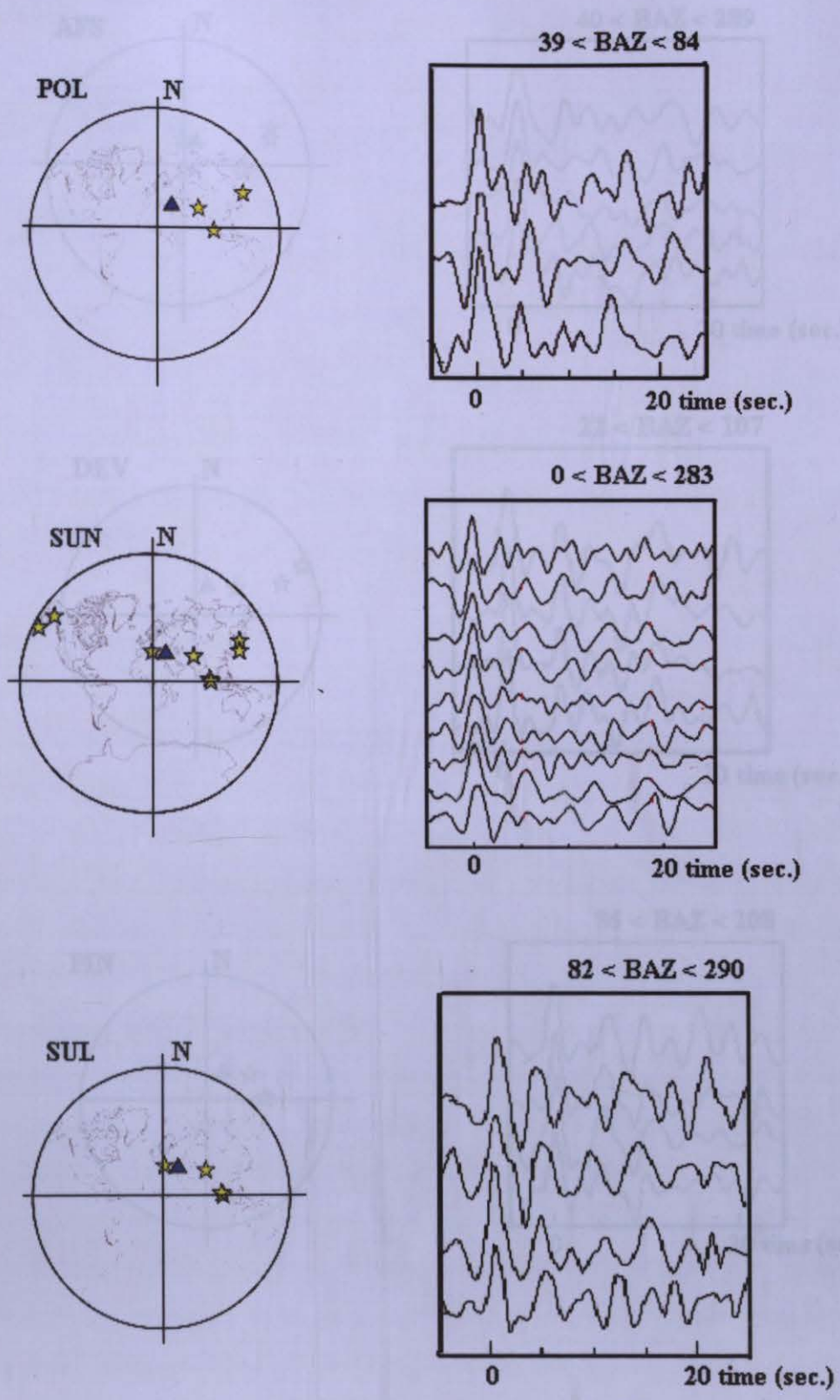

Figure 3.11 Same as the Figure 3.10, but it is shown for POL, SUN and SUL broadband stations.


AFS
N

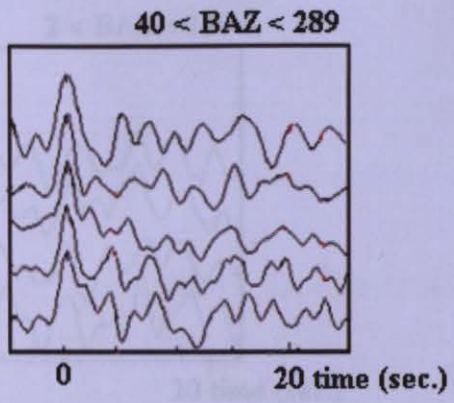
40 < BAZ < 289
0
20 time (sec.)


DEV
N

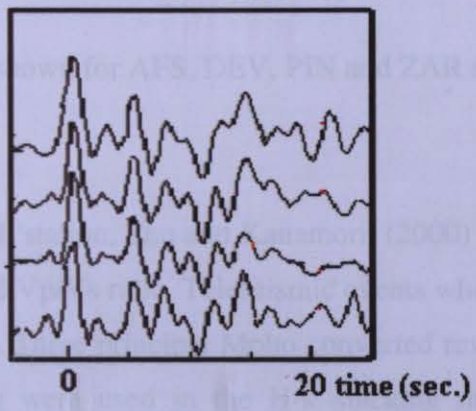
22 < BAZ < 107
0
20 time (sec.)


PIN
N

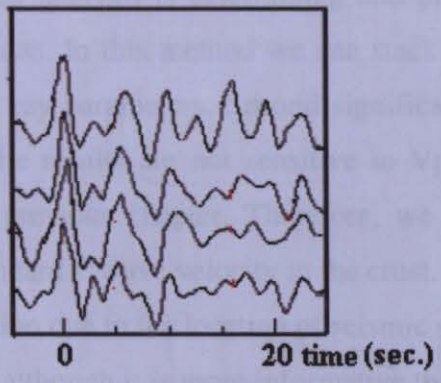
86 < BAZ < 108
0
20 time (sec.)

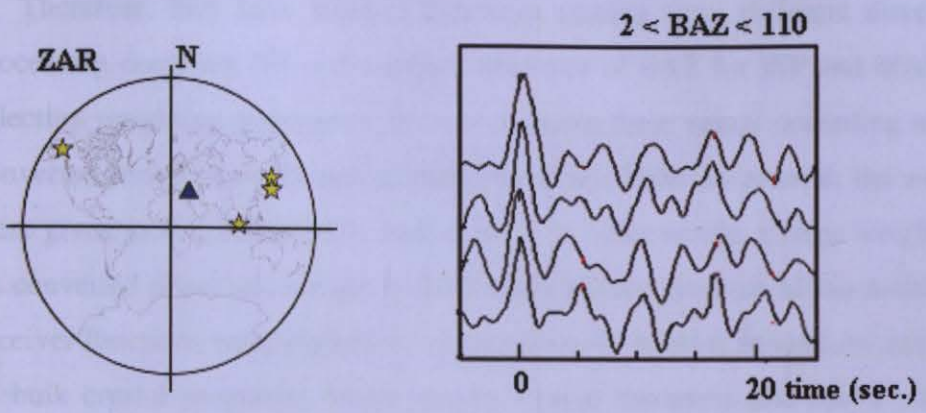

Figure 3.12 Same as the Figure 3.10, but it is shown for AFS, DEV, PIN and ZAR short period stations.

After identifying receiver functions for each station, Zhu and Kanamori, (2000) method has been applied to determine crustal thickness and Vp/Vs ratio. Teleseismic events which are used in H-κ stacking, were listed in APPENDIX A. Three principal Moho converted reverberations which are visible at most stations recording were used in the H-κ stacking method. H-κ stacking technique is based on the transformation of the amplitude of receiver functions, in time domain, into the crustal thickness (H) and Vp/Vs ratio (κ) as explained in detail in Chapter II. The most significant step in H- κ stack analysis is determining and placing ray parameter in header information of receiver functions. In this method we can stack events at different distances, with correspondingly different ray parameters. Second significant step is determining P wave as a fixed value. Although the results are not sensitive to Vp, method requires assumed Vp value as we mentioned in previous chapter. Therefore, we generally chose 6.3 km/s for Vp value in the analysis as a standard P wave velocity in the crust.

Obtained receiver response can vary with direction due to the location of seismic stations in different tectonic regions. From this point of view, although it is more informative that analyse receiver function separately in terms of their BAZ range, we apply the technique to all traces coming from different directions and distances to get average crustal estimates for each temporary station due to not having any dominant BAZ range and much RF traces as Zhu and Kanamori (2000) suggested. However, ISP and MALT have a lot of receiver functions because we processed data between the 2000 and 2005 time period for these permanent stations.

Therefore, they have receiver functions coming from different directions and we prefer processing dominant NE and southern direction of BAZ for ISP and MALT. Another step is selecting weighting parameters. We have chosen these values according to the visibility of the converted Moho phase Ps and its multiples PpPs, PpSs. In general, the weights w_1, w_2 and w_3 were given as 0.7, 0.2 and 0.1, respectively. In other words, a large weight of 70% is given to Ps converted phase and weight of 20% and 10% are given to Moho multiples. As a result, all receiver functions were stacked by using above mentioned parameters and the best estimations of bulk crustal properties which are the crustal thickness and *Vp/Vs* ratio can be found by stacking three phases coherently. Moreover, trade off between crustal thickness and Vp/Vs ratio can be reduced by incorporating the later converted phases. By determining Vp/Vs value, we can get information about the medium and rock composition that is affected by several factors such as temperature, partial melting, crustal fluids and anisotropy.

The global average of Poisson's ratio that depends on different kind of continental crust, correspond to Vp/Vs ratio of 1.78. When the phases cannot be observed clearly and not stacked consistently, this average Vp/Vs ratio is fixed in the process.

After the all steps mentioned above, H-κ stack analysis was applied to all stations and crustal thickness and Vp/Vs ratio were found as an output of the method. H-κ stack analysis for each station is represented in Figure 3.13 to 3.27. Stacking surface is shown on top, this surface with 1σ-confidence ellipse is shown at the bottom. Corresponding radial receiver functions and their determined phases are shown on right hand side of each figure. Furthermore, obtained crustal thickness, Vp/Vs ratio and result of bootstrap replications are written on the top of each image.

AFS

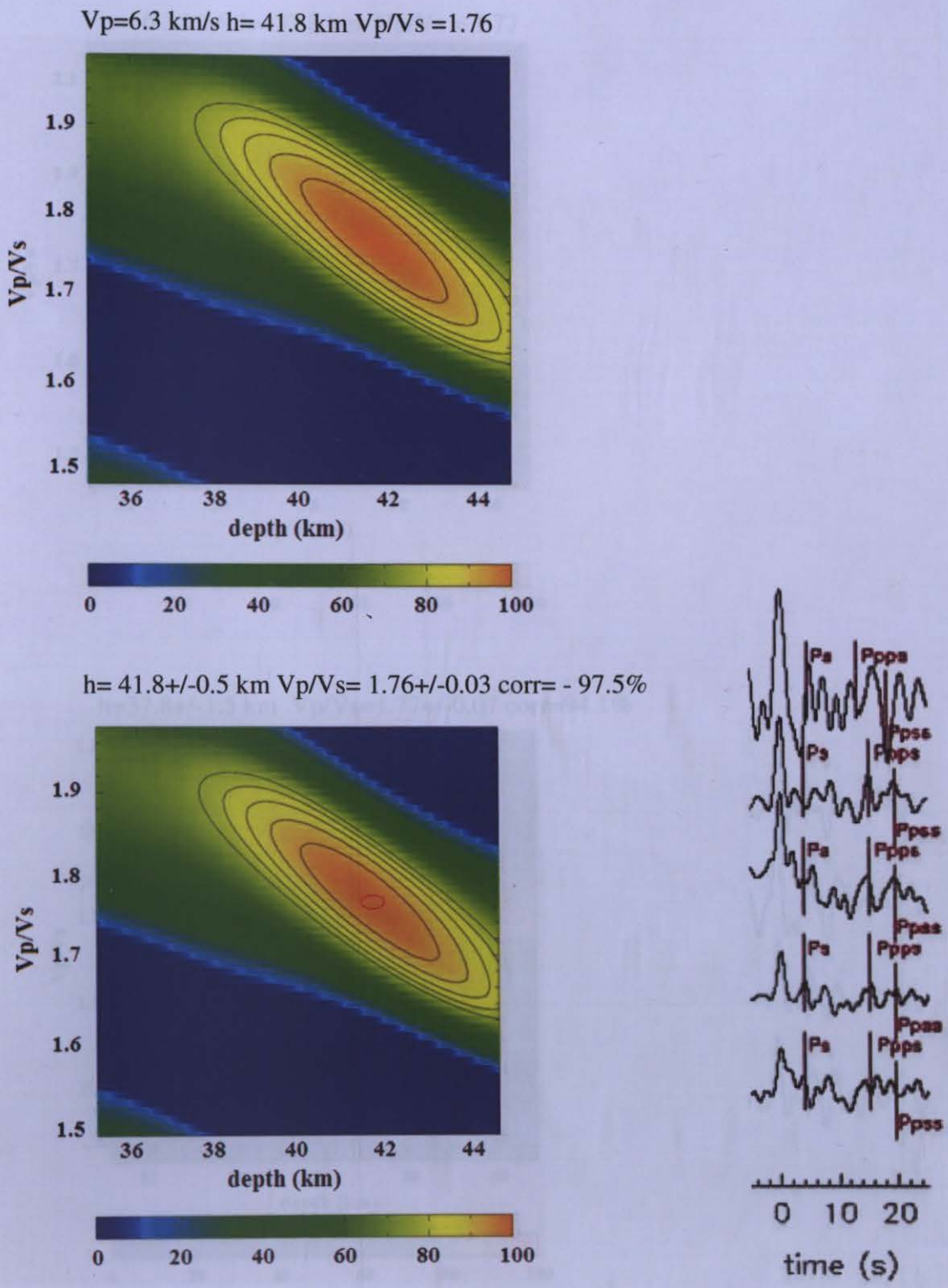

Figure 3.13 Result of the H-κ stacking method for AFS broadband station. The best estimation of thickness is 41.8km with a Vp/Vs ratio of 1.76.

DEV

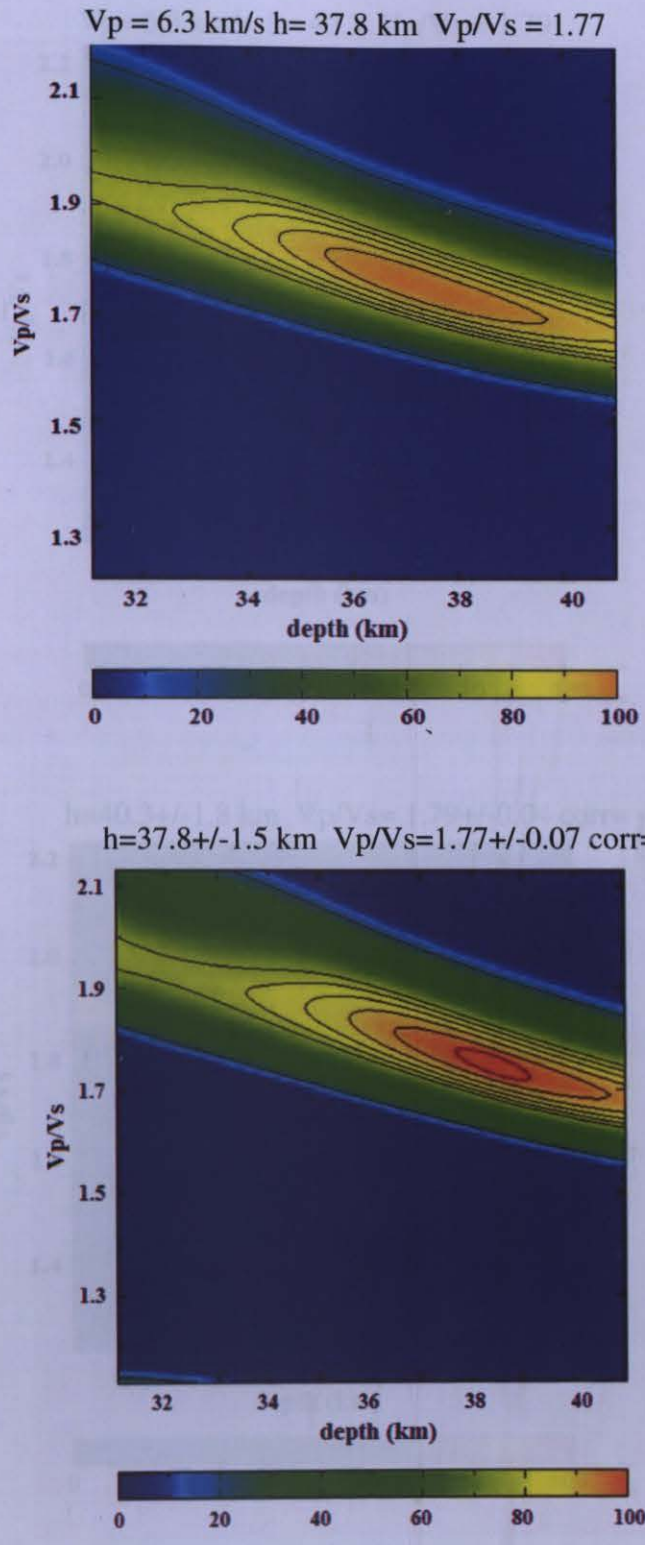

Figure 3.14 Result of the H-κ stacking method for DEV broadband station. The best estimation of thickness is 37.8km with a Vp/Vs ratio of 1.77.

PIN

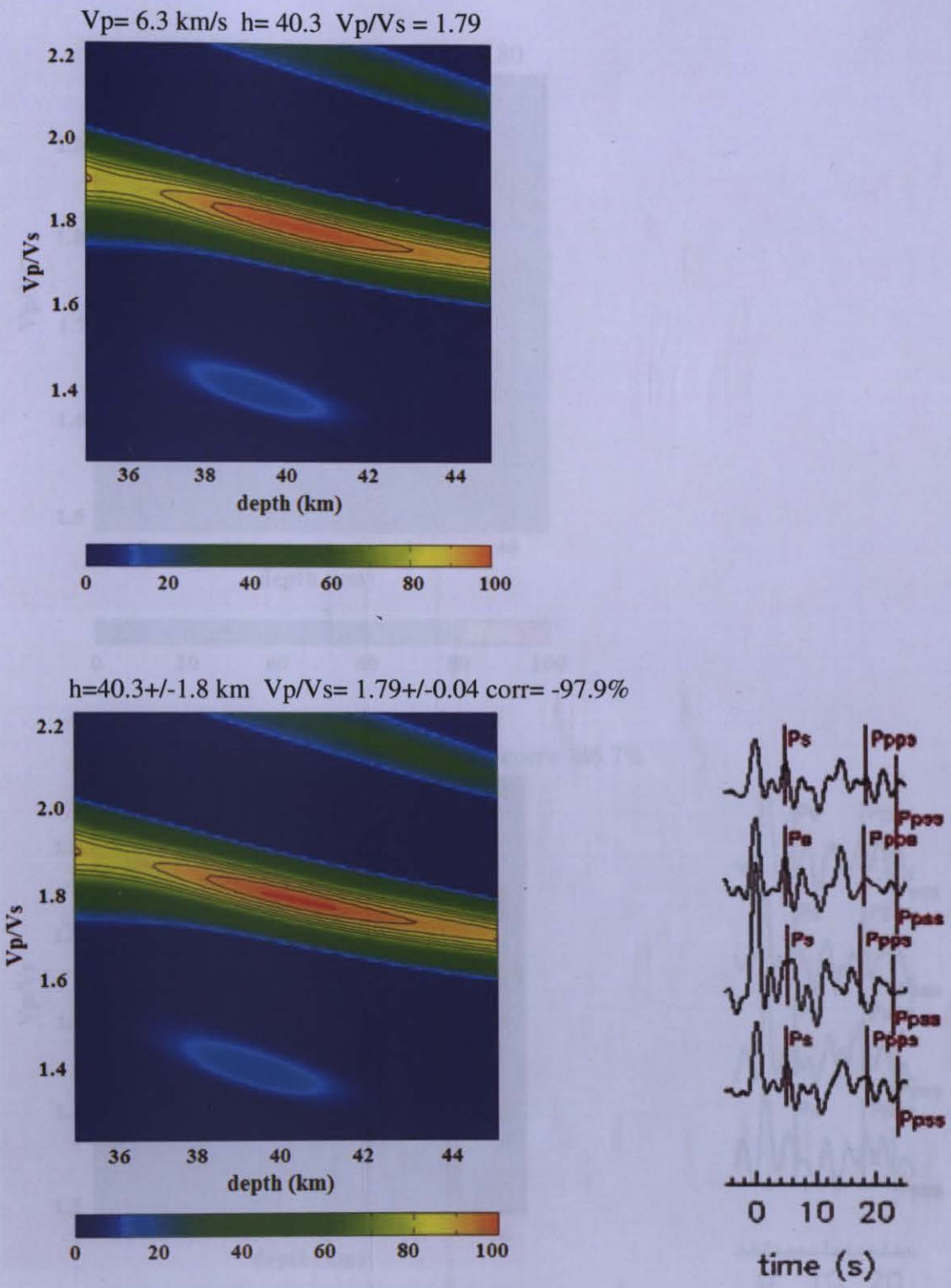

Figure 3.15 Result of the H-κ stacking method for PIN broadband station. The best estimation of thickness is 40.3km with a Vp/Vs ratio of 1.79.

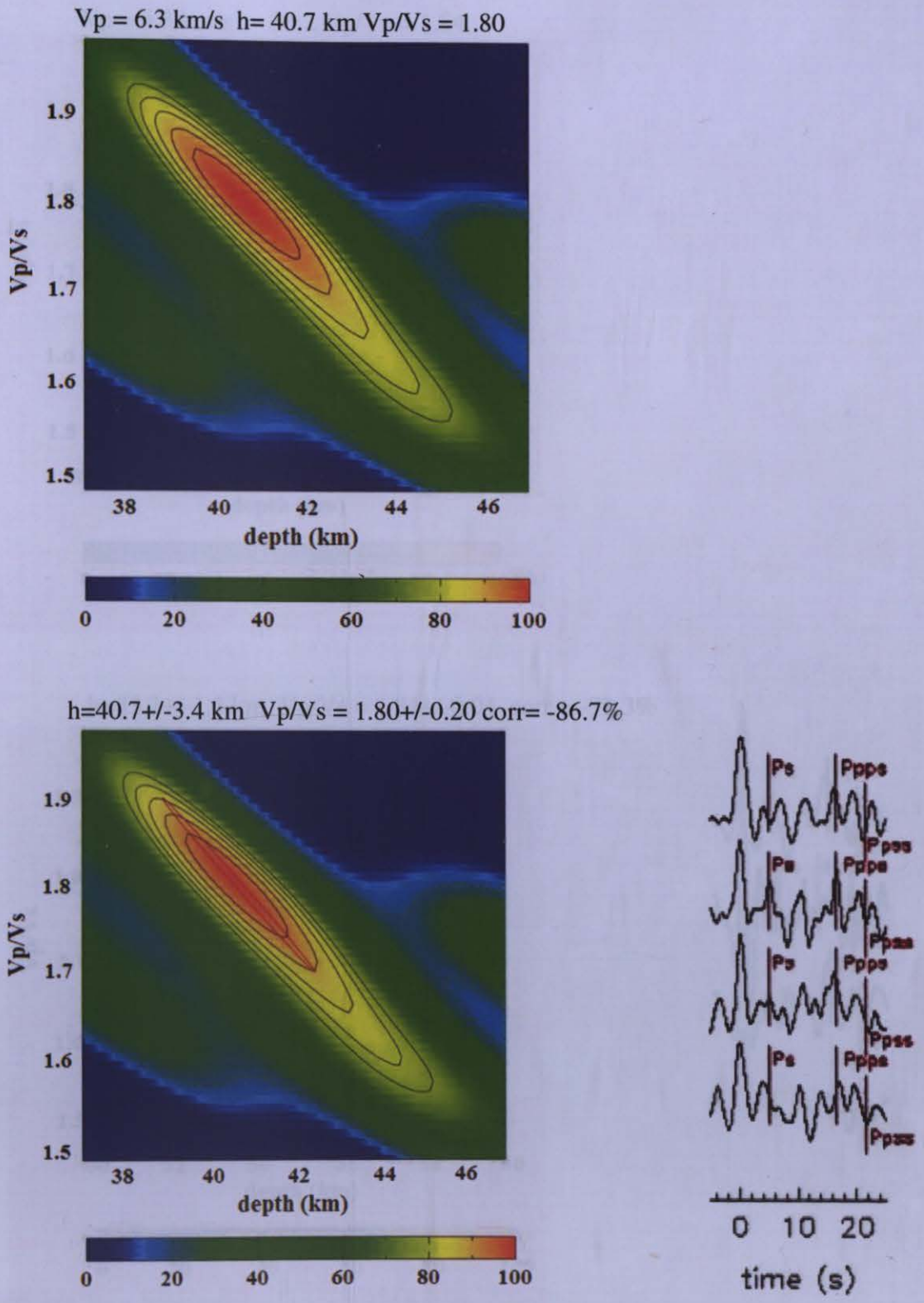

Figure 3.16 Result of the H-κ stacking method for ZAR broadband station. The best estimation of thickness is 40.7km with a Vp/Vs ratio of 1.80.

AVO

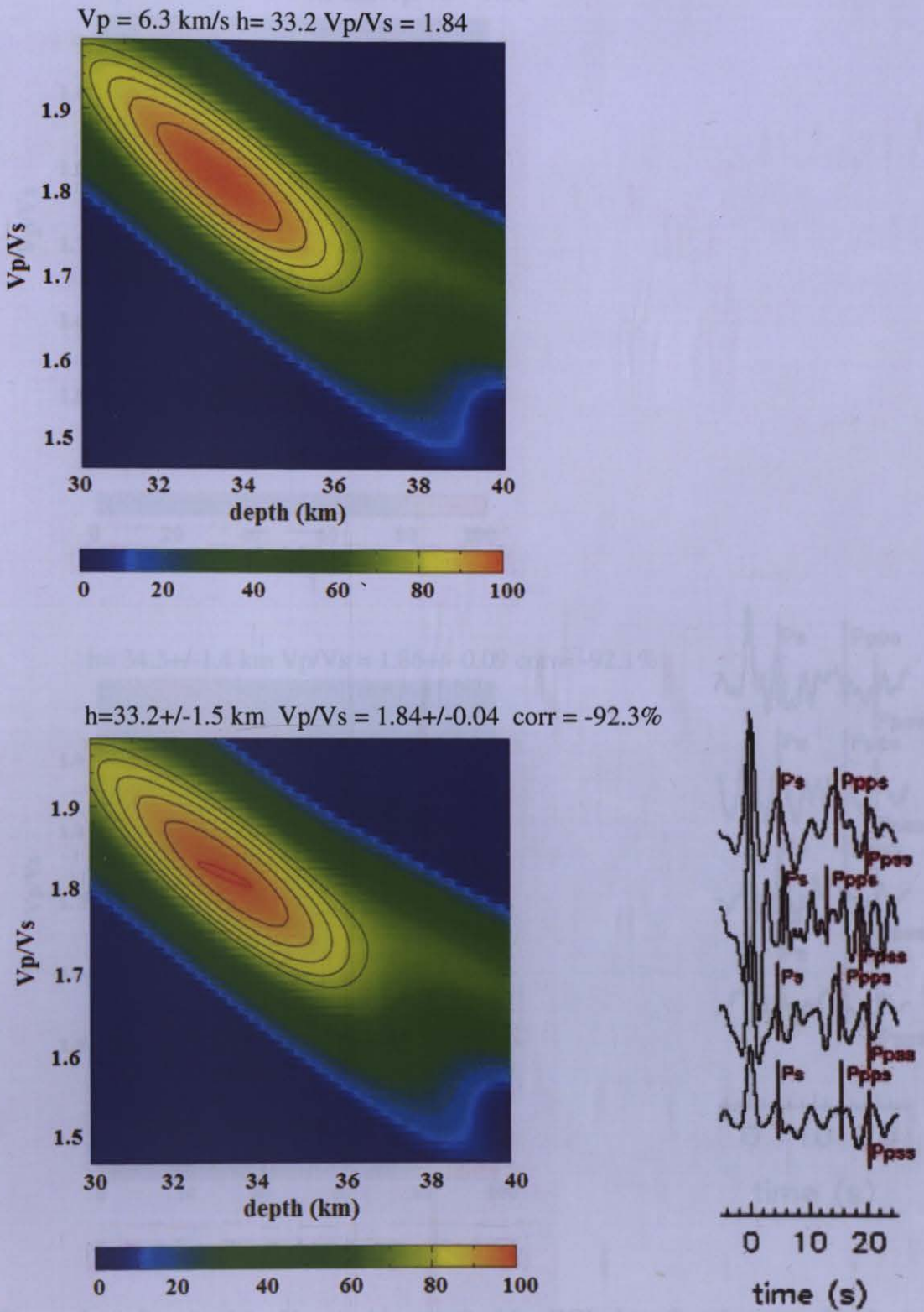

Figure 3.17 Result of the H-κ stacking method for AVO broadband station. The best estimation of thickness is 33.2km with a Vp/Vs ratio of 1.84.

BOL

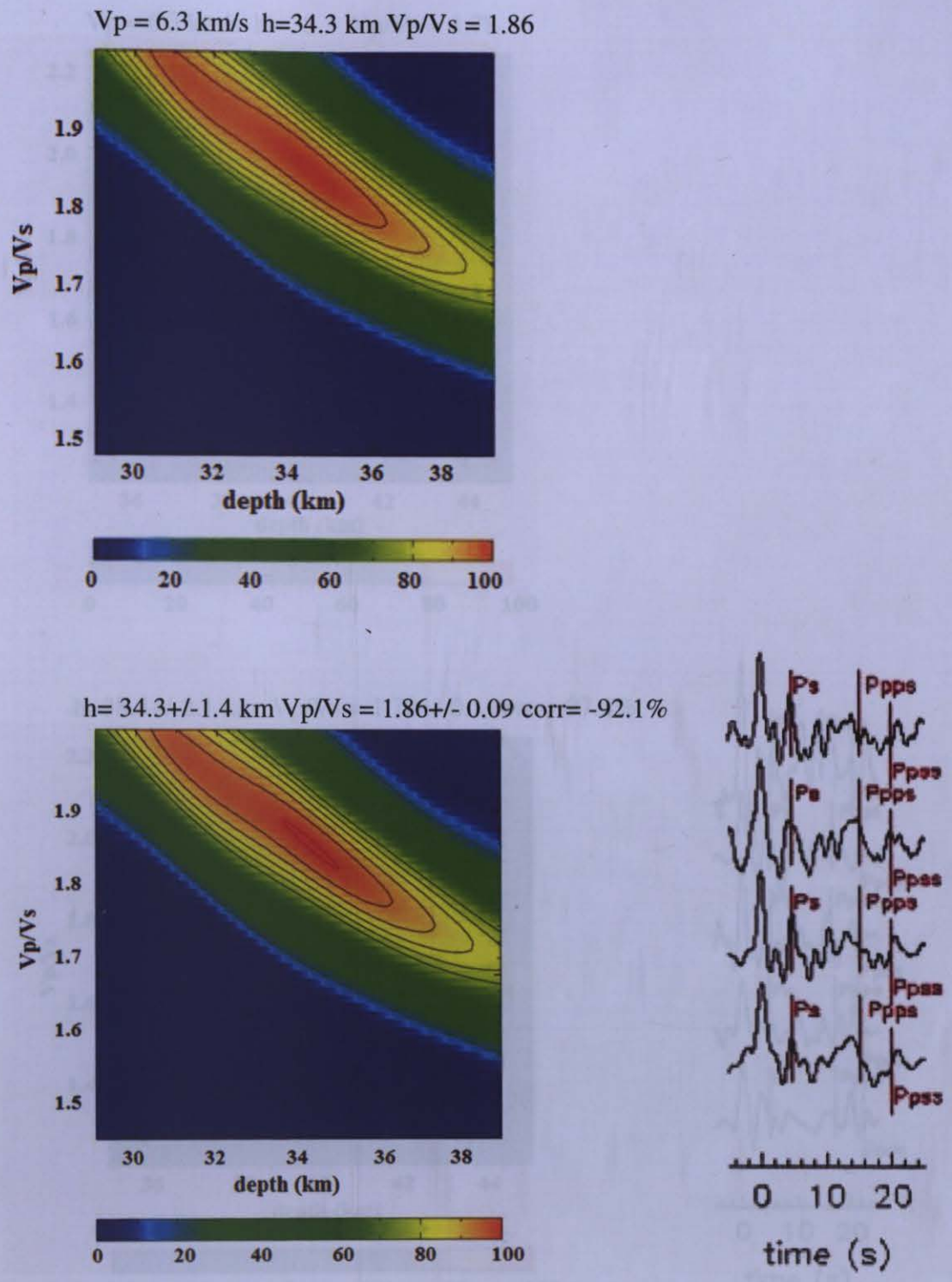

Figure 3.18 Result of the H-κ stacking method for BOL broadband station. The best estimation of thickness is 34.3km with a Vp/Vs ratio of 1.86.

KAR

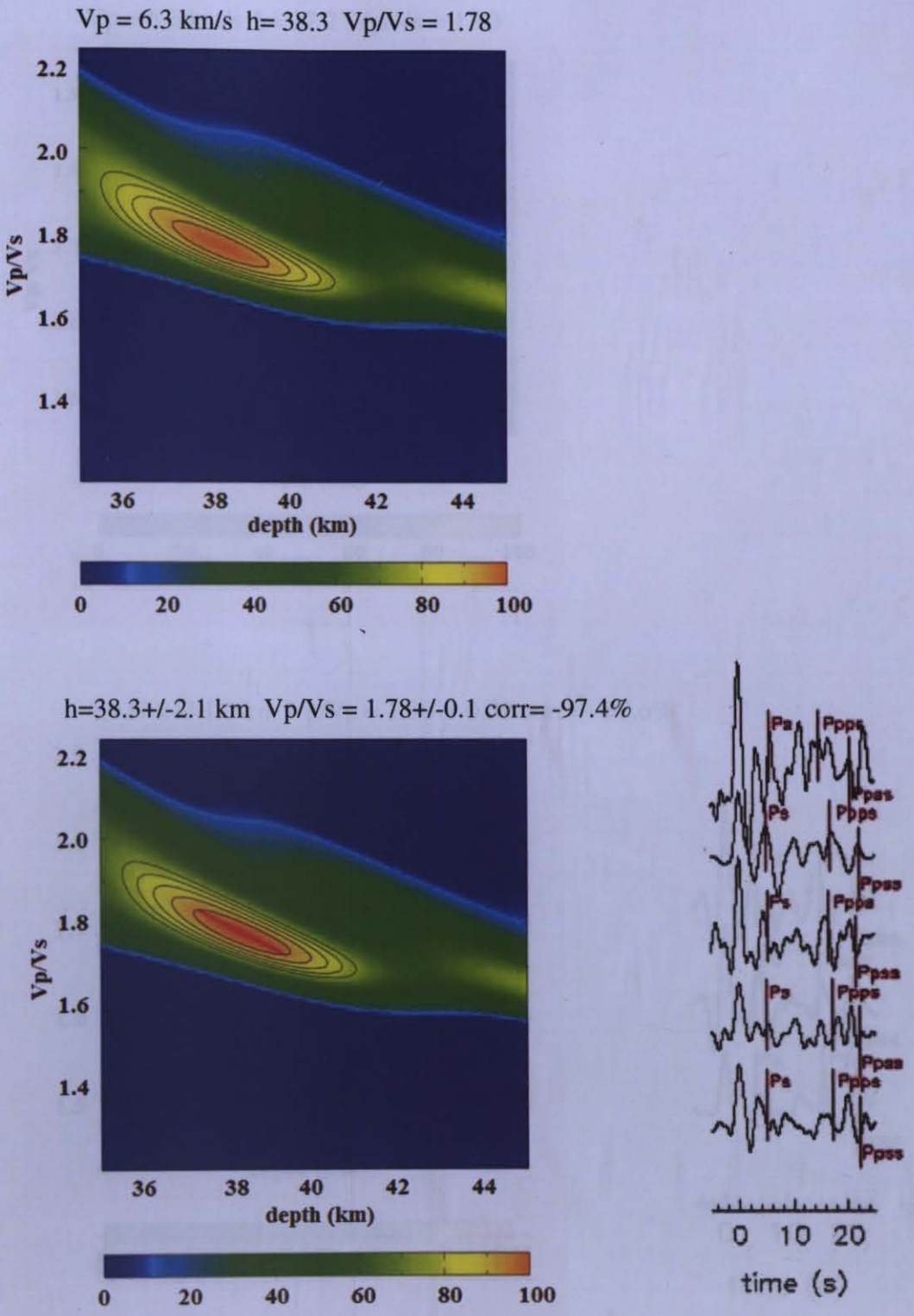

Figure 3.19 Result of the H-κ stacking method for KAR broadband station. The best estimation of thickness is 38.3 km with a Vp/Vs ratio of 1.78.

POL

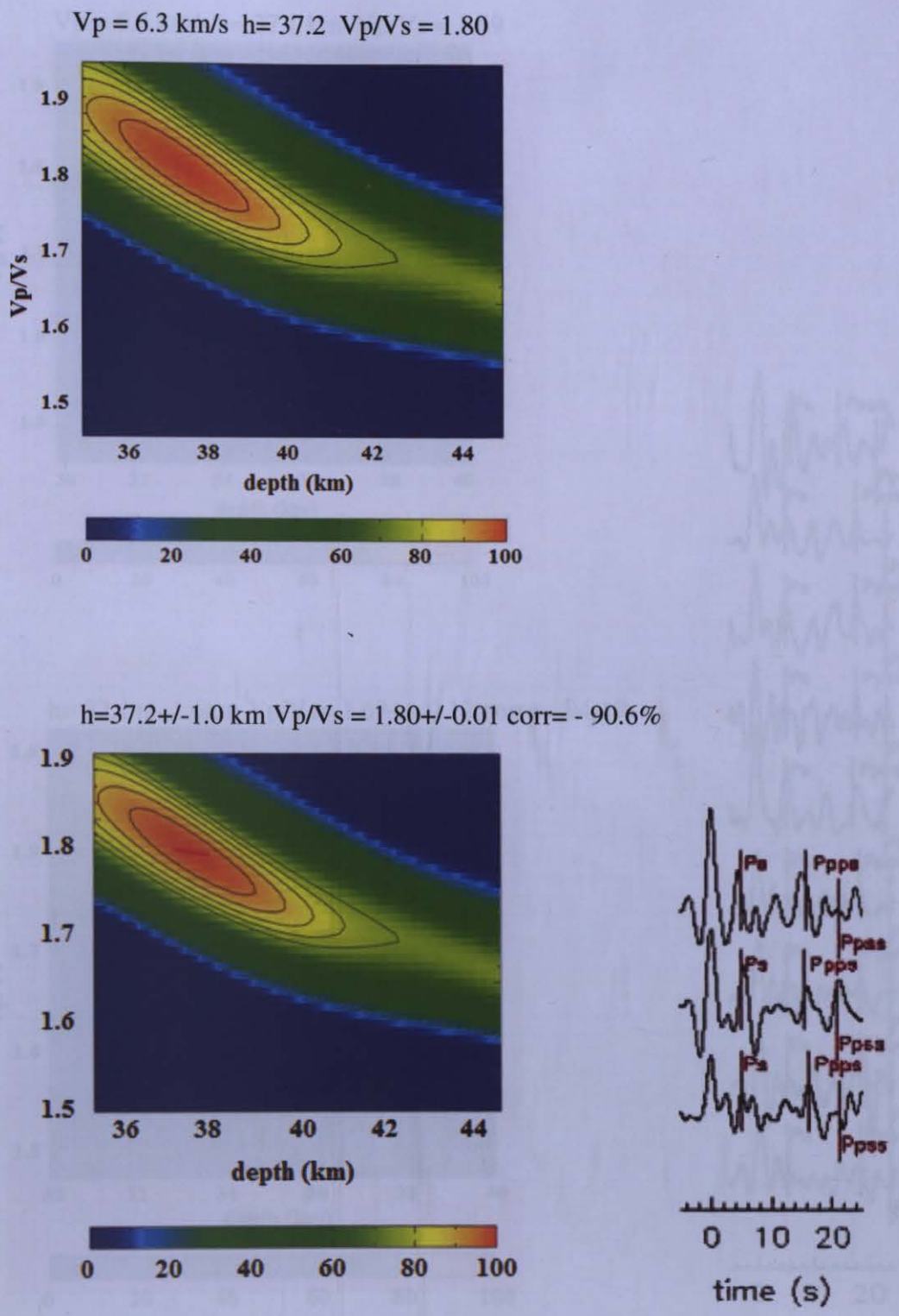

Figure 3.20 Result of the H-κ stacking method for POL broadband station. The best estimation of thickness is 37.2km with a Vp/Vs ratio of 1.80.

SUN

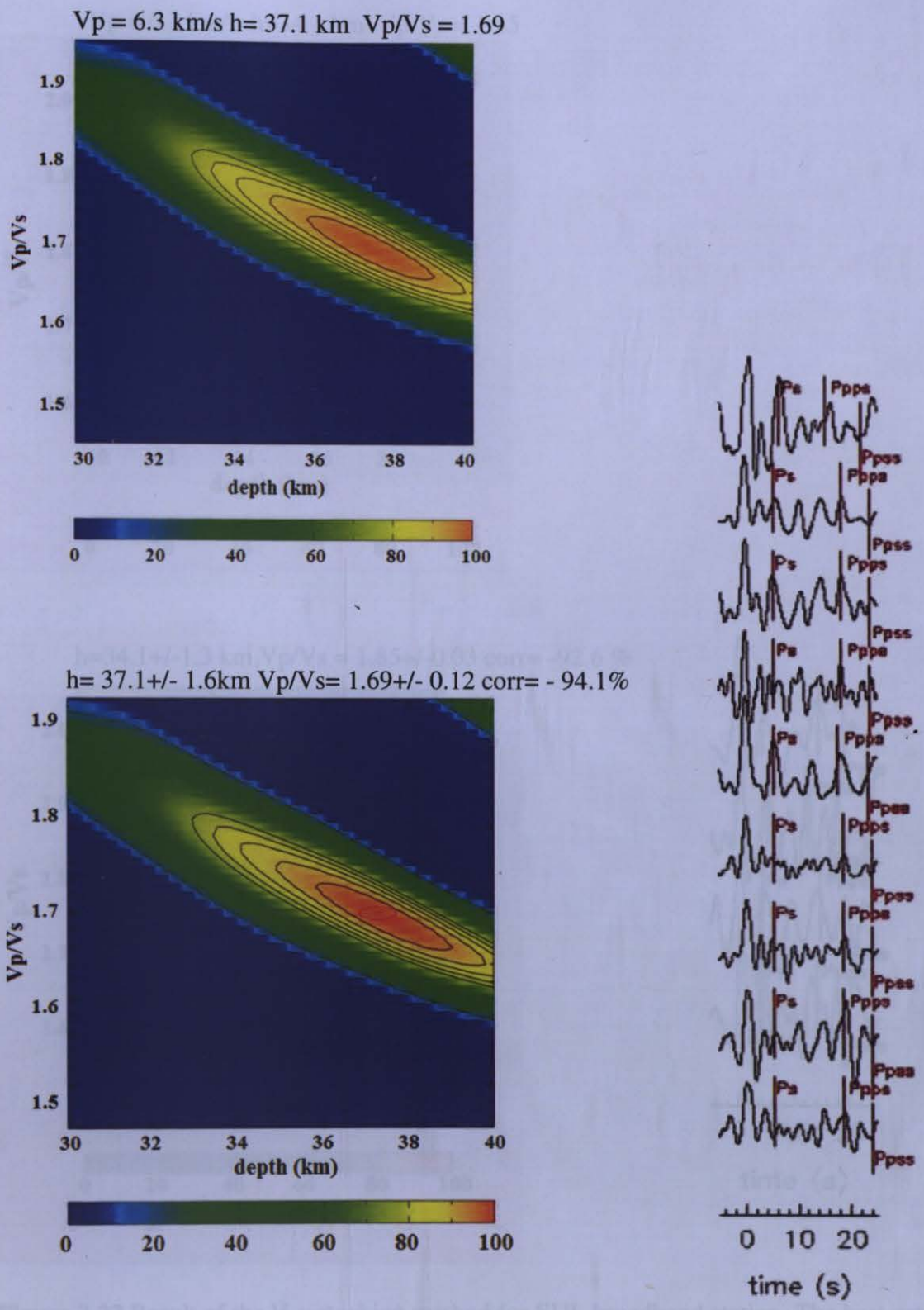

Figure 3.21 Result of the H-κ stacking method for SUN broadband station. The best estimation of thickness is 37.1 km with a Vp/Vs ratio of 1.69.

SUL

Vp = 6.3 km/s h=34.1 km Vp/Vs = 1.85

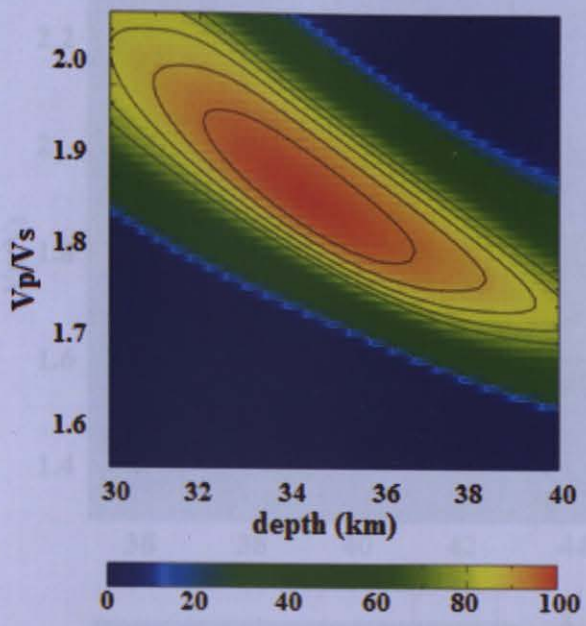

h=34.1+/-1.3 km Vp/Vs = 1.85+/-0.03 corr= -92.6 %

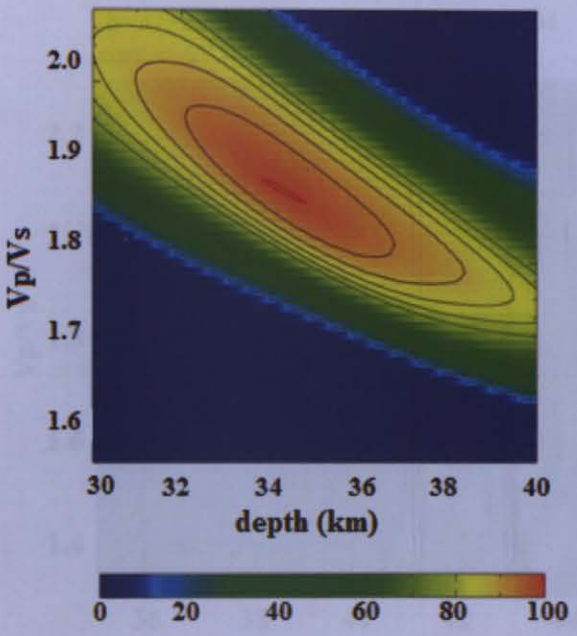

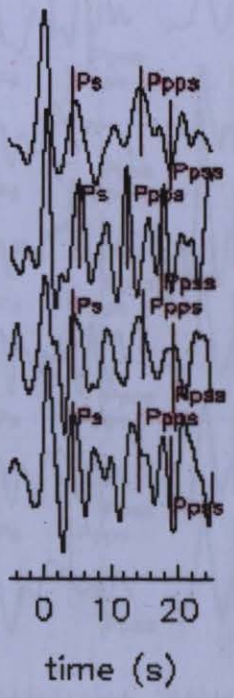

Figure 3.22 Result of the H-κ stacking method for SUL broadband station. The best estimation of thickness is 34.1km with a Vp/Vs ratio of 1.85.

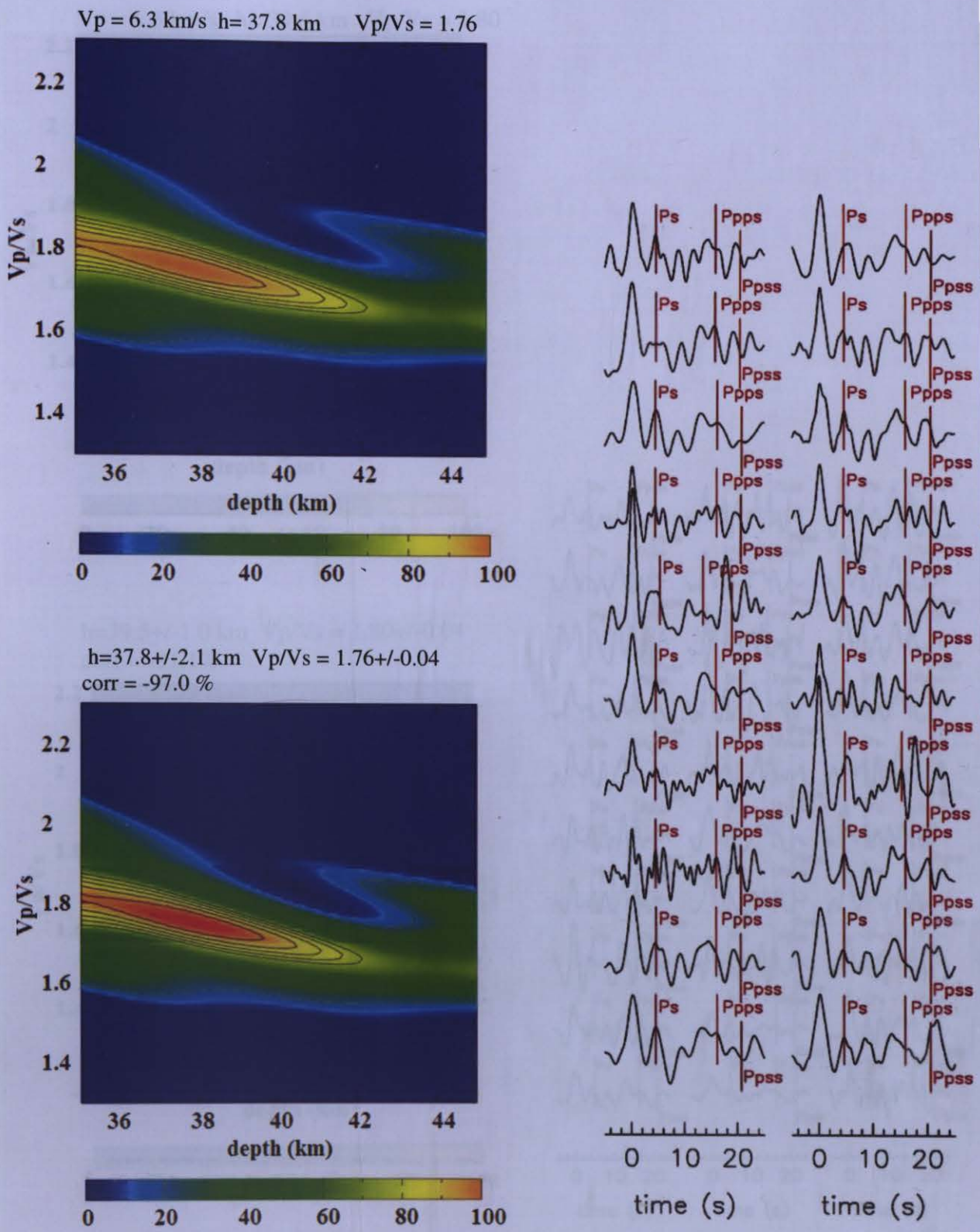

Figure 3.23 Result of the H-κ stacking method for ANTO broadband station. The best estimation of thickness is 37.8km with a Vp/Vs ratio of 1.76.

ISP

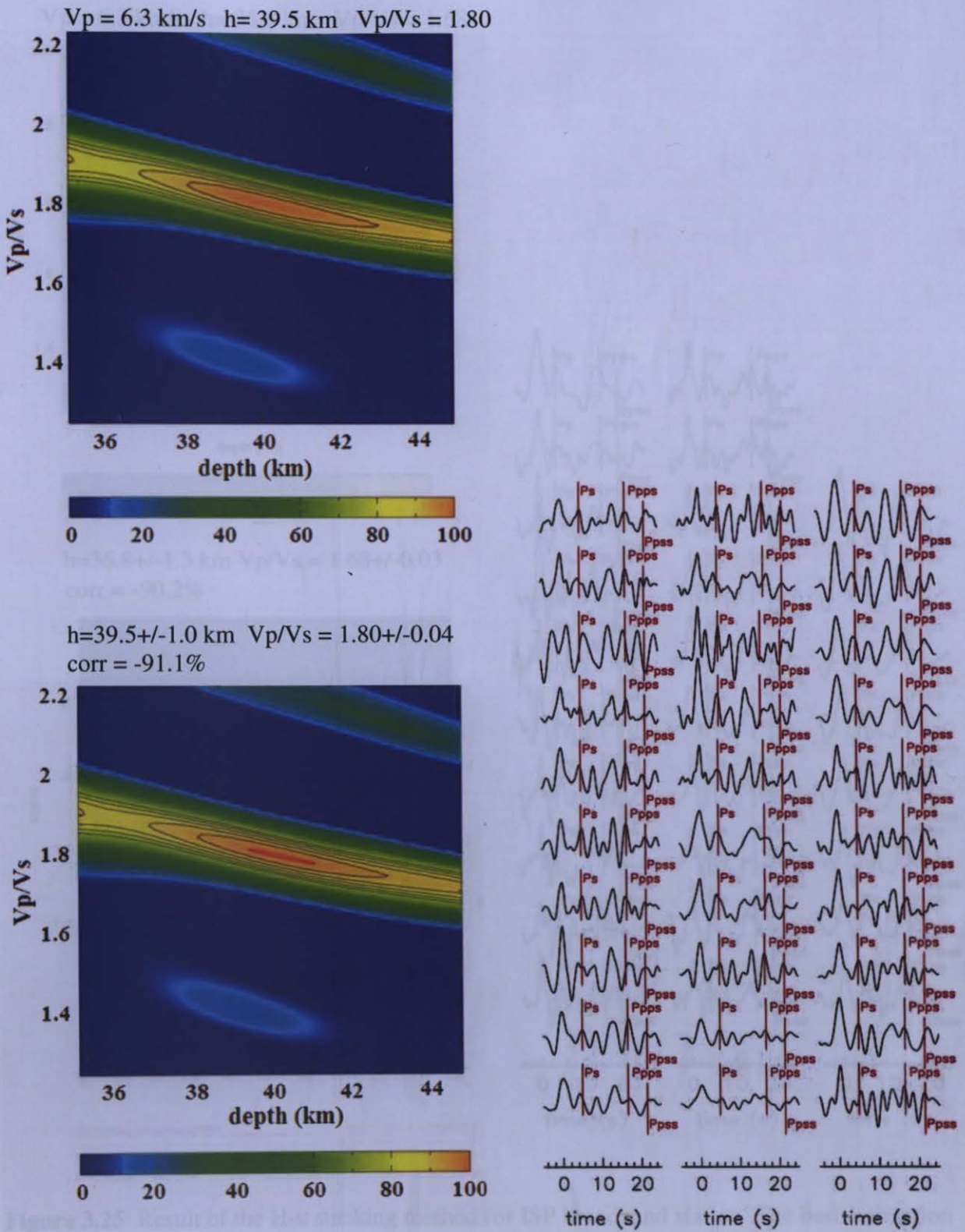

Figure 3.24 Result of the H-κ stacking method for ISP broadband station. The best estimation of thickness is 39.5 km with a Vp/Vs ratio of 1.80. Events coming from NE direction was used in analysis.

ISP

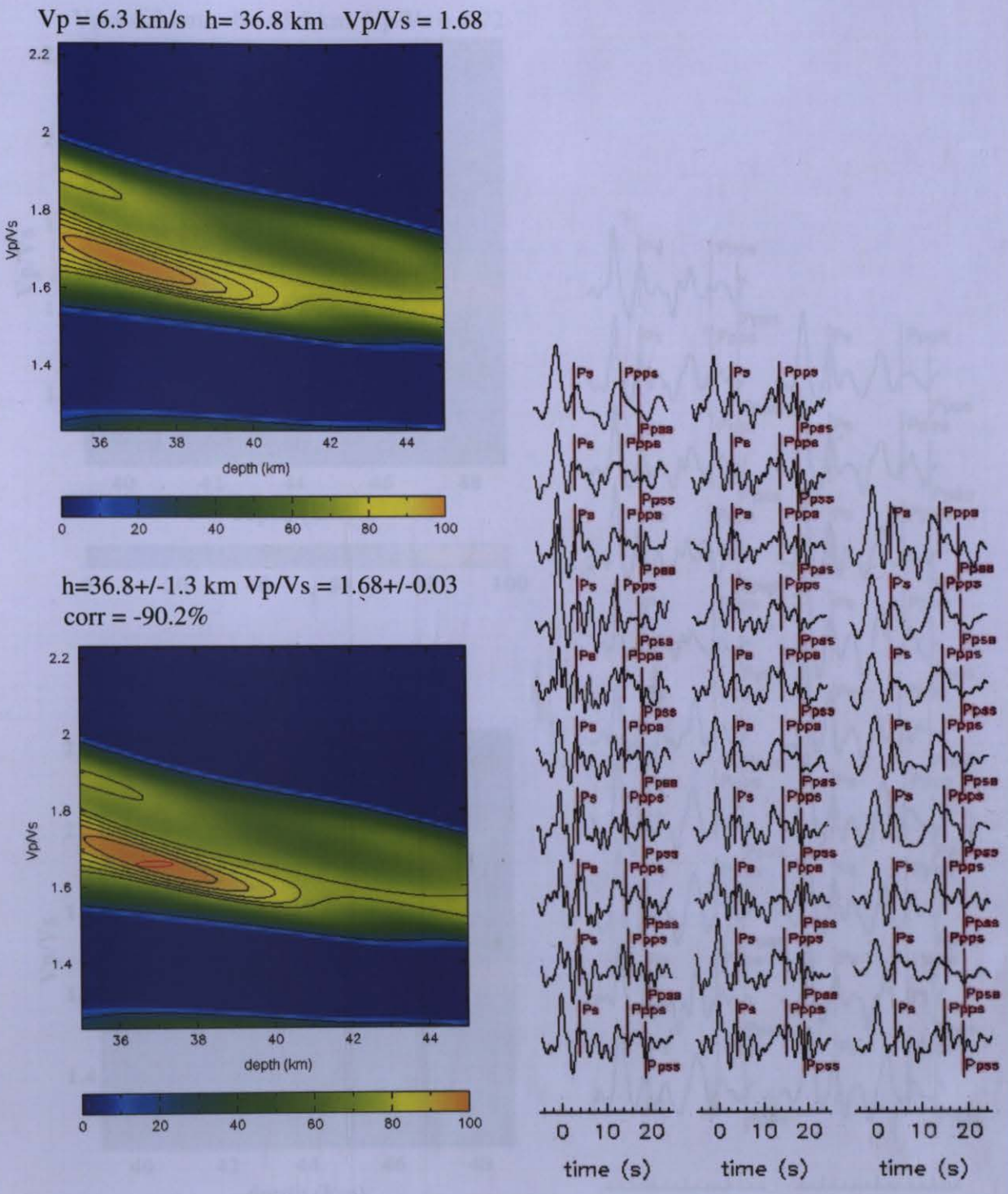

Figure 3.25 Result of the H-κ stacking method for ISP broadband station. The best estimation of thickness is 36.8 km with a Vp/Vs ratio of 1.68. Events coming from southern direction was used in analysis.

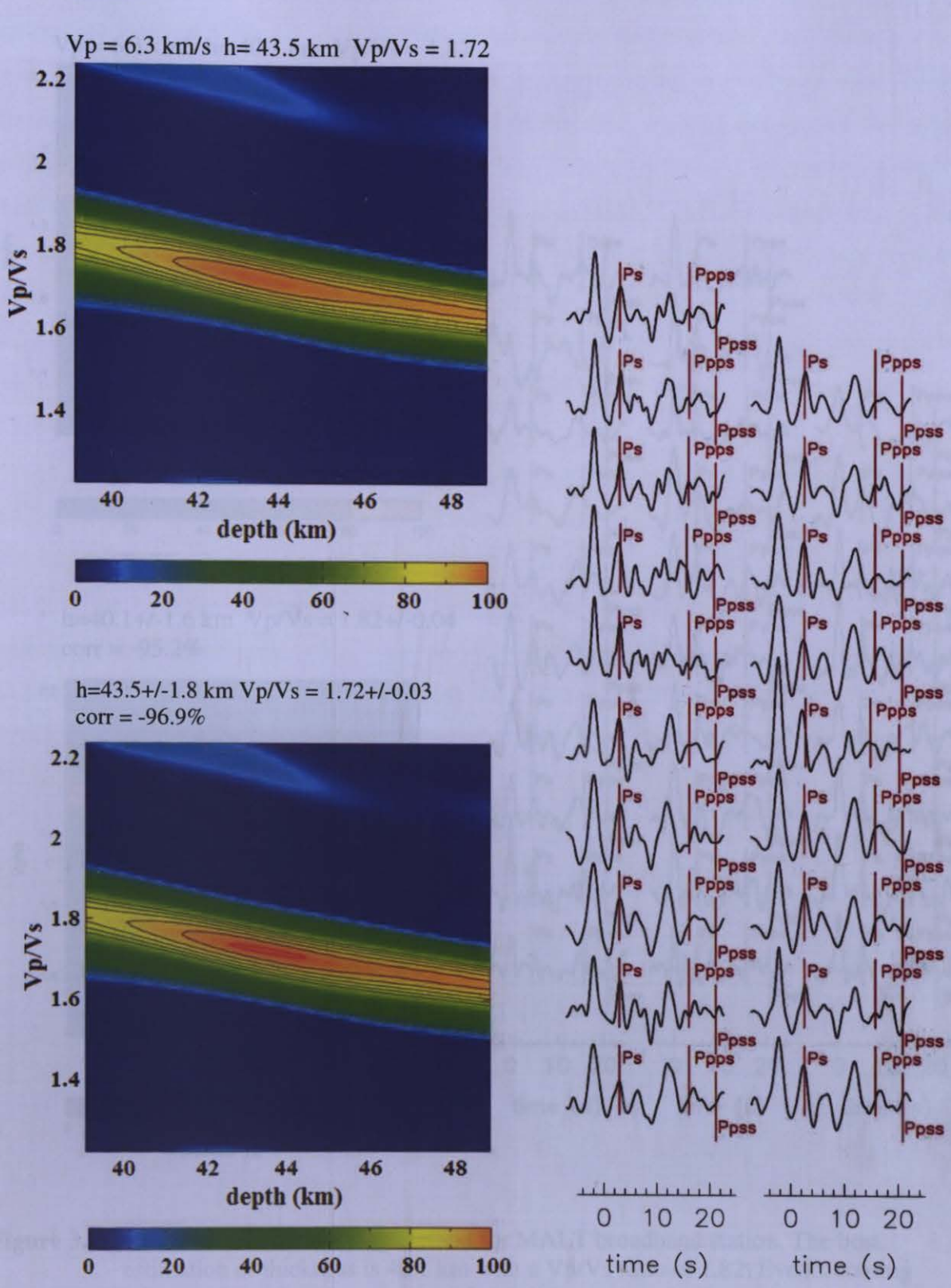

Figure 3.26 Result of the H-κ stacking method for MALT broadband station. The best estimation of thickness is 43.5km with a Vp/Vs ratio of 1.72. Events coming from NE direction was used in analysis.

MALT

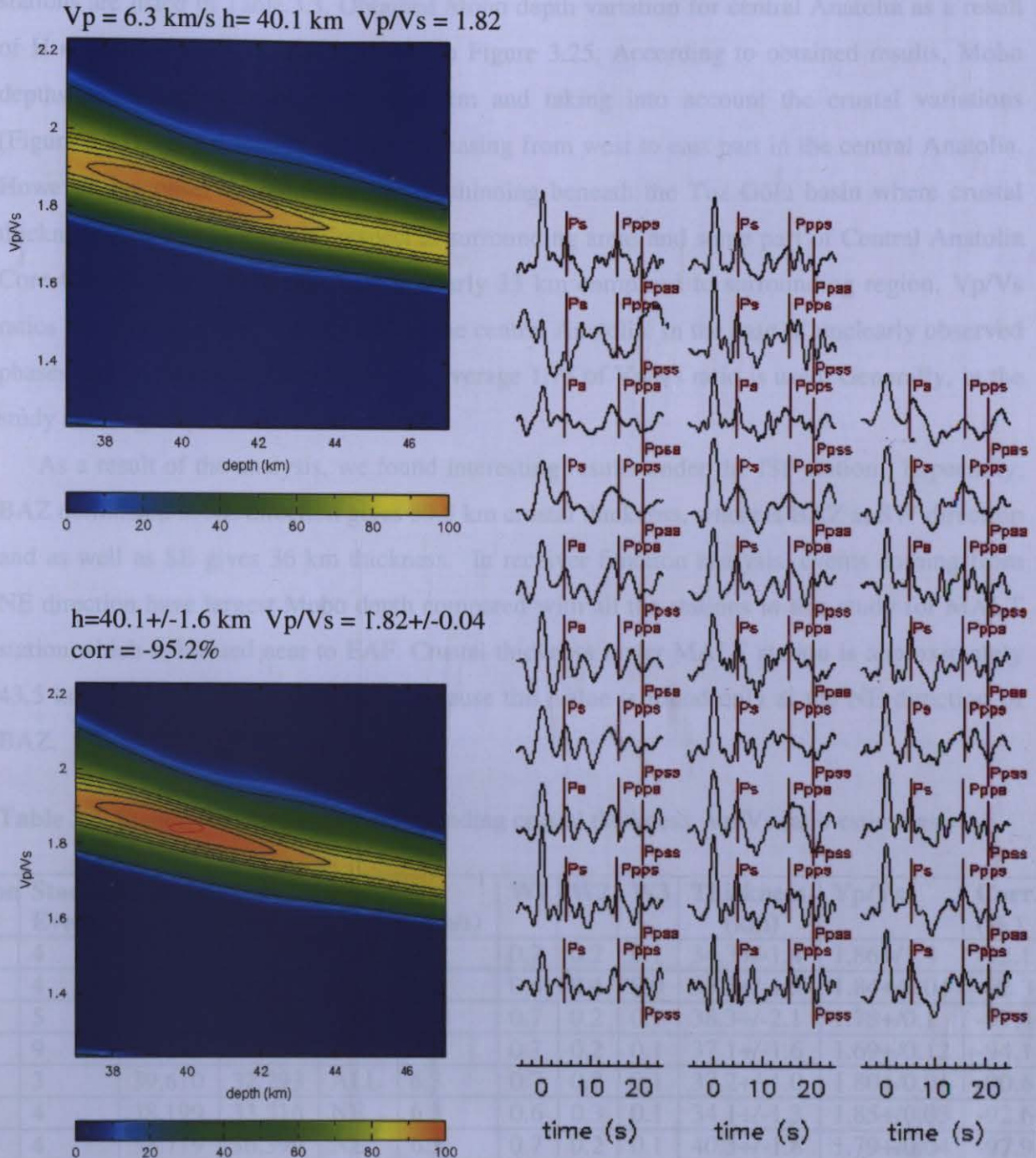

Figure 3.27 Result of the H-κ stacking method for MALT broadband station. The best estimation of thickness is 40.1 km with a Vp/Vs ratio of 1.82. Events coming from southern direction was used in analysis.

H and Vp/Vs ratio results which were found as a result of stacking analysis for all 13 stations are listed in Table.3.3. Obtained Moho depth variation for central Anatolia as a result of H-κ stacking analysis is also shown in Figure 3.25. According to obtained results, Moho depths are changing from 33 to 43.5 km and taking into account the crustal variations (Figure 3.25), crustal thicknesses are increasing from west to east part in the central Anatolia. However, we observe significant crustal thinning beneath the Tuz Gölü basin where crustal thickness is nearly 34 km with respect to surrounding areas and some part of Central Anatolia Core Complex where the thickness is nearly 33 km compared to surrounding region. Vp/Vs ratios are changing from 1.69 to 1.86 in the central Anatolia. In the case of unclearly observed phases and uncoherently stacked events, average 1.78 of Vp/Vs ratio is used. Generally, in the study area high Vp/Vs ratios were found.

As a result of the analysis, we found interesting results under the ISP station. Especially, BAZ dominated at NE direction gives 39.5 km crustal thickness, whereas BAZ at SW direction and as well as SE gives 36 km thickness. In receiver function analysis, events coming from NE direction have largest Moho depth compared with all the stations in this study for MALT station which is located near to EAF. Crustal thickness under MALT station is approximately 43.5 km. This is a very crucial point because this value is found only at the NE direction of BAZ.

Table 3.3 Station Locations and corresponding crustal thickness, Vp/Vs ratio estimates.

Station	Stacked Events	Lat. (deg)	Lon. (deg)	Baz	Vp (km/s)	W1	W2	W3	Thickness (km)	Vp/Vs	Corr. (%)
BOL	4	38.718	30.950	ALL	6.3	0.7	0.2	0.1	34.3+/-1.4	1.86+/1.4	-92.1
AVO	4	38.995	34.931	ALL	6.3	0.6	0.4	0.0	33.2+/-1.5	1.84+/0.04	-92.3
KAR	5	39.915	36.991	ALL	6.3	0.7	0.2	0.1	38.3+/-2.1	1.78+/0.1	-97.4
SUN	9	40.179	34.630	ALL	6.3	0.7	0.2	0.1	37.1+/-1.6	1.69+/0.12	-94.1
POL	3	39.610	32.293	ALL	6.3	0.7	0.2	0.1	37.2+/-1.0	1.80+/0.01	-90.6
SUL	4	38.199	33.516	NE	6.3	0.6	0.3	0.1	34.1+/-1.3	1.85+/0.03	-92.6
PIN	4	38.719	36.399	NE	6.3	0.7	0.2	0.1	40.3+/-1.8	1.79+/0.04	-97.9
AFS	5	38.419	36.923	NE	6.3	0.7	0.2	0.1	41.8+/-0.5	1.76+/0.03	-97.5
ZAR	4	39.902	37.650	ALL	6.3	0.7	0.2	0.1	40.7+/-2.4	1.80+/0.2	-86.7
DEV	4	38.353	35.492	ALL	6.3	0.7	0.2	0.1	37.6+/-1.5	1.77+/0.07	-94.1
ANTO	20	39.87	32.79	ALL	6.3	0.7	0.2	0.1	37.8+/-2.1	1.76+/0.04	-97.0
ISP	33	38.31	38.43	NE	6.3	0.7	0.2	0.1	39.5+/-1.0	1.80+/0.04	-91.1
ISP	25	38.31	38.43	S	6.3	0.7	0.2	0.1	36.8+/-1.3	1.68+/-0.03	-90.2
MALT	19	37.84	30.51	NE	6.3	0.7	0.2	0.1	43.5+/-1.8	1.72+/0.03	-96.9
MALT	28	37.84	30.51	S	6.3	0.7	0.2	0.1	40.1+/-1.6	1.82+/-0.04	-95.2

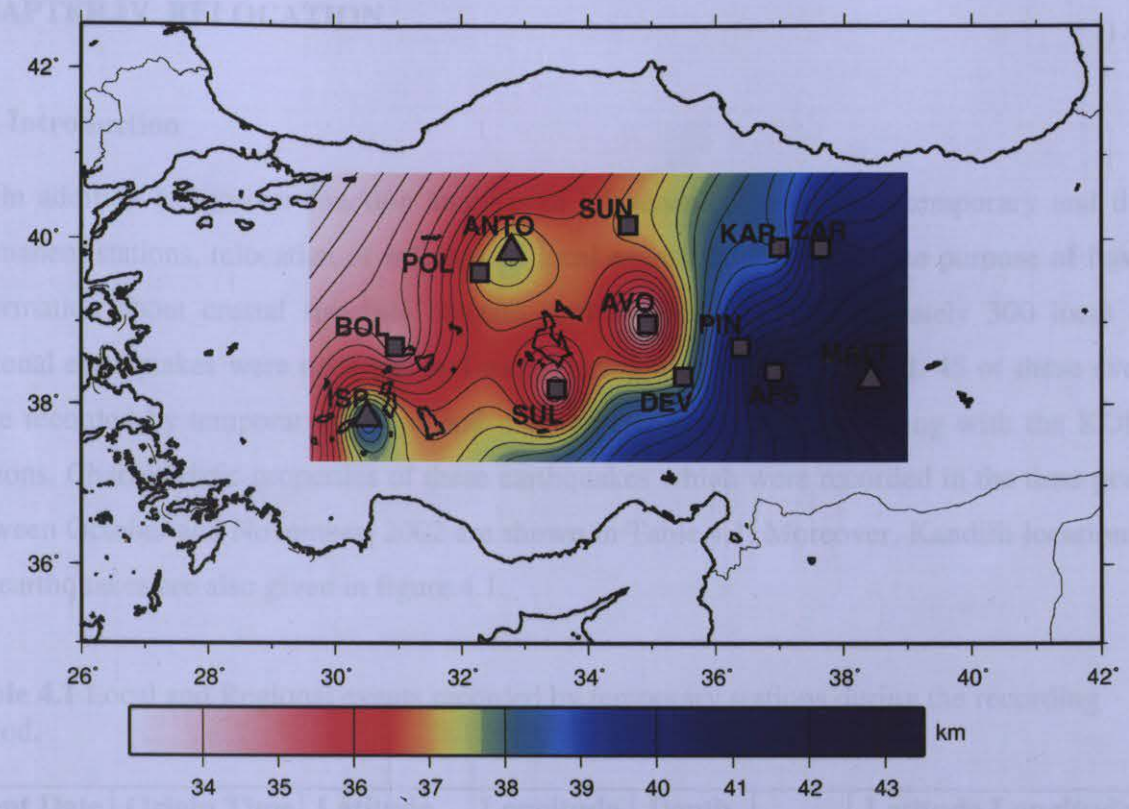

Figure 3.28 Moho depth variation in Central Anatolia

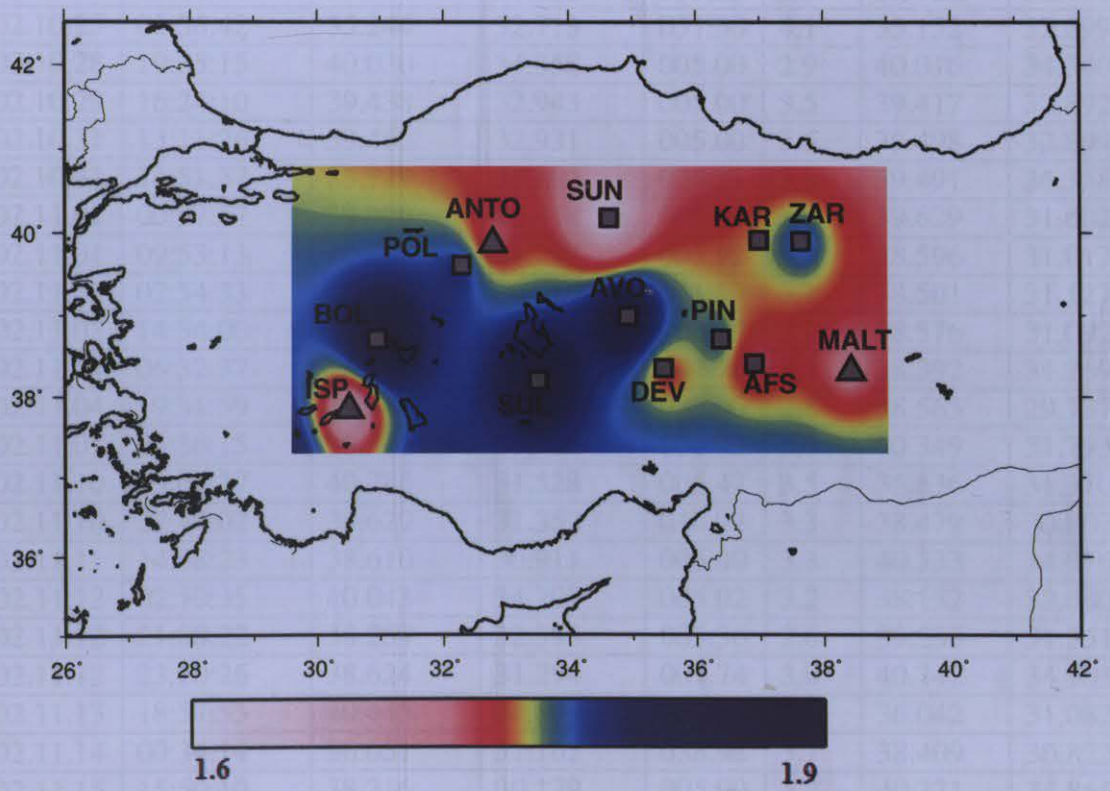

Figure 3.29 Crustal Vp/Vs ratio variation in Central Anatolia

CHAPTER.IV. RELOCATION

4.1. Introduction

In addition to receiver function analysis of teleseismic events from temporary and three permanent stations, relocation of selected 45 local events were used for the purpose of having information about crustal structure beneath central Anatolia. Approximately 300 local and regional earthquakes were occurred in Turkey during the recording period. 45 of these events were recorded by temporary stations and they were relocated by combining with the KOERI stations. Characteristic properties of these earthquakes which were recorded in the time period between October and November, 2002 are shown in Table.4.1. Moreover, Kandilli locations of the earthquakes are also given in figure.4.1.

Table 4.1 Local and Regional events recorded by temporary stations during the recording period.

Event Date yy:mm:dd	Origin Time (Local)	Latitude From KOERI Location	Longitude	Depth (km)	Mag.	Latitude From New Location	Longitude
2002.10.24	07:24:30	37.535	36.062	017.05	3.3	37.703	36.112
2002.10.25	01:56:42	35.244	32.713	051.50	4.1	35.152	32.699
2002.10.28	19:35:15	40.030	34.358	005.00	2.9	40.016	34.340
2002.10.29	16:24:10	39.438	32.943	005.00	3.5	39.417	32.892
2002.10.31	13:11:26	39.462	32.931	005.00	3.5	39.498	32.899
2002.10.31	14:51:37	35.729	31.192	026.31	3.8	39.491	36.358
2002.11.01	00:57:57	39.379	36.418	005.00	3.2	39.629	31.602
2002.11.01	09:53:13	40.404	31.227	005.92	3.3	38.596	31.017
2002.11.03	02:54:33	38.668	30.979	011.17	3.2	38.501	31.127
2002.11.03	14:34:00	38.645	31.188	006.55	2.9	38.576	31.092
2002.11.04	06:32:37	38.691	31.078	004.76	3.1	38.392	31.269
2002.11.04	19:31:59	38.544	31.395	032.00	2.8	38.565	29.737
2002.11.07	04:36:15	38.576	29.726	008.02	3.7	40.349	31.793
2002.11.10	09:04:37	40.785	31.528	006.47	3.5	36.636	31.310
2002.11.10	22:44:02	36.629	31.352	010.94	3.3	38.479	30.807
2002.11.11	14:08:23	38.610	30.911	005.00	3.3	40.333	34.076
2002.11.12	02:10:35	40.043	34.705	005.02	3.2	38.132	32.080
2002.11.12	21:00:22	38.259	32.393	005.36	2.6	39.235	31.351
2002.11.12	23:20:26	38.624	31.294	007.74	3.0	40.342	34.903
2002.11.13	18:57:55	40.445	34.809	066.49	2.8	36.042	31.082
2002.11.14	00:34:14	36.051	31.105	038.98	3.7	38.409	30.822
2002.11.15	15:50:10	38.216	30.179	005.00	3.2	40.371	34.865
2002.11.15	17:38:09	40.456	34.875	005.00	3.3	40.711	29.965
2002.11.18	18:49:43	40.740	29.961	007.42	3.1	38.037	38.427

2002.11.19	01:25:35	38.056	38.404	005.00	4.6	40.907	31.616
2002.11.19	14:43:31	40.933	31.599	005.00	3.7	38.536	30.814
2002.11.19	15:16:45	38.609	30.885	009.12	2.9	37.938	30.527
2002.11.19	19:12:40	37.863	30.372	010.76	3.2	40.341	37.064
2002.11.19	20:43:46	40.446	36.938	008.32	2.6	38.615	31.241
2002.11.20	23:14:46	38.620	31.326	009.26	2.9	38.695	31.026
2002.11.21	09:40:16	38.654	31.022	006.37	3.5	36.709	31.981
2002.11.21	20:43:16	36.730	31.991	005.19	3.3	35.566	36.656
2002.11.22	01:34:52	35.893	36.356	013.03	3.9	38.403	31.468
2002.11.23	12:38:24	38.502	31.428	005.00	2.7	40.932	31.455
2002.11.23	17:27:19	40.936	31.375	005.00	3.1	38.630	31.325
2002.11.23	17:48:56	38.505	31.131	005.50	3.3	37.881	29.367
2002.11.24	00:57:18	37.841	29.437	007.20	3.3	38.642	31.049
2002.11.24	21:54:08	38.672	31.069	011.98	2.8	35.785	31.590
2002.11.25	01:31:01	35.732	31.472	002.87	3.6	39.869	32.954
2002.11.25	13:45:46	39.835	32.951	005.00	2.9	41.009	30.616
2002.11.25	18:36:36	40.938	30.842	031.62	2.3	40.524	34.007
2002.11.26	04:33:49	38.495	35.836	005.00	0.0	38.522	35.729
2002.11.27	02:06:04	40.331	32.171	005.00	3.2	40.249	32.110
2002.11.27	07:41:00	40.241	33.824	005.03	3.4	40.161	33.730
2002.11.28	01:37:25	35.454	31.329	005.00	3.7	35.656	31.305

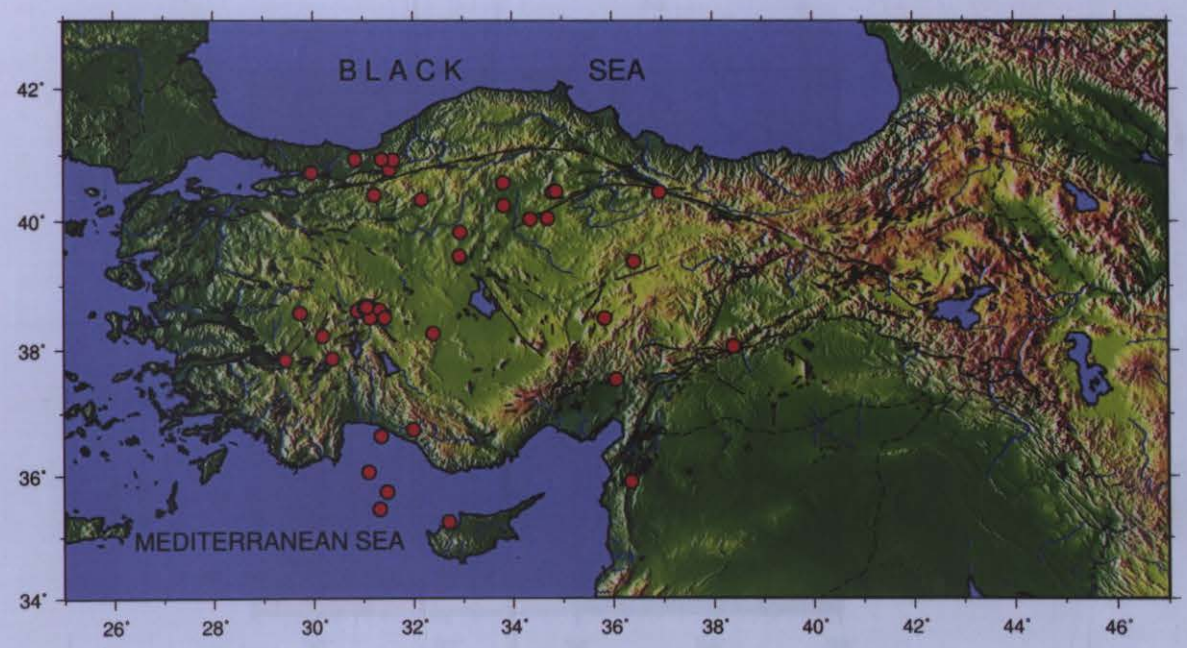

Figure 4.1 Location of 45 earthquakes from existing KOERI catalog.

4.2. Relocation Procedure

For determining hypocenter of local events, HYPO71 program was performed by using accurate station coordinates, reliable first motion of selected earthquakes and a reasonable crustal structure model. In the first case, location procedure was applied with the velocity model that is used by KOERI for all over the Turkey (Table.4.2). Addition to the temporary stations, we also used permanent KOERI stations. Average residual values obtained from relocation procedure give us information about crustal structure beneath the region. Although positive and negative residual values are related to crustal thickness, they can be indicator of low or high velocity layers. Therefore, a residual map was created by using Kandilli velocity model (Fig.4.2.).

Table 4.2 Velocity model used in first case for relocation.

Velocity (km/s)	Thickness (km)
4.500	00.000
5.910	5.4000
7.800	31.600
8.300	89.200

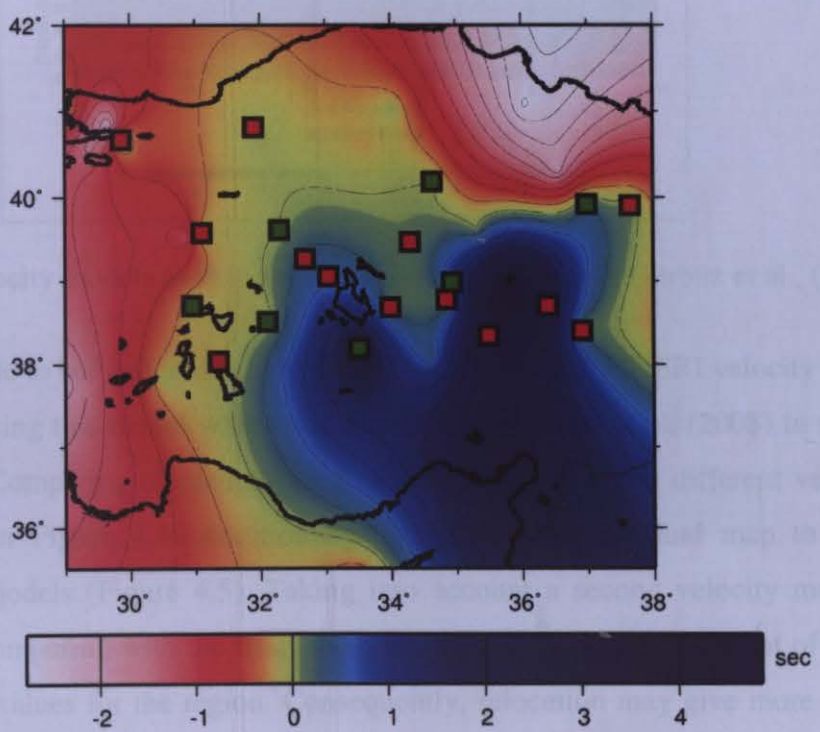

Figure 4.2 Residual map created by using Kandilli velocity model.

As a second case, we tried to locate the same events with HYPO71 by using a different velocity model which has been proposed by Gürbüz et al., (2003) and average Vp/Vs ratio which was obtained by H-κ stacking analysis. In Figure 4.3, velocity-depth structure is presented for three direction of profile, north, west and south, respectively. These profiles are also shown in Figure 3.1 with the blue triangles. The average crustal thickness and corresponding velocity from these three structural model was employed in the relocation process.

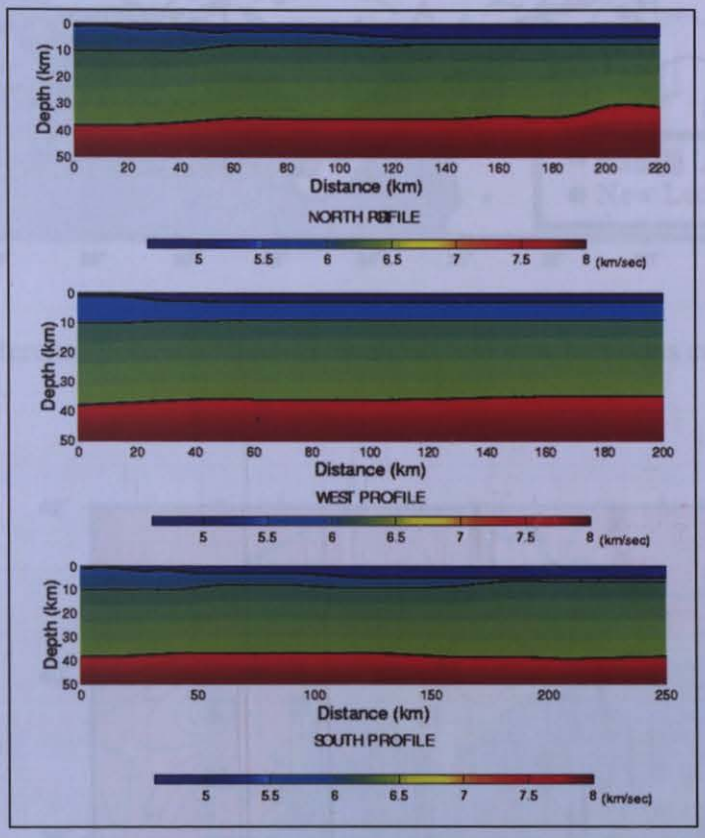

Figure 4.3 Velocity models used in for three direction of profile Gürbüz et al., (2003).

It is possible to see difference between the locations from KOERI velocity model and new locations, by using this model which was obtained by Gürbüz et al, (2003) in relocation as an initial model. Comparing of earthquake locations from these two different velocity model is demonstrated in Figure 4.4. Additionally, we plotted the residual map to see difference between two models (Figure 4.5). Taking into account a second velocity model for central Anatolia and comparing with the first model shows clearly an improvement of epicenters with lower residual values for the region. Consequently, relocation may give more accurate results in the case of supporting with reasonable crustal structure model and parameters obtained from receiver function.

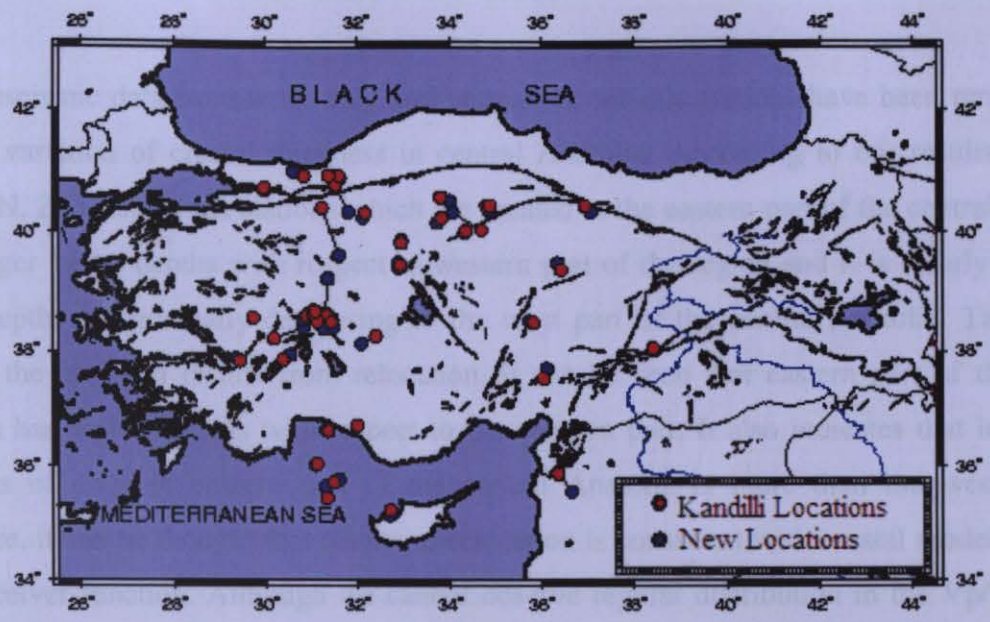

Figure 4.4 Difference between Kandilli locations and new locations calculated from second velocity model.

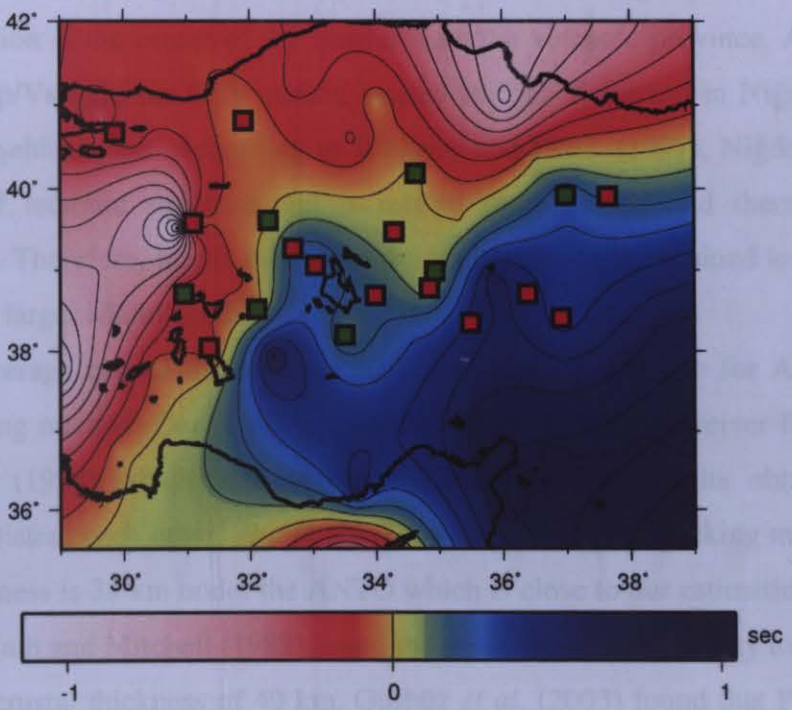

Figure 4.5 Residual map created by using velocity model from Gürbüz et al., (2003).

CHAPTER.V. CONCLUSION AND DISCUSSION

Teleseismic data from temporary and permanent seismic stations have been processed to identify variation of crustal thickness in central Anatolia. According to our results, MALT, AFS, PIN, ZAR and KAR stations which are located in the eastern part of the central Anatolia have larger Moho depths with respect to western part of the region and it is clearly seen that Moho depths are gradually decreasing to the west part of the central Anatolia. Taking into account the obtained results from relocation, it can be seen that eastern part of the central Anatolia has high residuals with respect to the western part. It also indicates that in general, thickness of crust in eastern part of the central Anatolia is more than the western part. Therefore, it can be thought that results of relocation is consistent with crustal model obtained from receiver function. Although we cannot observe regular distribution in the Vp/Vs ratios, lower Vp/Vs ratios were determined in the eastern part of the central Anatolia with respect to western part of the region. This can be related to Quaternary volcanism. However, AVO station that is located in Nevşehir region gives us 1.84 for Vp/Vs ratio corresponding to crustal thickness of 33.2 km. This higher ratio compared to the surrounding region indicates a volcanic region. This region is the center of the central Anatolia volcanic province. Additionally, we found a lower Vp/Vs ratio for DEV station located in CAF Zone and in Niğde which is also close to the Nevşehir region. According to Whitney and Dilek (1997), Niğde massif permits reconstruction of tectonic structure that is related to thickened and thermally weakened continental crust. Therefore, this is thought to be compatible with obtained lower Vp/Vs ratio corresponding to larger Moho depth.

We found average crustal thickness of 37.8 and 1.76 Vp/Vs ratio for ANTO station by using H-κ stacking method. Our result is compatible with previous receiver function study of Saunders et al., (1998) which used waveform inversion. The results obtained from two methods are consistent each other. Zhu et al., (2006) also used H-κ stacking method and found that crustal thickness is 38 km under the ANTO which is close to our estimation for the region. Whereas Mindevalli and Mitchell (1989) found the shear wave (Sn) velocity to be 4.2 km/s and an approximate crustal thickness of 40 km, Gurbüz *et al.* (2003) found that Pn velocity is 7.8 km/sec. and the crust is 36 km thick under Keskin area using seismic refraction method.

As a result of the H-κ stacking analysis, various values in the thickness of crust beneath ISP station which is located in so-called ISP angle area where Hellenic and Cyprus arcs intersect are found in terms of different BAZ ISP. There are some proposed phenomena related to tectonic characteristics of the region. It is known that there are two adjacent subduction zones in the region; The Hellenic arc to the west and the Cyprian arc to the east. Moreover, although the African and Eurasian lithospheric plates converge at rate of 1 cm/year, deformation of Aegean is fast and intense and, convergence across Hellenic trench is greater than 4 cm/year and that is evidenced by geodetic measurement (McClusky at al, 2000). Comparing our result obtained from ISP station with the tectonic properties of the region, we observed that changes in thickness of the crust is dependent on the direction of coming earthquakes. This phenomenon may be explained with accurate internal deformation of the crust that is certainly proved by the existence of major active crustal fault by seismic activity which may leads to anisotropy in the crust. Especially, BAZ dominated at NE direction gives larger Moho depth than BAZ at SW direction and as well as SE. It may be explained by complex asthenospheric flow due to retreat of subducted slab along the Hellenic arc. Also, probable interrelation between overriding lithosphere and strong asthenosphere in the region are responsible for these variations in back azimuths.

The distribution of BAZ is not uniform that leads to obtaining different values in the crustal thickness for MALT station. Obtained high value of crustal thickness for NE comparing with southern direction of BAZ under this station may be supported by different models that were proposed for East Anatolia region. It is well known that East Anatolia Plateau is a product of collision between Eurasian and Arabia plates. Recent seismic observations have been interpreted to indicate only slightly thickened crust in the collision zone (Zor et al., 2003) and N-S shorthening by complex folding and thrusting of East Anatolia accretionary complex produce average 2 km topography. The area which MALT station is placed may be subject to a more active thrusting of African plate than Eurasion plate. This situation leads to thinner crustal thickness in Southern direction of BAZ than NE direction. High Moho depth in NE direction of BAZ may presumably be associated with thickening of the trapped lithosphere after collision between Eurasian and Arabian plates.

REFERENCES

A. Barka, K. Kadinsky-Cade, 1988. Strike-slip fault geometry in Turkey and its influence on earthquake activity, 1988, *Tectonics,* 7, 663-684.

Al -Lazki, A.I., E. Sandvol, D. Seber, M. Barazangi, N. Türkelli, and R. Mohamad, 2004. Pn tomographic imaging of mantle lid velocity and anisotropy at the junction of the Arabian, Eurasian and African plates, *Geophys. J. Int.,* 158, 1024-1040.

Ammon, C.J., G.E. Randall, and G. Zandt 1990. On the non-uniqueness of receiver function inversions, *J. Geophys. Res.,* 95, 15,303–15,318.

Ammon, C.J., 1991. The isolation of Receiver Effects from Teleseismic P Waveforms, *Bull. Seismi. Soc. Am.*, 81, 2504-2510.

Aydan, Ö., 1997. Seismic characteristics of Turkish earthquakes. Turkish Earthquake Foundation, TDV/TR 97-007, pp.41.

Barka, A., 1996. Slip distribution along the North Anatolian fault associated with large earthquakes of the period 1939–1967: Seismological Society of America Bulletin, v. 86, p. 1238–1254.

Barka and K. Kadinsky-Cade, 1988. Strike-slip fault geometry in Turkey and its influence on earthquake activity, Tectonics, 7, pp.663-684.

Barka, A., and Reilinger, R., 1997. Active tectonics of the eastern Mediterranean region deduced from GPS, neotectonic, and seismicity data: Annali Geofisica, v. 40, p. 587–610.

Baker, G. E., J. B. Minster, G. Zandt, and H. Gurrola, 1996. Constraints on crustal structure and complex Moho topography beneath Piñon Flat, California from teleseismic receiver functions, *Bull. Seism. Soc. Amer.*, 86, 1830-1844.

Burdick, L.J. and Langston, C.A., 1977. Modelling crust-structure through the use of converted phases in teleseismic body-wave-forms, *Bull. Seism. Soc. Am.* 67, 677-691.

Canıtez, N., Toksöz M.N., 1980. Crustal structure beneath Turkey, EOS TRANS. AGU, 61, 290.

Cassidy, J. F. 1992. Numerical experiments in broadband receiver function analysis, *Bull. Seismol. Soc. Am.,* 82, 1453– 1474.

Çakır, O. and Erduran, M., 2004. Constraining crustal and uppermost mantle structure beneath station TBZ (Trabzon, Turkey) by receiver function and dispersion analyses, *Geophys. J. Int.,* 158, 955-971.

Cassidy, J.F., 1995. Receiver Function Analysis of Canadian National Network, *Canadian Journal of Earth Sciences,* 32,939-950.

Cemen, İ., M.C. Göncüoğlu and K. Dirik, 1999. Structural Evolution of the Tuzgölü Basin in Central Anatolia, Turkey, *Geol. J.,* 107, 693-706.

Chevrot, S., van der Hilst, R.D., 2000. The Poisson ratio of the Australian crust: geological and geophysical implications, *Earth Planet. Sci. Lett.* 183, 121–132.

Dey-Sarkar, S.K., and Wiggins, R.A., 1976. Source deconvolution of teleseismic P wave arrivals between 14-40 degrees, *J. Geophys. Res.,* 81, 3633-3641.

Dewey, J.F., M.R. Hempton, W.S.F. Kidd, F. Saroglu, and A. M. C. Şengör, 1986. Shortening of continental lithosphere: The neotectonics of Eastern Anatolia – a young collision zone, in M. P. Coward, and A. C. Ries, eds. *Collision Tectonics, Geol. Soc. London Spec. Pub.*, 19, (R. M. Shackleton volume), 3 – 36.

Dirik, K., 2001. Neotectonic evolution of the nortwestward arched segment of the Central Anatolian Fault Zone, Central Anatolia, Turkey, *Geodinamica Acta,* 14, 147-158

Dirik, K., M.C. Göncüoğlu and H. Kozlu, 1999. Stratigraphy and pre-Miocene tectonic evolution of the southwestern part of the Sivas Basin, Central Anatolia, Turkey, *Geol. J.* 34, 303-319.

Efron, B. and Tibshirani, R., 1991. Statistical data analysis in the computer age, *Science,* 253,390-395.

Endrun, B., L. Cerenna, T. Meier, M. Bohnhoff and H. P. Harjes, 2005. Modeling the influence of Moho topography on receiver functions: A case study from the central Hellenic subduction zone. *Geophys. Res. Lett.* 32, L12311, doi: 10.1029/2005GL023066.

Froger, J.L., J.F. Lenat, J. Chorowicz, J. L. Le Pennec, J. L. Bourdier, O. Köse, O. Zimitoğlu, N. M. Gündoğdu, A. Gourgaud, 1998. Hidden calderas evidenced by multisources geophysical data; example of Cappadocian calderas, Central Anatolia, *J. Volcanol. and Geothermal Res.* 185, 99-128.

Göncüoglu, M.C., Toprak, V., Kuşcu, I., Erler, A. and Olgun E.,1991. Geology of the western part of the Central Anatolian Massif, Part 1: Southern Section: Unpubl. Report No.2909, Turkish Petroleum Company Report.

Görür N., Oktay F. Y., Seymen I. and Şengör A. M. C. 1984. Paleotectonic evolution of the Tuzgölü basin complex, central Turkey: sedimentary record of a Neo-Tethyan closure, Geological Society of London, Special Publication 17: 467-482.

Gürbüz, C. and Evans, J.R., 1991, A seismic refraction study of the western Tuz Gölü basin, central Turkey, *Geophys. J. Int.,* 106, 239-251.

Gürbüz, C., T. Bekler, M.N. Toksöz, S. Kuleli, D. Kalafat, and C. A. Schultz, 2003. Seismic refraction studies and crustal structure in Anatolia. Commision on controlled- source Seismology, 12 International Workshop, Mountain Lake, Virginia, October 7-11, 74-78.

Helmberger, D. and Wiggins R.A., 1971. Upper mantle structure of the Midwestern United States, *J. Geophys. Res.*, 76, 3229-3245.

Hearn, T.M. and J. F. Ni, 1994. Pn velocities beneath continental collision zones: the Turkish-Iranian plateau, *Geophys. J. Int.*, 117, 273-283.

Ilkişik, O.M., A. Gürer, T. Tokgöz, C. Kaya, 1997. Geoelectromagnetic and geothermic investigations in the Ihlara Valley geothermal field, *J. Volcanol. and Geothermal Res.* 78, 297-308.

Innocenti, F., Mazzuoli, R., Pasquare, G., Radicati di Brozolo, F. and Villari, L. 1975. The Neogene calcalkaline volcanism of the Central Anatolia: geochronological data on Kayseri-Niğde area. *Geol. Mag.* 112, pp.349-360.

Innocenti, F., Mazzuoli, R., Pasquare, G., Radicati di Brozolo, F. and Villari, L.,1982. Tertiary and Quaternary volcanism of the Erzurum-Kars area (Eastern Turkey): geochronological data and geodynamic evolution, *J. Volc. Geotherm. Res.*, 13, 223-240.

Jackson, J.A., and D. McKenzie, 1988. The relationship between plate motions and seismic moment tensors and the rates of active deformation in the Mediterranean and Middle East, *Geophys. J.*, 93, 45–73.

Julia, J., and J. Mejia, 2004. Thickness and VP/VS ratio variation in the Iberian crust, Geophys. J. Int., 156, 59– 72.

Julia, J., F. Mancilla and J. Morales, 2005. Seismic signature of intracrustal magmatic intrusions in the Eastern Betics (Internal Zone), SE Iberia, *Geophys. Res. Lett.*, 32, L16304, doi:10.1029/2005GL023274.

Ketin, I., 1973. Umumi Jeoloji (General Geology), Published by ITÜ, 4th Ed.

Koçyiğit, A., and A. Beyhan, 1998. A new intracontinental transcurrent structure: the Central Anatolian Fault Zone, Turkey, *Tectonophysics,* 284, 317-336.

Koper, K. D., M. E. Wysession, and D. A. Wiens, 1999. Multimodal Function Optimization with a Niching genetic Algorithm:ASeismological Example, Bull. Seismol. Soc. Am., 89(4), 978–988.

Kuleli, S., E. Zor, N. Türkelli, E. Sandvol, D. Şeber and M. Barazangi, 2001. The IMS Belbaşı Seismic Array (BRAR) in Central Turkey, *Seism. Res. Lett.*, 72, 60-69.

Langston, C.A. 1979. Structure under Mount Rainier,Washington, inferred from teleseismic body waves, J. Geophys. Res., 84, 4749–4762.

Langston, C.A., 1977. Corvallis, Oregon, crustal and upper mantle structure from teleseismic P and S waves, *Bull. Seis. Soc. Am.*, 67, 713-724.

Langston, C.A., 1994. An integrated study of crustal structure and regional wave propagation for southeastern Missouri, *Bull. Seis. Soc. Am.*, 84, 105-118.

Levin, V., and J. Park, 1997. Crustal anisotropy in the Ural Mtns foredeep from teleseismic receiver functions, *Geophys. Res. Lett.*, 24, 1283-1286.

Liggoria, J.P., and C.J. Ammon 1999. Iterative deconvolution and receiver function estimation, *Bull. Seismol. Soc. Am.*, 89, 1395– 1400.

Ligorria, J.P., 2000, The Mantle-Crust Transition beneath North. America, Ph.D. Thesis, Department of Earth and Atmospheric. Sciences St. Louis University.

Mangino, S. and K. Priestley 1998. Crustal structure in the Caspian Sea region, *Geophys. J. Int.*, **133**, 640-648.

McKenzie, D.P., 1970. Plate tectonic of the Mediterranean region, *Nature,* 226, 239- 243.

McKenzie, D., 1972. Active tectonics of the Mediterranean region, *Geophys. J. Roy. Ast. Soc.* 30, 109-185.

McNamara, D.E., and T.J. Owens, 1993. Azimuthal shear wave velocity anisotropy in the Basin and Range province using Moho Ps converted phases, *J. Geophys. Res.*, 98, 12,003-12,017.

Mindevalli, O.Y. and B.J. Mitchell, 1989. Crustal structure and possible anisotropy in Turkey from seismic surfacewave dispersion, *Geophys. J. Int.*, 98, 93-106.

Oral, M.B., R.E. Reilinger, M.N.Toksöz, R.W. King, A.A. Barka, I. Kinik, and O. Lenk, 1995. Global Positioning system offers evidence of plate motions in Eastern Mediterranean, *EOS.*

Owens, T.J., Nyblade, A.A., Gurrola, H., & Langston, C.A., 2000. Mantle transition zone structure beneath Tanzania, East Africa, *Geophys. Res. Lett.* 27, 827-830.

Owens, T.J., Zandt, G., and Taylor, S.R., 1984. Seismic evidence for an ancient rift beneath the Cumberland Plateau, Tennessee: A detailed analysis of broadband teleseismic P waveforms, *J. Geophys. Res.* 89, 7783-7795.

Owens, T. J., 1987. Crustal structure of the Adirondacks determined from broadband teleseismic waveform modeling, *J. Geophys. Res.*, 92, 6391– 6401.

Ozalaybey, S., M. K. Savage, A. F. Sheehan, J. N. Louie, and J. N. Brune, 1997. Shear-wave velocity structure in the northern Basin and Range Province from the combined analysis of receiver functions and surface waves, *Bull. Seism. Soc. Am.*, 87, 183–199.

Pasquare, G., Poli, S., Vezzoli, L., Zanchi, A., 1988. Continental Arc Volcanism and Tectonic Setting in Central Anatolia, Turkey. *Tectonophysics* 146, 217-230.

Peng, X., and E.D. Humphreys, 1997. Crustal velocity structure of northwestern Nevada from teleseismic receiver function analysis, *Bull. Seis. Soc. Am.*, 87, 745-754.

Phinney, R. A., 1964. Structure of earths crust from spectral behavior of long-period body waves, *J. Geophys. Res.,* 69, 2997-3017.

Sandvol, E., Şeber, D., Calvert, A. and Barazangi, M., 1998. Grid search modelling of receiver functions: Implications for crustal structure in the Middle East and North Africa, *J. Geophys. Res.* 103, 26899-26917.

Saunders, P., K. Preistley, and T. Taymaz, 1998. Variations in the crustal structure beneath western Turkey, *Geophys. J. Int.*,134,373-389.

S.C. McClusky, S. Balassanian, A. Barka, C. Demir, S. Ergintav, et al., 2000. Global Positioning System constraints on plate kinematics and dynamics in the eastern Mediterranean and Caucusus, *J. Geophys. Res.*, 105: 5695-5719.

Şeber, D., Marisa Vallve, Eric Sandvol, David Steer, and Muawia Barazangi. *Geographic Information Systems (GIS) in earth sciences: An application to the Middle East region*, GSA Today, February 1997.

Şengör, A.M.C., and W.S.F. Kidd, 1979. The post-collisional tectonics of the Turkish-Iranian Plateau and a comparison with Tibet, *Tectonophysics,* 55, 361– 376.

Şengör, A.M.C. and Y. Yılmaz, 1981. Tethyan evolution of Turkey, a plate tectonic approach. Tectonophysics, 75, 181-241.

Şengör A.M.C., Gorur N., Saroglu F., 1985. Strike-slip faulting and related basin formation in zones of tectonic escape: Turkey as a case study, In: Biddle K.D., Christie-Blick N. (eds.) Strike-slip deformation, basin formation, and sedimentation. SEPM Spec., 1.17, 227-264.

Şengör, A.M.C. and Yılmaz, Y., 1983. Türkiye'de Tetisin evrimi levha tektoniği açısından bir yaklaşım: *Geo. Soc.Turk. Earth. Scien. Spe Publ. 1.*

Şengör, A.M.C., S. Ozeren, E. Zor, and T. Genc, 2003. East Anatolian high plateau as a mantle-supported, N-S shortened domal structure, *Geophys. Res. Lett.,* 30(24), 8045, doi:10.1029/2003GL017858.

Temel A. 1992. Geochemistry and Petrology of the Cappadocian Explosive Volcanism. Hacettepe University Ph.D. Thesis, Ankara, Turkey, 209 p.

Temel, A., Gündoğdu, M.N., Gourgaud, A., Le Pennec, J.-L., 1998. Ignimbrites of Cappadocia (Central Anatolia, Turkey): petrology and geochemistry. *Jour. of Volc. And Geotherm. Res.* 85, 447-471.

Velis, D.R. and Ulrych, T.J., 2001. Simulated annealing ray tracing in complex 3-D media: Geophysical Journal International, 145, 2, 447-459.

Vinnik, L.P. and Kosarev, G.L. 1981. Determination of crustal parameters from observations of teleseismic body waves. Proc. Acad. Sci. USSR, 261, 1091-1095.

Walter, W. R., 1993. Source parameters of the June 29 Little Skull Mountain earthquake from complete regional waveforms at a single station, Geophys. Res. Lett., 20 , 403–406.

Wilson, D., Aster, R., Ni, J. and Grand, S., 2005. Imaging the seismic structure of the crust and upper mantle beneath the Great Plains, Rio Grande Rift, and Colorado Plateau using receiver functions, *J. Geophys. Res.* 110.

Whitney, D.L., and Y. Dilek, 1997. Core complex development in central Anatolia, Turkey, *Geology*, 25,1023-1026.

Zandt, G. and Ammon, C.J., 1995. Continental crust composition constrained by measurements of crustal Poisson's ratio, *Nature,* 374, 152-154.

Zandt, G., Myers, S.C., and Wallace, T.C., 1995. Crustal and mantle structure across the Basin and Range - Colorado Plateau boundary at 37°N latitude and implications for Cenozoic extensional mechanism, *J. Geophys. Res.* 100, 10529-10548.

Zelt, B.C. & Ellis, R.M., 1998. Receiver function studies in the Trans-Hudson orogen, Saskatchewan, *Can.J.Earth Sci.,* 36, 585-603.

Zelt, B.C. and Ellis, R.M. 1999. Teleseismic receiver function analysis in the Trans-Hudson Orogen, Saskatchewan. *Canadian Journal of Earth Sciences*, 36: 585-603.

Zhang, J., Langston, C.A., 1995. Dipping structure under Doubes, Belgium, determined by receiver function modeling, *Bull. Seismol. Soc. Am.* 85, 254– 268.

Zhu, H. & Kanamori, H., 2000. Moho depth variation in southern California from teleseismic receiver functions, *J. Geophys. Res.* 105, 2969-2980.

Zhu, L., B.J. Mitchell, N. Akyol, I. Çemen and K. Kekovali, 2006. Crustal thickness variations in the Aegean region and implications for the extension of continental crust, *J. Geophys. Res.,* 111, B01301, doi: 10.1029/2005JB003770.

Zor, E., The shear wave velocity structure of the eastern Marmara Region by using receiver function analysis, Ph.D. Thesis, *Bogazici Univ. Library,* Turkey, 2002.

Zor, E., E. Sandvol, C. Gurbuz, N. Türkelli, D. Şeber and M. Barazangi, 2003. The crustal structure of the East Anatolian plateau (Turkey) from receiver functions, *Geophys. Res. Lett.* 30(24), 8044, doi:10.1029/2003GL018192.

APPENDIX A

This section shows teleseismic events that are used in H-κ stacking analysis.

A.1. AFS Station Stacked Events

Event ID	Lat. (deg.)	Lon. (deg.)	Dist (km)	BAZ (deg.)	Depth (km)	Mag.
2002.321.0453.7342.0.1.eqr	47.95	146.42	8341	41.33792	470	5.80
2002.307.0337.7342.0.1.eqr	38.89	141.98	8759	50.70971	39	6.4
2002.306.0946.7342.0.1.eqr	2.95	96.39	7591	107.6582	27	6.4
2002.306.0126.7342.0.1.eqr	2.82	96.08	7575	107.9928	30	7.6
2002.304.1032.7342.0.1.eqr	41.79	14.87	1488	288.2487	100	5.90

A.2. AVO Station Stacked Events

Event ID	Lat. (deg.)	Lon. (deg.)	Dist (km)	BAZ (deg.)	Depth (km)	Mag.
2002.307.2212.7298.0.1.eqr	63.52	-147.44	8581	1.087406	44	8.50
2002.298.0249.7298.0.1.eqr	25.21	123.73	8383	70.64163	87	5.3
2002.304.1032.7298.0.1.eqr	41.79	14.87	1488	286.7377	100	5.90
2002.321.0453.7298.0.1.eqr	47.95	146.42	8341	40.36048	470	5.80

A.3. BOL Station Stacked Events

Event ID	Lat. (deg.)	Lon. (deg.)	Dist (km)	BAZ (deg.)	Depth (km)	Mag.
2002.311.1514.7286.0.1.eqr	51.20	179.33	9455	19.30281	33	6.60
2002.321.0453.7286.0.1.eqr	47.95	146.42	8341	38.63897	470	5.80
2002.306.0946.7286.0.1.eqr	2.95	96.39	7591	103.5311	27	6.4
2002.307.2212.7286.0.1.eqr	63.52	-147.44	8581	359.2626	44	8.50

A.4. DEV Station Stacked Events

Event ID	Lat. (deg.)	Lon. (deg.)	Dist (km)	BAZ (deg.)	Depth (km)	Mag.
2002.297.2153.7591.0.1.eqr	6.03	94.42	7203	106.2061	64	6.2
2002.307.0337.7591.0.1.eqr	38.89	141.98	8759	49.20981	39	6.4
2002.311.1514.7591.0.1.eqr	51.20	179.33	9455	22.30191	33	6.60
2002.324.2132.7591.0.1.eqr	35.41	74.51	3726	86.43827	33	6.5

A.5. KAR Station Stacked Events

Event ID	Lat. (deg.)	Lon. (deg.)	Dist (km)	BAZ (deg.)	Depth (km)	Mag.
2002.307.2212.7300.0.1.eqr	63.52	-147.44	8581	2.038713	44	8.50
2002.321.0453.7300.0.1.eqr	47.95	146.42	8341	41.67060	470	5.80
2002.305.2209.7300.0.1.eqr	35.52	74.65	3734	86.31390	33	5.4
2002.306.0946.7300.0.1.eqr	2.95	96.39	7591	108.3797	27	6.4
2002.304.1032.7300.0.1.eqr	41.79	14.87	1488	283.5493	100	5.90

A.6. PIN Station Stacked Events

Event ID	Lat. (deg.)	Lon. (deg.)	Dist (km)	BAZ (deg.)	Depth (km)	Mag.
2002.297.2153.7288.0.1.eqr	6.03	94.42	7203	107.0244	64	6.2
2002.306.0946.7288.0.1.eqr	2.95	96.39	7591	106.8732	27	6.4
2002.306.0126.7288.0.1.eqr	2.82	96.08	7575	106.8944	30	7.6
2002.324.2132.7288.0.1.eqr	35.41	74.51	3726	86.81722	33	6.5

A.7. POL Station Stacked Events

Event ID	Lat. (deg.)	Lon. (deg.)	Dist (km)	BAZ (deg.)	Depth (km)	Mag.
2002.321.0453.7428.0.1.eqr	47.95	146.42	8341	39.42000	470	5.80
2002.324.2132.7428.0.1.eqr	35.41	74.51	3726	83.61287	33	6.5
2002.297.2153.7428.0.1.eqr	6.03	94.42	7203	103.8682	64	6.2

A.8. SUN Station Stacked Events

Event ID	Lat. (deg.)	Lon. (deg.)	Dist (km)	BAZ (deg.)	Depth (km)	Mag.
2002.307.2212.7350.0.1.eqr	63.52	-147.44	8581	0.9538586	44	8.50
2002.331.0135.7350.0.1.eqr	54.67	-160.74	9493	8.896484	33	5.6
2002.321.0453.7350.0.1.eqr	47.95	146.42	8341	40.62836	470	5.80
2002.307.0337.7350.0.1.eqr	38.89	141.98	8759	49.83943	39	6.4
2002.324.2132.7350.0.1.eqr	35.41	74.51	3726	85.73047	33	6.5
2002.297.2153.7350.0.1.eqr	6.03	94.42	7203	105.7041	64	6.2
2002.306.0946.7350.0.1.eqr	2.95	96.39	7591	106.7337	27	6.4
2002.306.0126.7350.0.1.eqr	2.82	96.08	7575	107.0659	30	7.6
2002.304.1032.7350.0.1.eqr	41.79	14.87	1488	282.5707	100	5.90

A.9. SUL Station Stacked Events

Event ID	Lat. (deg.)	Lon. (deg.)	Dist (km)	BAZ (deg.)	Depth (km)	Mag.
2002.324.2132.7447.0.1.eqr	35.41	74.51	3726	82.05480	33	6.5
2002.306.0946.7447.0.1.eqr	2.95	96.39	7591	105.1193	27	6.4
2002.304.1032.7447.0.1.eqr	41.79	14.87	1488	289.9371	100	5.90
2002.297.2153.7447.0.1.eqr	6.03	94.42	7203	105.4042	64	6.2

A.10. ZAR Station Stacked Events

Event ID	Lat. (deg.)	Lon. (deg.)	Dist (km)	BAZ (deg.)	Depth (km)	Mag.
2002.307.2212.7456.0.1.eqr	63.52	-147.44	8581	2.341329	44	8.50
2002.321.0453.7456.0.1.eqr	47.95	146.42	8341	41.96850	470	5.80
2002.307.0337.7456.0.1.eqr	38.89	141.98	8759	51.36353	39	6.4
2002.306.0126.7456.0.1.eqr	2.82	96.08	7575	51.36353	30	7.6

A.11. ANTO Station Stacked Events

Event ID	Lat. (deg.)	Lon. (deg.)	BAZ (deg.)	Dist (km)	Depth (km)	Mag.
ANTO.2002.06.27.05.50.35.110.eqr	-6.96	104.18	107.4073	8944.096	11	6.90
ANTO.2002.11.02.01.26.10.700.eqr	2.82	96.08	105.5978	7550.273	30	7.60
ANTO.2004.02.22.06.46.27.40.eqr	-1.56	100.49	105.8766	8239.189	42	6.30
ANTO.2004.04.23.01.50.30.220.eqr	-9.36	122.84	97.15280	1067.618	65	6.70
ANTO.2004.05.11.08.28.48.280.eqr	0.41	97.82	106.2353	7872.061	21	6.20
ANTO.2004.05.28.12.38.44.270.eqr	36.29	51.61	97.72949	1696.845	17	6.30
ANTO.2004.07.25.14.35.19.60.eqr	-2.43	103.98	104.1335	8592.104	582	7.30
ANTO.2004.11.11.21.26.41.150.eqr	-8.15	124.87	94.93833	10764.09	10	7.50
ANTO.2004.12.26.09.20.01.610.eqr	8.88	92.38	103.2956	6799.394	16	6.60
ANTO.2005.01.01.06.25.44.820.eqr	5.10	92.30	106.5323	7069.970	11	6.70
ANTO.2005.01.01.19.08.07.800.eqr	7.34	94.46	10.30833	7084.188	55	6.10
ANTO.2005.02.09.13.27.25.340.eqr	4.80	95.12	104.7006	7324.625	44	6.00
ANTO.2005.02.26.12.56.52.620.eqr	2.91	95.59	105.8810	7503.221	36	6.80
ANTO.2005.03.13.03.31.23.150.eqr	27.09	61.89	108.8883	3031.789	54	6.00
ANTO.2005.04.03.00.59.21.420.eqr	0.37	98.32	105.9181	7916.911	30	6.00
ANTO.2005.04.08.05.48.37.880.eqr	-0.22	97.73	106.7958	7912.489	20	6.30
ANTO.2005.04.10.10.29.11.280.eqr	-1.64	99.61	106.5548	8172.822	19	6.70
ANTO.2005.04.11.06.11.11.820.eqr	2.17	96.76	105.6231	7654.576	24	6.10
ANTO.2005.04.16.16.38.03.900.eqr	1.81	97.66	105.2625	7755.536	31	6.40
ANTO.2005.05.10.01.09.05.100.eqr	-6.23	103.14	107.5702	8804.731	17	6.40

A.12. ISP Station Stacked Events coming from NE direction

Event ID	Lat. (deg.)	Lon. (deg.)	BAZ (deg.)	Dist. (km)	Depth (km)	Mag.
ISP.2000.01.28.14.21.07.340.eqr	43.05	146.84	41.70991	9149.489	61	6.80
ISP.2000.06.03.08.54.49.200.eqr	35.55	140.46	50.66190	8710.422	62	6.20
ISP.2000.06.07.21.46.55.900.eqr	26.86	97.24	80.30702	9113.880	33	6.50
ISP.2000.07.20.18.39.18.820.eqr	36.51	140.98	49.65529	8946.839	47	6.20
ISP.2000.08.19.17.26.27.940.eqr	43.82	147.17	40.98043	8644.097	62	6.00
ISP.2000.10.06.04.30.19.150.eqr	35.46	133.13	54.59658	8972.710	10	7.40
ISP.2000.10.03.04.13.30.490.eqr	40.28	143.12	45.68539	1010.598	33	6.30
ISP.2001.01.02.07.30.03.780.eqr	6.75	126.81	80.84855	8694.772	33	6.40
ISP.2001.03.24.06.27.53.580.eqr	34.08	132.53	56.01859	8929.576	50	6.80
ISP.2001.04.26.17.48.57.470.eqr	43.10	145.92	42.14609	9710.875	86	6.00
ISP.2001.06.14.19.48.47.850.eqr	51.16	-179.83	18.56547	9786.852	18	6.50
ISP.2002.05.25.05.36.31.970.eqr	53.81	-161.12	6.867835	8940.578	33	6.40
ISP.2002.08.24.18.40.53.440.eqr	43.11	146.12	42.03637	9944.704	42	6.10
ISP.2002.03.08.18.27.53.190.eqr	5.87	124.27	83.09057	9932.082	23	6.00
ISP.2002.03.05.21.16.09.130.eqr	6.03	124.25	82.97718	7927.685	31	7.50
ISP.2002.06.28.17.19.30.270.eqr	43.75	130.67	48.83735	3909.386	566	7.30
ISP.2002.11.20.21.32.30.810.eqr	35.41	74.51	80.22733	4021.350	33	6.50
ISP.2003.02.24.02.03.41.450.eqr	39.61	77.23	72.32758	9835.354	11	6.30
ISP.2003.05.26.23.13.29.720.eqr	6.76	123.71	82.73268	8238.726	565	6.90
ISP.2003.07.27.06.25.31.950.eqr	47.15	139.25	42.20987	8909.301	470	6.80
ISP.2003.03.15.19.41.28.700.eqr	52.25	160.39	28.60214	8610.348	30	6.10
ISP.2003.06.16.22.08.02.140.eqr	55.49	160.00	26.73181	9583.501	174	6.90
ISP.2003.06.23.12.12.34.470.eqr	51.44	176.78	20.38102	9708.975	20	7.00
ISP.2003.12.09.12.44.01.680.eqr	51.33	-179.27	18.17444	9121.790	33	6.20
ISP.2004.04.03.23.02.00.870.eqr	36.43	141.01	49.69947	3573.097	31	6.00
ISP.2004.04.05.21.24.04.000.eqr	36.51	71.03	79.73276	8879.254	187	6.60
ISP.2004.04.11.18.06.12.480.eqr	42.92	144.84	42.82959	8593.827	41	6.10
ISP.2004.06.10.15.19.57.750.eqr	55.68	160.00	26.60969	8906.162	188	6.90
ISP.2004.07.08.10.30.49.160.eqr	47.20	151.30	36.47584	9085.007	128	6.40
ISP.2004.09.05.10.07.07.820.eqr	33.07	136.62	54.64653	8904.011	14	7.20
ISP.2004.12.06.14.15.11.890.eqr	42.90	145.23	42.64600	9141.739	35	6.80
ISP.2005.04.10.22.22.15.710.eqr	35.60	140.40	50.65668	9682.312	43	6.10
ISP.2005.06.14.17.10.16.640.eqr	51.23	179.41	18.97480	9149.489	51	6.80

A.13. ISP Station Stacked Events coming from Southern direction

Event ID	Lat. (deg.)	Lon. (deg.)	BAZ (deg.)	Dist. (km)	Depth (km)	Mag.
ISP.2000.06.06.09.58.06.770.eqr	23.05	146.84	105.100	7944.096	233	6.30
ISP.2000.08.24.11.36.45.370.eqr	35.55	130.46	105.835	8550.273	324	6.50
ISP.2000.09.12.16.27.24.580.eqr	26.86	87.24	105.945	9239.189	145	6.10
ISP.2001.01.26.03.16.40.500.eqr	36.51	120.98	101.437	4067.618	234	6.00
ISP.2001.02.13.19.28.30.260.eqr	43.82	-147.17	104.873	6872.061	456	6.30
ISP.2001.03.15.01.22.43.370.eqr	35.46	138.16	99.690	3696.845	123	6.60
ISP.2001.08.05.05.16.16.890.eqr	50.27	143.12	96.956	9592.104	87	6.00
ISP.2002.06.27.05.50.35.110.eqr	6.75	126.81	105.590	20764.09	167	6.30
ISP.2002.10.03.19.05.10.670.eqr	34.04	132.53	98.875	7799.394	96	6.10
ISP.2002.11.02.01.26.10.700.eqr	33.12	145.92	103.222	9069.970	86	6.30
ISP.2002.11.02.09.46.46.700.eqr	51.16	179.83	102.905	6084.188	108	6.20
ISP.2003.07.15.20.27.50.530.eqr	53.81	-161.38	130.156	4324.625	154	6.70
ISP.2004.07.25.14.35.19.60.eqr	43.11	136.17	102.195	2503.221	86	6.40
ISP.2004.12.26.09.20.01.610.eqr	5.84	134.28	100.608	5031.789	94	6.80
ISP.2004.12.29.01.50.52.570.eqr	43.03	138.09	99.4650	6916.911	143	6.30
ISP.2004.12.29.05.56.47.540.eqr	44.08	142.53	100.126	8912.489	47	6.60
ISP.2005.01.01.19.08.07.800.eqr	34.17	138.54	100.529	4172.822	79	6.10
ISP.2005.01.04.09.13.12.250.eqr	41.05	122.32	99.0258	9654.576	107	6.30
ISP.2005.02.22.02.25.22.770.eqr	18.89	131.51	100.219	6755.536	65	6.30
ISP.2005.03.28.16.09.36.530.eqr	32.98	86.45	103.129	9804.731	96	6.10
ISP.2005.03.30.16.19.41.100.eqr	43.07	146.56	103.539	8844.096	158	6.60
ISP.2005.04.11.06.11.11.820.eqr	43.15	137.89	103.292	6550.273	48	6.20
ISP.2005.04.16.16.38.03.900.eqr	32.12	164.87	102.978	9239.189	59	6.40
ISP.2005.04.28.14.07.33.700.eqr	32.92	135.45	103.298	4067.618	175	6.10

A.14. MALT Station Stacked Events coming from NE direction

Event ID	Lat. (deg.)	Lon. (deg.)	BAZ (deg.)	Dist. (km)	Depth (km)	Mag.
MALT.2000.06.15.11.10.46.210.eqr	29.37	132.08	64.35631	8345.714	10	6.10
MALT.2000.06.25.06.34.42.880.eqr	31.18	131.21	63.27849	8161.179	10	6.00
MALT.2000.07.01.07.01.55.580.eqr	34.22	139.13	56.67410	8560.142	10	6.80
MALT.2000.07.08.18.57.44.470.eqr	34.05	139.13	56.81208	8571.665	10	6.60
MALT.2000.07.15.01.30.30.500.eqr	34.32	139.26	44.96205	8436.146	10	6.10
MALT.2000.08.19.17.26.27.940.eqr	43.82	147.17	73.73545	5342.147	62	6.00
MALT.2000.09.12.00.27.58.620.eqr	35.39	99.34	56.52563	8562.838	10	6.30
MALT.2000.11.13.15.57.21.610.eqr	42.49	144.76	47.17633	8378.490	33	6.00
MALT.2000.12.22.10.13.01.110.eqr	44.79	147.20	44.17804	8368.884	140	6.30
MALT.2001.03.23.11.30.10.520.eqr	44.07	148.05	44.34355	8472.189	33	6.00
MALT.2001.03.24.06.27.53.580.eqr	34.08	132.53	60.13199	8078.411	50	6.80
MALT.2001.06.24.13.18.51.710.eqr	44.19	148.51	44.02857	8491.498	33	6.00

MALT.2001.08.13.20.11.23.400.eqr	41.05	142.31	49.51882	8317.958	38	6.40
MALT.2003.05.26.09.24.33.400.eqr	38.85	141.57	51.67504	8418.038	68	7.00
MALT.2003.12.01.01.38.31.960.eqr	42.90	80.51	68.21125	3561.066	10	6.00
MALT.2004.09.05.10.07.07.820.eqr	33.07	136.62	58.91298	8451.842	14	7.20
MALT.2004.09.05.14.57.18.610.eqr	33.18	137.07	58.58982	8478.118	10	7.40
MALT.2004.11.11.10.02.47.330.eqr	42.14	144.34	47.65966	8375.854	32	6.10
MALT.2004.12.06.14.15.11.890.eqr	42.90	145.23	46.62200	8379.806	35	6.80

A.15. MALT Station Stacked Events coming from Southern direction

Event ID	Lat. (deg.)	Lon. (deg.)	BAZ (deg.)	Dist. (km)	Depth (km)	Mag.
MALT.2000.06.04.16.28.26.170.eqr	63.52	-147.44	110.687	8149.48	27	6.0
MALT.2000.06.07.23.45.26.680.eqr	54.67	-170.74	110.737	7710.42	78	6.30
MALT.2000.06.09.08.00.24.150.eqr	47.95	146.42	110.909	8113.88	48	6.80
MALT.2000.06.18.14.44.13.310.eqr	38.89	261.98	120.731	9946.83	123	6.10
MALT.2000.08.24.11.36.45.370.eqr	35.41	44.51	111.268	7644.09	167	6.00
MALT.2000.09.22.18.22.03.150.eqr	6.03	74.42	109.637	7972.71	98	6.50
MALT.2000.10.25.09.32.23.970.eqr	2.95	86.39	110.327	3010.59	43	6.80
MALT.2001.02.13.19.28.30.260.eqr	2.82	63.08	121.809	7694.77	236	6.10
MALT.2001.09.02.02.25.54.90.eqr	41.79	24.87	120.388	9929.57	145	6.40
MALT.2001.09.07.02.45.59.00.eqr	63.52	187.44	934.377	9810.87	98	6.60
MALT.2001.12.09.18.15.02.600.eqr	54.67	190.74	109.747	9686.85	59	6.80
MALT.2002.01.15.07.12.58.30.eqr	51.33	189.27	148.213	8970.57	196	6.80
MALT.2002.05.14.16.56.10.420.eqr	36.43	241.01	113.441	9984.70	447	6.50
MALT.2003.12.26.01.56.52.440.eqr	36.51	81.03	110.621	9933.08	261	6.60
MALT.2004.04.16.21.57.05.410.eqr	42.92	194.84	109.726	8926.68	86	6.60
MALT.2004.05.11.08.28.48.280.eqr	55.68	240.00	109.869	4909.38	168	6.10
MALT.2004.12.26.15.06.33.240.eqr	47.20	141.30	110.534	7021.35	389	6.00
MALT.2004.12.26.19.19.55.570.eqr	33.07	186.62	110.018	8835.35	69	6.20
MALT.2005.01.01.06.25.44.820.eqr	42.90	115.23	110.992	9238.72	68	6.70
MALT.2005.02.22.02.25.22.770.eqr	35.60	160.40	109.350	7909.30	245	6.40
MALT.2005.02.26.12.56.52.620.eqr	51.23	189.41	112.651	7610.34	39	6.10
MALT.2005.03.13.03.31.23.150.eqr	51.33	179.27	109.419	8583.50	288	6.10
MALT.2005.03.30.16.19.41.100.eqr	36.43	111.01	109.400	8708.97	65	6.60
MALT.2005.04.03.00.59.21.420.eqr	36.51	78.03	110.302	7121.79	118	6.30
MALT.2005.04.08.05.48.37.880.eqr	42.92	194.84	110.061	5573.09	104	6.30
MALT.2005.04.10.10.29.11.280.eqr	-1.64	72.61	109.943	7879.25	73	6.00
MALT.2005.04.10.17.24.39.400.eqr	2.17	94.76	111.107	4593.82	56	6.70